1-1-2014

Aging of a Polymer Core Composite Conductor Under Combined Ozone and Temperature Conditions

James M. Middleton
University of Denver

AGING OF A POLYMER CORE COMPOSITE CONDUCTOR UNDER COMBINED OZONE AND TEMPERATURE CONDITIONS

A Dissertation

Presented to

The Faculty of the Daniel Felix Ritchie School of Engineering and Computer Science

University of Denver

In Partial Fulfillment

Of the Requirements for the Degree

Doctor of Philosophy

By

James M. Middleton

August 2014

Advisor: Dr. Maciej Kumosa

Author: James M. Middleton
Title: AGING OF A POLYMER CORE COMPOSITE UNDER COMBINED OZONE AND TEMPERATURE CONDITIONS
Advisor: Dr. Maciej Kumosa
Degree Date: August 2014

ABSTRACT

The next generation High Temperature Low Sag Polymer Core Composite Conductors (HTLS PCCC) can experience harsh in-service environments including high temperature and highly concentrated ozone. In some extreme cases, it is possible that the conductors will experience temperatures of up to 180^{o}C and ozone concentrations as high as 1% (10,000 ppm). Therefore, the primary goal of this research was to determine the most damaging aging conditions which could negatively affect the in-service life of the conductors. This included characterizing the aging in ozone and at high temperature of the HTLS PCCC hybrid composite rods and neat resin. It was found that exposure to 1% ozone for up to three months at room temperature did not negatively affect the flexural performance of either the neat resin epoxy, or the hybrid composite rods. When aged up to a year at 140°C no detrimental effect on flexural performance of the composite was observed, as opposed to aging at 180°C, which had a very negative effect on the properties. The aging of the epoxy at 140°C was driven almost entirely by temperature and the effect of 1% ozone, even at that temperature, was insignificant for aging times up to ninety days. A finite element model was developed and showed the residual stresses developed after aging at 140°C for a year were minimal, but for temperatures higher than 160°C were substantial. From this it was determined that the aging was thermally driven,

and atmospheric high temperatures were the most damaging conditions for the PCCC conductors.

ACKNOWLEDGEMENTS

I dedicate this work to my family. I truly hope to make them proud.

I would like to thank and express my gratitude to Dr. M. Kumosa, my advisor. His continual support financially, academically, and morally made this research possible. I would also like to thank Dr. Brian Burks for the incredible amount of help he gave on not just experimental and theoretical, but also on modeling. This work was performed for the Western Area Power Administration, Tri-State Generation and Transmission Association, Inc., and the Bonneville Power Administration under contracts 36532A-272803, 36570A-272803, and 36863A-272803, respectively. I am especially grateful to Mr. R. Clark and Mr. A. Turner of WAPA, Mr. A. Mander and Mr. S. Anderson of Tri-State, and Mr. M. Staats of BPA for their most generous support of this study. It was also supported by the National Science Foundation (NSF) under the Grant Opportunities for Academic Liaison with Industry (GOALI) with the contract #CMMI-1232520. Research was conducted at the NSF Center For Novel High Voltage/Temperature Materials and Structures at DU. I thank Composite Technology Development for the use of their facilities, Jon Buckley of the University of Denver for test fixture manufacturing and Lindau Chemicals Inc., for supplying the epoxy resin and hardener. I am grateful to Professors D. Stedman, D. Smith and A. Chughtai for their contributions in helping create the ozone aging laboratory, and Dr. P. Predecki for his advice and help when I was stuck. And finally, I would like to thank my friends, who not only encouraged me, but also made life a bit more enjoyable when there was a lot of stress.

TABLE OF CONTENTS

Table of Contents.....v

Chapter 1: Introduction.....1

1.1 This Study.....1

1.1.1 Current Power Demands.....1
1.5.2 ACCC Transmission Lines.....4
1.5.3 Goals.....9

1.1 Polymers.....10
1.2 Viscoelasticity.....12
1.3 Aging.....16

1.3.1 Thermal.....21
1.3.2 Chemical.....27
1.3.3 Hygrothermal.....31

1.4 Computational Modeling.....37

1.4.2 Finite Element Analysis.....37

Chapter 2: Materials.....38

2.1 Introduction.....38
2.2 Materials.....39

2.2.1 High Temperature Aliphatic Epoxy.....39
2.2.2 PCCC Rods.....41

Chapter 3: Experimental Methods.....42

3.1 Introduction.....42
3.2 Aging Conditions.....42
3.3 Mass Loss, Density Change and Volumetric Shrinkage.....44
3.3 Flexure Strength.....45
3.4 Dynamic Mechanical Analysis.....47

3.5 Nanoindentation 52
3.6 Fourier Transform Infrared Spectroscopy 53
3.7 Dimensional Relaxations 54
3.8 Representative Volume Element Models 55
3.8.1 Representative Volume Elements and Repeating Unit Cell Modeling 55
3.8.2 RVE Model 56
3.8.3 Axis Symmetric Model 59

Chapter 4: Aging in Ozone at Room Temperature 61
4.1 Introduction 61
4.2 Mass, volumetric, density, and Void Content Changes in Aged Neat Resin 62
4.3 Nanohardness 63
4.4 Mechanical Properties of Neat Resin and Rod Specimens 64
4.5 Glass Transition Temperature 70
4.6 FTIR Analysis 71
4.7 Overall Effect of Chemical Changes on Mechanical Properties of Neat Resin and Composite Rod Specimens 76
4.8 Conclusions 78

Chapter 5: Aging of Neat Resin and PCCC in Atmospheric High Temperature 80
5.1 Introduction 80
5.2 Aging of the Hybrid Composite Rods 80
5.3 Aging of the Neat Resin 90
5.4 Conclusions 93

Chapter 6: The Combined Effect of High Temperature and Ozone 95
6.1 Introduction 95
6.2 Hybrid Composite Rods 96
6.2.1 Mechanical Performance of the Hybrid Composite Rods 96
6.2.2 Oxidation of the Hybrid Composite Rods 99
6.2.3 Hardness of Aged Hybrid Composite Rods 101
6.3 Aged Neat Resin 102
6.3.1 Mass Loss and Volumetric Shrinkage 102
6.3.2 Flexure Testing of Aged Neat Resin 105
6.3.3 Dynamic Mechanical Analysis of Aged Neat Resin 107
6.3.4 Nanoindentation of Aged Neat Resin 113
6.3.5 FTIR of Aged Neat Resin 118
6.3.6 Statistical Analysis 120
6.4 Conclusions 121

6.5 The Most Damaging Aging Condition 122

Chapter 7: Residual Stresses From Physical Aging Using Finite Element Modeling 124

7.1 Introduction 124
7.2 Representative Volume Element Model 124
7.3 Thermorheological Relaxations 129
7.4 RVE Modeling 131
7.3 Axis Symmetric Model 151
7.4 Discussion of the RVE Model 156
7.5 Conclusions 160

Chapter 8: Conclusions and Recommendations for Future Research 162

8.1 Conclusions 162
8.1.1 Major Conclusion of This Study 162
8.1.2 Other Important Conclusions 162
8.2 Future Research Suggestions 167

REFERENCES 171

LIST OF TABLES

Table 1: Glass fiber material properties used for RVE model. 57

Table 2: Mechanical properties of aged resin specimens as a function of aging time. 65

Table 3: Aging condition designations 96

Table 4: Stiffness matrix components of carbon fiber.....127

Table 5: Material properties of the ECR glass fiber and epoxy matrix used for RVE modeling. 128

Table 6: Generalized Maxwell model constants used for RVE modeling. 132

LIST OF FIGURES

Figure 1.1: Overview of power consumption and production in the US from 1949-2011. 2

Figure 1.2: US power production from 1949-2011 of different sources. 3

Figure 1.3: ACSR conductor.....5

Figure 1.4: Reactions for the creation of a cycloaliphatic epoxy resin. 6

Figure 1.5: Two commercially available cycloaliphatic epoxy resins. 7

Figure 1.6: Schematic of A). Composite core B). CFC and GFC. 8

Figure 1.7: The viscoelastic phase lag of the material response with an applied stress. ..13

Figure 1.8: Maxwell model of viscoelasticity. 14

Figure 1.9: Closed loop system of the free-volume concept. 17

Figure 1.10: Flexural strength as a function of postcure temperature and time. 26

Figure 1.11: Most common form of oxidation in polymers. 28

Figure 1.12: General reaction of polymers when different types of energies are introduced.....32

Figure 1.13: Hygrothermal cycles of aged epon 862. 35

Figure 3.1: Chamber in which the hybrid composite rods were aged……..…44

Figure 3.2: 4 point loading configuration with modified saddled loading pins and Teflon® tape at points of contact. 46

Figure 3.3: Schematics of DMA set ups available. 48

Figure 3.4: Schematic of the material properties calculated from DMA. 52

Figure 4.1: Mass loss and density change as a function of aging time.....62

Figure 4.2: Reduced modulus profiles for unaged and aged neat resin specimens.....63

Figure 4.3: Nanohardness profiles for unaged and aged neat resin specimens.....64

Figure 4.5: Loads at failure of aged resin specimens as a function of aging time with 1 σ error bars. 66

Figure 4.6: Displacements at failure of aged resin specimens as a function of aging time with 1 σ error bars. 66

Figure 4.7: Loads at failure for aged ACCC rods as a function of aging time with 1 σ error bars. 67

Figure 4.8: Mid-span deflections at failure for aged ACCC rods as a function of aging time with 1 σ error bars.....68

Figure 4.9: Storage modulus of aged resin for varying aging times as a function of frequency.....69

Figure 4.10: Loss modulus of aged resin for varying aging times as a function of frequency.....69

Figure 4.11: Damping (tan δ) of aged resin for varying aging times as a function of temperature at 1Hz. 70

Figure 4.12: Tg as a function of aging time for neat resin specimens.....71

Figure 4.13: FTIR spectra of aged neat resin samples for varying time lengths. 72

Figure 4.14: FTIR spectra of aged neat resin samples for varying time lengths. 73

Figure 4.15: FTIR spectra of an aged composite rod for varying time lengths. 74

Figure 4.16: FTIR spectra of an aged composite rod for varying time lengths. 75

Figure 5.1: Load at failure of hybrid composite rods in 4 point flexure as a function of aging time.....82

Figure 5.2: Displacement at failure of hybrid composite rods as a function of aging time. 82

Figure 5.3: Flexural modulus of hybrid composite rods as a function of aging time. 83

Figure 5.4: Dark field micrographs showing the oxidation layer of A180C specimens aged for (a) 3 months (b) 6 months (c) 9 months and (d) 12 months.. 86

Figure 5.5: SEM surface micrographs of A). 0 months, B). 3 months, C). 6 months and D). 12 months aged hybrid composite rods. 87

Figure 5.6: Schematic of hardness test set up.. 88

Figure 5.7: Rockwell hardness of hybrid composite rods aged in high temperature. 89

Figure 5.8: (a) Dimensional relaxations curves for various isothermal aging temperatures and (b) linearized Arrhenius plot for activation energy determination. 90

Figure 5.9: Load at failure of aged neat resin specimens with ±σ. 92

Figure 5.10: Displacement at failure of neat resin specimens aged at high temperature with ±σ. 92

Figure 5.11: Flexural modulus of neat resin aged at high temperature with ±σ. 93

Figure 6.1: Load at failure of hybrid composite rods as a function of aging time with ± 1 σ. 97

Figure 6.2: Mid-span deflection of hybrid composite rods as a function of aging time with ± 1 σ. 98

Figure 6.3: Flexural modulus of hybrid composite rods as a function of aging time with ± 1 σ. 98

Figure 6.4: Photomicrographs of A). AR, B). 1ORT, C). A140C, and D). CE140C specimens aged for three months. 100

Figure 6.5: Comparison of surface discoloration in A). AR, B). 1ORT, C). A140C, and D). CE140C specimens aged for three months. 100

Figure 6.6: Surface damage of a specimen aged at 180°C for three months. 101

Figure 6.7: Rockwell hardness of hybrid composite rods aged in various conditions as a function of aging time.....102

Figure 6.8: Mass loss of samples aged in various conditions as a function of aging time. 103

Figure 6.9: Volumetric shrinkage as a function of aging time of samples aged in various conditions with ± 1 σ.. 104

Figure 6.10: Loads at failure of neat resin specimens as a function of aging time with ± 1 σ.....105

Figure 6.11: Crosshead displacement at failure of neat resin specimens as a function of aging time with ± 1 σ.....106

Figure 6.12: Flexure modulus of neat resin specimens as a function of aging time with ± 1 σ.....107

Figure 6.13: Storage modulus as a function of frequency at varying time lengths: (A) seven days (B) fourteen days (C) thirty days and (D) ninety days.....109

Figure 6.14: Damping (tan δ) as a function of temperature for various aging conditions and time lengths: (A) seven days (B) fourteen days (C) thirty days and (D) ninety days. 112

Figure 6.15: The evolution of Tg as a function of aging time and aging condition with ± 1 σ.....113

Figure 6.16: Reduced modulus of aged specimens for A). 7 days, B). 14 days, C). 30 days and D). 90 days.....115

Figure 6.17: Nanohardness of specimens aged for A). 7 days, B). 14 days, C). 30 days and D). 90 days.....118

Figure 6.18: FTIR spectra of A140C aged specimens.....119

Figure 6.19: FTIR spectra of CE140C aged specimens. 119

Figure 6.20: FTIR spectra of A180C specimens.....120

Figure 7.1: A). Geometry of square fiber array FE model B). hexagonal fiber array geometry. 125

Figure 7.2: (A) Dimensional relaxations of aged neat resin specimens (B) plot of ln(τ) vs. 1/T for determining activation energy. 130

Figure 7.3: Plot of the measured dimensional relaxations and the created shear relaxations. 131

Figure 7.4: An example of the typical radial, hoop, and axial COMSOL stress plots as a function of arc length. 133

Figure 7.5. (A) Maximum radial stress of the CFC measured at 45° (B) maximum radial stress of the GFC measured at 45° for square packing.. 135

Figure 7.6: (A) Hoop stress of the CFC measured at 45° (B) hoop stress of the GFC measured at 45° for square packing. 136

Figure 7.7: (A) Axial stress of the CFC measured at 45° (B) axial stress of the GFC measured at 45° for square packing. 137

Figure 7.8: (A) Maximum radial stress of the CFC at 0° (B) maximum radial stress of the GFC measured at 0° for square packing. 139

Figure 7.9: (A) Hoop stress of the CFC at 0° (B) hoop stress of the GFC at 0° for square fiber packing. 140

Figure 7.10: (A) Axial stress of the CFC at 0° (B) axial stress of the GFC at 0° for square fiber packing. 141

Figure 7.11: (A) Maximum radial stress of the CFC measured at 30° (B) maximum radial stress of the CFC measured at 30° for hexagonal packing. 143

Figure 7.12: (A) Hoop stress of the CFC at 30° (B) hoop stress of the GFC at 30° for hexagonal fiber packing. 144

Figure 7.13: (A) Axial stress of the CFC at 30° (B) axial stress of the GFC at 30° for hexagonal fiber packing. 145

Figure 7.14: (A) Axial stress of a the CFC square packing at 45° (B) axial stress of the hexagonal packing CFC at 30°. 146

Figure 7.15: Comparison of stresses for CFC aged for 12 months at a 45° for the square fiber packing. 148

Figure 7.16: Comparison of CFC axial stresses for a specimen aged up to a year at 180°C at a 45° for the square fiber packing. 149

Figure 7.17: Schematic of what the axis symmetric FE model represents. 152

Figure 7.18: Stress convergence plot of the CFC axis symmetric model with a constant fiber radius. 154

Figure 7.19: Stress convergence plot of CFC axis symmetric model with a constant matrix radius.....154

Figure 7.20: Stresses created from aging for 12 months of the CFC axis symmetric model with a constant fiber radius.....155

Figure 7.21: Stresses created from aging for 12 months of the CFC axis symmetric model with a constant matrix radius. 156

Figure 7.22: A schematic of an (a) square RUC and (b) a hexagonal RUC……...159

CHAPTER 1: INTRODUCTION

1.1 THIS STUDY

1.1.1 CURRENT POWER DEMANDS

Polymers are an important material and have extensive applications due to their versatility and ability to be tailored. Applications run the gamut from household items such as plastic cups and plates, to biomedical materials, to automotive components such as car frames or bumpers [78]. If the polymer is reinforced with fibers such as glass or carbon, the applications and possibilities are significantly increased. Fiber reinforced polymers can have applications that range from aeronautical to structural such as transmission lines.

Since 1949, the amount of energy produced and consumed has been growing significantly. Albeit, by about 1960, the amount of energy consumed in the U.S., had surpassed the amount of energy produced (**Figure 1.1**). This trend has continued until this very day (79). Clearly there exists a need for ratification in the energy industry. One of those ratifications is the implementation of a new way to transport power.

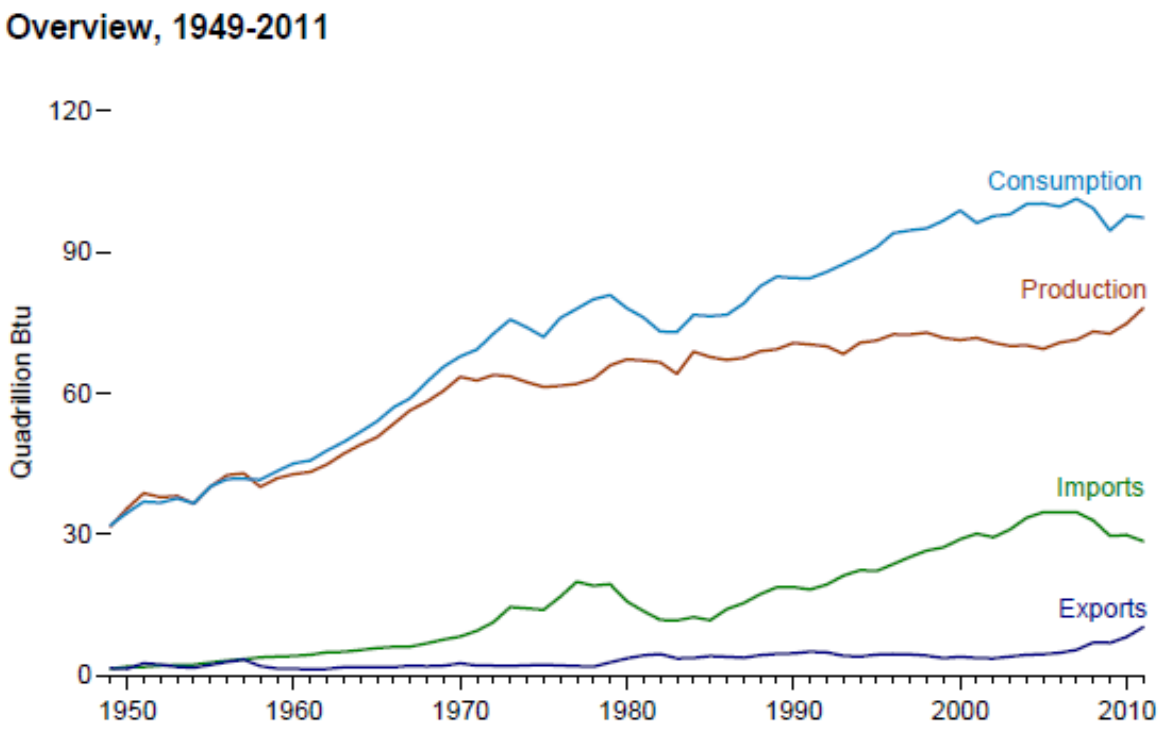

Figure 1.1: Overview of power consumption and production in the US from 1949-2011.[1]

[1] From [79].

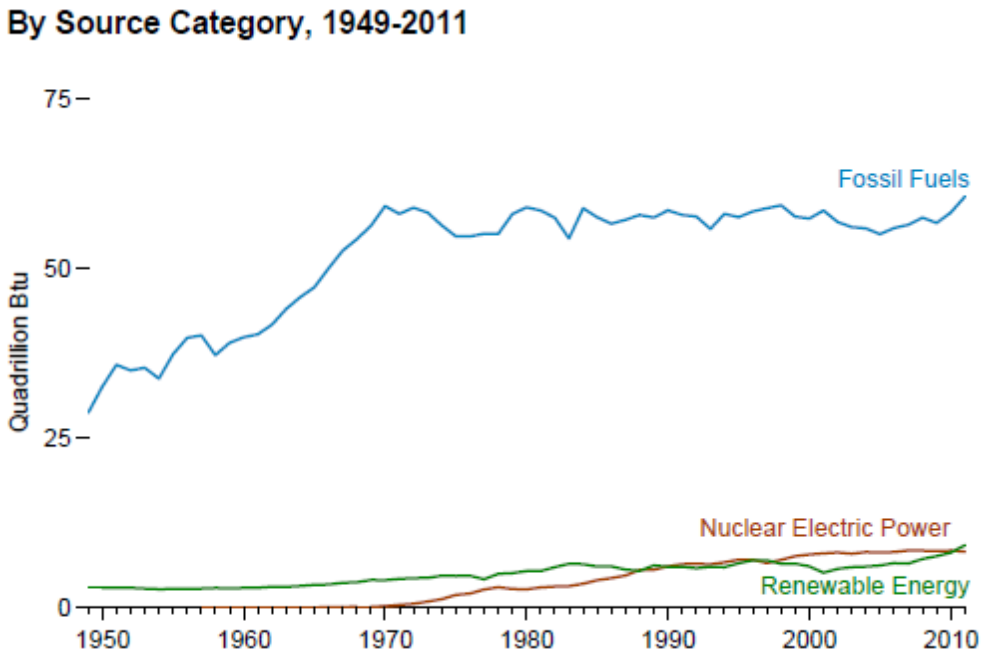

Figure 1.2: US power production from 1949-2011 of different sources.[2]

Using clean, renewable and nuclear energy is a potential way to meet the ever growing consumer demands. It can be seen from **Figure 1.2** that the use of nuclear and renewable energy has been on an overall incline since 1949. However, adding to power production through the use of renewable or nuclear sources requires time-consuming and costly infrastructure investments. Given the existing gap between consumption and production, a more immediate solution would be useful. A 2004 study prepared for Energy Delivery Group at Edison Electric Institute and the Office of Electric Transmission and Distribution of the US DOE concludes that additions to electric power transmission capacity appreciably lag increases in consumer demand. Improving upon

[2] From [79].

current transmission technology to increase capacity significantly without the need for major changes to current infrastructure could be of great benefit in timely solving problem of meeting consumer demand.

1.5.2 ACCC TRANSMISSION LINES

Aluminum conducting steel reinforced (ACSR) has a steel core for strength, and aluminum wrapped around it mostly for conduction (**Figure 1.3**). The steel is load bearing, but is not strong enough to bear the entire load. Therefore an aluminum alloy is used instead of pure aluminum, which makes the ACSR design strong enough. However, the aluminum alloy reduces conductivity compared to the conductivity achieved with a more pure aluminum.

Figure 1.3: ACSR conductor. The outer lighter in color strands are the conducting aluminum, and the inner darker in color strands are strength reinforcing steel core.[3]

The aluminum used in the current transmission lines has a relatively high coefficient of thermal expansion (CTE): 23.6 μm/m-^{o}C [80]. Steel on the other hand has a lower CTE, but is highly elastic. With these two properties, transmission lines experience a phenomenon called sag. As the lines heat up and expand, they stretch and sag lower. It is possible that the lines will sag low enough for a flash over if there is an object below the line. This creates a power surge that may possibly result in power outages. Recently, a new bill was introduced that restricts the amount of sagging a power line can experience before a large fine is imposed. Therefore the need to reduce sagging is important. Thus power companies are faced with an interesting engineering problem: a new way to transport more power while mitigating sag.

[3] Image courtesy of Google Images

For structural applications in the presence of HV fields, cycloaliphatic epoxy resins are a common choice of matrix material. They have high resistance to ultraviolet degradation and arc-tracking due to their fully saturated molecular structures. This makes them an ideal candidate for such applications [61]. They exhibit low viscosity and can have relatively high T_g. Such resins are expected to be used in PCC conductors since aging and electrical arc-tracking are major problems. Cycloaliphatic epoxy resins are prepared by converting tetrahydrobenzaldehyde by Tischenko condensation to form an olefin which is epoxidised with a peracid following the reactions shown below in **Figure 1.4**.

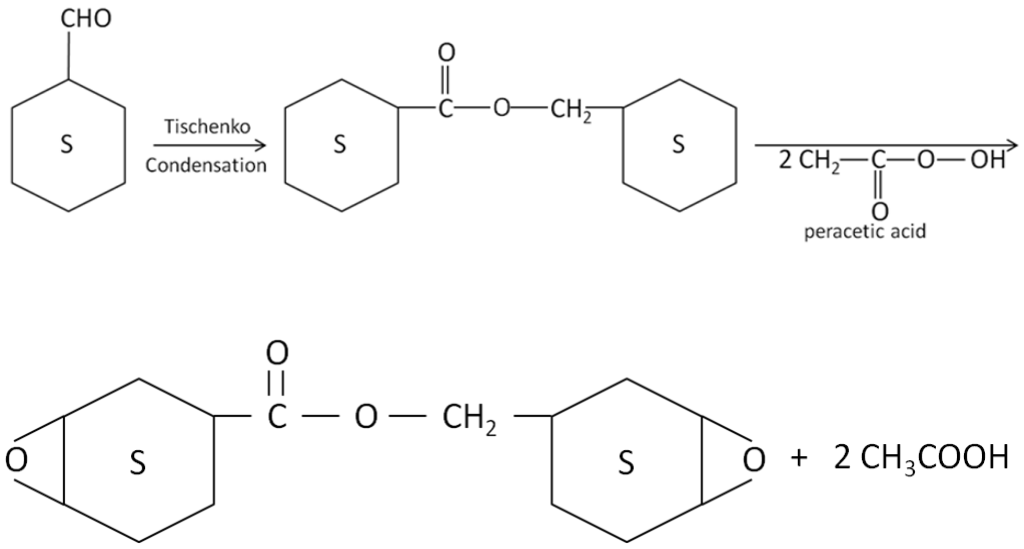

Figure 1.4: Reactions for the creation of a cycloaliphatic epoxy resin.

Two commercially available cycloaliphatic epoxy resin monomer structures are presented in **Figure 1.4**. They exhibit significantly different T_g, viscosity, as well as mechanical and electrical properties. For outstanding electrical properties in outdoor environments, any of the cycloaliphatic epoxy resins (**Figure 1.4**) can be used if cured with fully saturated acid anhydrides [61]. However, if electrical performance is not a primary requirement but low viscosity coupled with high T_g are of paramount importance, then the epoxy structure shown in **Figure 1.5B** would be the more appropriate material. This resin is cured at high temperature by nadic-methyl anhydride and its glass transition temperature can exceed 180°C.

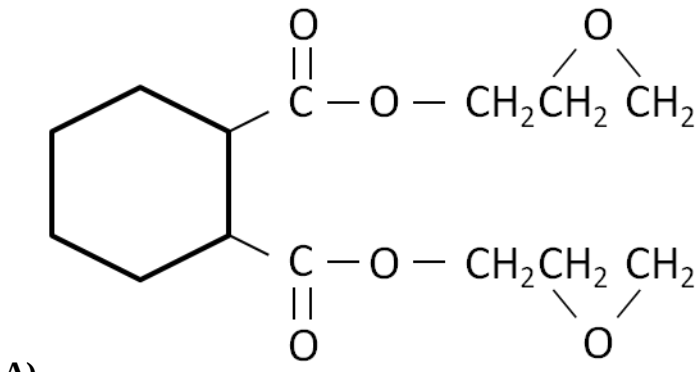

A).

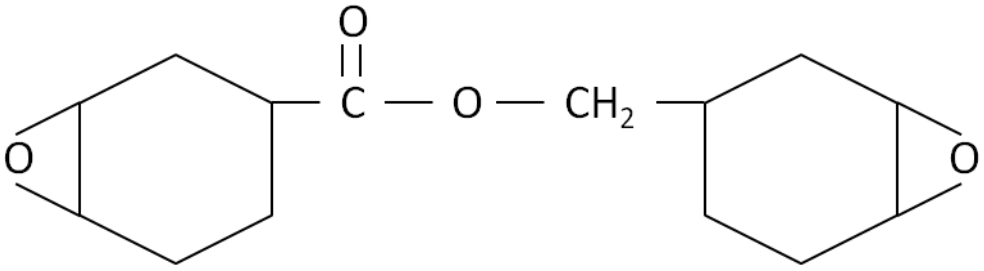

B).

Figure 1.5: Two commercially available cycloaliphatic epoxy resins.

This PCCC has many advantages which have been reported in literature in the past [13, 81, 82]. The first is that carbon has a slightly negative CTE [83, 84]. This mitigates sagging due to the carbon shrinking upon heating. Another advantage is that the composite core is strong enough to be able to bear the entire load allowing for a more pure aluminum to be used as the conductor reducing the amount of loss during transport of the power. Furthermore, the composite core is relatively small, so there can be more aluminum strands used. Consequently, the wires can be made into a trapezoidal design allowing for more conducting material (**Figure 1.6A**). With these advantages the lines can transport significantly more power than the ACSR design [85].

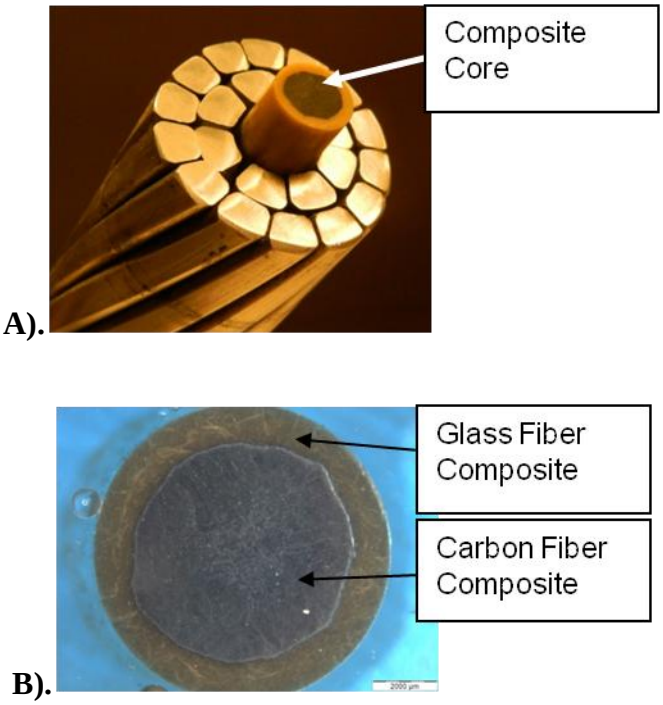

Figure 1.6: Schematic of A). Composite core B). CFC and GFC.

A great advantage of this design is that the power companies do not have to change the infrastructure. The PCCC design only requires that the current transmission line be replaced. No alterations to the infrastructure are needed.

The PCCC cores experience harsh environments that cause excessive bending, dynamic mechanical loading, pollution, partial discharges, and other environmental conditions that can cause aging [10, 12-14, 86-89]. For unidirectional glass fiber and carbon fiber polymer composites, the matrix dominated properties are especially vulnerable [6, 90-92]. Therefore it is necessary to understand and characterize the aging of the polymer matrix of the PCCC.

1.5.3 GOALS

The design life of transmission lines is desired to be decades long. It is therefore important to characterize the aging of the matrix of the HV transmission lines. Thus the goals of this research project were three fold: (1) characterize the aging of a cycloaliphatic resin that would potentially be used as the matrix of high voltage transmission lines, (2) characterize the aging of PCCC rods of one particular design, and (3) determine the most damaging aging condition for both the resin and the composite rods. The scope of aging is large and broad, so for this research only two mechanisms were considered: ozone and temperature and a combination thereof. The overall goal was to characterize the aging of both the neat resin and hybrid composite rods for the aging conditions chosen. This research also makes comments on future studies that could

possibly result in ways to enhance the neat resin and composite rods life, by increasing resistance to aging.

1.1 POLYMERS

Polymers are made through a process called polymerization in which long chains are made from repeating monomers, where the mer is the building block for the polymer. This process can happen in different ways, namely: chain growth and step growth. The former, also known as addition polymerization, is done through reacting chains together from monomers that are chemically active. Step growth, or condensation polymerization, is much slower due to the fact that it is done by individual chemical reactions between the active chains [1].

Copolymers can be created by polymerizing two or more different types of monomers together. If the individual polymers that were in the solution show up in the chain as blocks, the polymer is said to be a block copolymer. Creating a blend can be done by mixing different polymeric molecules together that have been pre-polymerized. The length of the repeat chain, or polymeric molecule, determines the degree of polymerization. As an example, given a mer of $(C_2H_4)_n$, n is the degree of polymerization [1].

There are two types of polymers, thermoplastics and thermosets. Thermoplastics tend to be linear polymeric molecules and become soft and deformable upon heating.

They normally have high temperature plasticity because of high chain mobility. Or in other words, the chains readily slide by each other. Chain mobility is thermally activated and, in thermoplastics, the polymer chains are connected by weak van der Waals forces and are not chemically bonded. Therefore, with applied temperature the van der Waals forces are easily melted, allowing the chains to slide. The most common thermoplastic is polyethylene [1].

Unlike thermoplastics, thermosetting polymers become hard and rigid upon heating. Also, unlike thermoplastics, this phenomenon is not lost upon cooling. Thermosetting polymers tend to have a high amount of crosslinking, or chemical bonding of adjacent linear polymeric molecules. Crosslinking is a thermally driven process, and results in a reduction of chain mobility due to the covalent bonding of chains [1].

There are several ways to manufacture polymers. The two most predominant ways for thermoplastics are injection molding and extrusion molding. Injection molding has pellets of the polymer fed into a machine where the pellets are heated up, melted and then injected into a mold. Extrusion molding is similar albeit the polymer pellets are fed into an extruder where they are pushed along by a heated screw that melts the pellets. At the end of the screw is a die which the melted polymer is forced through [1].

The two most common processes for making thermosets are compression molding and transfer molding. Compression molding and injection molding are similar processes that involve resin being injected into a mold where compression is applied. The problem that occurs with compression molding is that for the product to be finalized, the mold has

to be cooled so the polymer will retain its shape. This increases processing time and makes it somewhat impractical especially for commercial use. With transfer molding on the other hand, the resin is already partially polymerized (and therefore retains its shape) when it is transferred into the closed mold where final crosslinking takes place [1].

1.2 VISCOELASTICITY

Polymers exhibit a property called viscoelasticity, which is to say the polymer is neither truly viscous nor is it truly elastic; elasticity is rate dependent. In other words if a periodic stress is applied to a polymer, the material response "lags" behind (**Figure 1.7**).

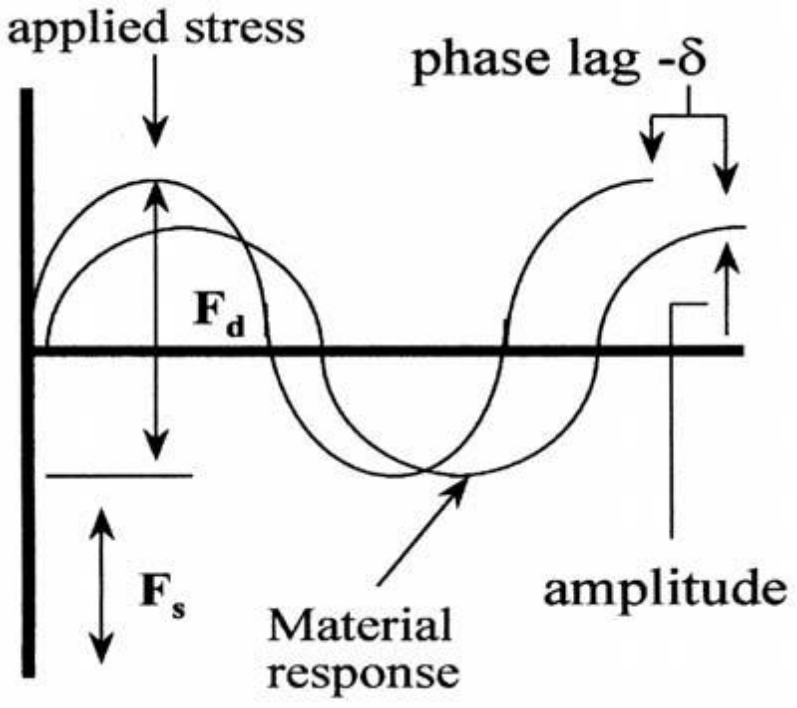

Figure 1.7: The viscoelastic phase lag of the material response with an applied stress.[4]

Consider a polymer in a liquid state. If a slow deformation is applied the polymer will exhibit viscous behavior. This results in the polymer eventually starting to flow. However, polymers behave elastically if the deformation is applied at such a short time period that the chains do not have enough time to reach a new equilibrium, and the polymer will return to some measure of its original shape. In low crosslink density polymers, the polymer will exhibit several regions. In the linear region of a stress-strain curve, the viscoelasticity of the polymer can be predicted by the Maxwell Model [2].

The Maxwell model contains a spring and dashpot in series (**Figure 1.8**).

[4] Figure from [105].

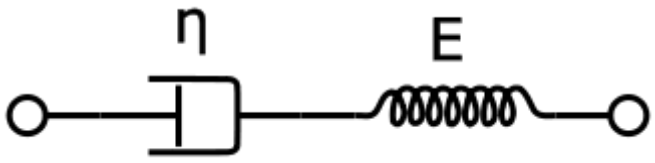

Figure 1.8: Maxwell model of viscoelasticity. The Dashpot has viscosity η and the spring has a stiffness of E.[5]

If a deformation is applied to the dashpot/spring system by some force, the dashpot dissipates the energy while the spring stores the energy. The overall deformation will be the summation of the dashpot displacement and the spring displacement (equation 1.1).

$$\delta_{total} = \delta_d + \delta_s \tag{1.1}$$

Where δ_{total} is the total displacement of the dashpot/spring system, δ_d is the displacement of the dashpot and δ_s is the displacement of the spring. Using the derivative of the dashpot displacement, the viscosity, η, can be calculated from equation 1.2:

$$\eta = -\frac{F}{\frac{d\delta_d}{dt}} \tag{1.2}$$

where F is the tensile force applied to the dashpot/spring system. Rewriting the equation as a derivative with respect to δ_{total} yields:

$$F + \frac{\delta_{total}}{G}\frac{dF}{dt} = -\eta\frac{d\delta_{total}}{dt} \tag{1.3}$$

[5] Figure from Google Images.

where G is the modulus of the solid. Replacing F by stress (σ) and $d\delta_{total}/dt$ with the strain rate $\dot{\varepsilon}$, equation 1.3 can be simplified to equation 1.4.

$$\frac{d\sigma}{dt} + \frac{\sigma}{\tau} = -\frac{\eta}{\tau}\dot{\varepsilon} \tag{1.4}$$

where τ is the relaxation time of the viscoelastic system and is calculated by equation 1.5.

$$\tau = \frac{\eta}{G} \tag{1.5}$$

The Generalized Maxwell model can be expanded to include n number of dashpot/spring systems connected in parallel. This will lead to a generalized stress

$$\sigma(t) = \sum_i \sigma_i(t) \tag{1.6}$$

where the subscript i refers to the ith dashpot/spring system. Equation 1.4 now becomes

$$\frac{d}{dt}\sigma_i(t) + \frac{1}{\tau_i}\sigma_i(t) = -\frac{\eta_i}{\tau_i}\dot{\varepsilon} \tag{1.7}$$

with the relaxation as

$$\tau_i = \frac{\eta_i}{G_i} \tag{1.8}$$

To change the form of equation 1.4 from an inhomogeneous first-order linear differential equation, both sides can be multiplied by an integration factor, $exp(t/\tau)$, thus transforming it into a integral. In generalized terms, the phenomenological model becomes

$$\sigma(t) = -\int_{-\infty}^{t} G(t-t')\dot{\varepsilon}\,(t)dt' \tag{1.9}$$

and

$$\sigma(t) = \int_{-\infty}^{t} M(t-t')\varepsilon(t,t')dt' \tag{1.10}$$

where *G(t)* and *M(t)* are the relaxation modulus and memory function respectively. They are related by

$$M(t) = -\frac{d}{dt}G(t) \tag{1.11}$$

In the above equations *t'* is some certain time and when *t' = t, ε(t,t) = 0* [2].

1.3 AGING

Using polymers in structural applications can be problematic due to a phenomenon known as aging. It has been shown that polymers, when below their glass transition temperature (T_g) are not in a state of thermodynamic equilibrium [3]. This state of non-equilibrium is unstable and the polymer therefore goes through a slow process in which it tends to equilibrate. As the material trends towards equilibrium, the properties of the material change over time. This change in properties has been coined "aging." Because the properties change over time, the transport mobility *M* is non-zero. This means that the concept of aging can be looked at as a free-volume concept: the transport

mobility of particles will mainly be dependent on the free-volume which is dependent on the packing of the system. Consequently, as the degree of packing increases, the free-volume decreases and vice versa [4].

Consider a specimen at a temperature above Tg, which is then cooled. Now apply the free-volume concept. As the polymer is cooled, the free-volume, which is essentially made up of "holes," redistributes and thereby reduces *M*. Therefore free-volume (v_{free}) dictates *M*, which dictates the rate at which the v_{free} changes (dv_{free}/dt). This closed loop system (**Figure 1.9**) leads to several conclusions [4].

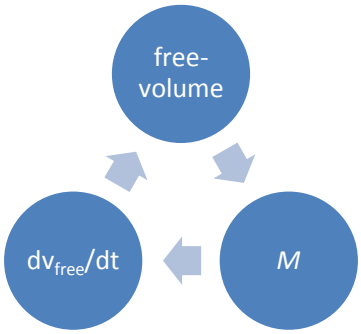

Figure 1.9: Closed loop system of the free-volume concept.

The first conclusion is that the volume-relaxation process is nonlinear. Second it shows that upon cooling, v_{free} has a limit; it cannot decrease indefinitely. Third, below T_g, *M* cannot be zero. A decrease in *M* requires a decrease is v_{free}, which implies that there is some mobility left to reduce. Therefore, *M* reduces asymptotically towards zero [4].

Aging results from many different factors. The most common is physical, or heat. Polymers are built upon monomers that are covalently bonded together repeatedly. With

the monomers repeating, a chain is created. In polymers such as polyethylene or epoxies, the chain can get infinitely long and create an amorphous material. The chains are held together by van der Waals forces, which are weak compared to the strong covalent bonds. Therefore, as the aging temperature increases, and gets closer and closer to the glass transition temperature, the more van der Waals bonds are melted. The melting of the van der Waals forces weakens chain interactions which can lead to a reduction in mechanical performance. If reinforced with a hardener, the T_g can be increased significantly due to crosslinking of the chains. Crosslinking connects chains via covalent bonds and therefore increases the temperature at which those bonds break and increases the temperature at which the polymer loses its properties. However, aging can be accelerated if aged in a non-inert environment giving rise to thermo-oxidation.

There are many different mechanisms in many different environments which cause aging. In most cases there is more than just heat present in in-service conditions. There can also be harmful chemicals present which can vary from chemically simplex air, which will cause oxidation, to complex chemicals such as insecticides or pollution; all result in the reduction of mechanical performance.

Aging consequently degrades mechanical performance of polymers and PMCs [5-8]. Ammar-Khodja showed that aging a carbon/epoxy composite with a T_g of 225^{o}C at atmospheric 180^{o}C up to 9000 hours, reduced the compressive strength by about 70%, and the elastic modulus about by 30% [9]. Burks *et al.* showed that aging a composite will increase the state of residual stresses. In a hybrid PMC that contains a glass fiber

composite (GFC) around a carbon fiber composite (CFC) used for transmission lines, Burks showed that the matrix in the GFC contains the highest state of stress which increased with aging time, impacting the fatigue performance of the composite [10].

PMCs have increased in use in industrial applications due to their lightweight yet desirable mechanical and material properties. However, in industrial applications, design life is of paramount importance. Most industrial applications occur in a harsh environment, which calls into question the long term reliability of the material. This creates interesting and complex challenges to overcome which include not just the initial mechanical and material properties of the PMC, but also the degradation of properties over time due to in-service aging conditions. Therefore the performance of aged PMCs is tantamount to knowing the unaged performance of the material. For PMCs, the matrix is the most susceptible to aging, especially in applications of long term high temperature exposure [11].

High voltage (HV) electric power transmission lines are an example of one such application. A current alternative for the present transmission line technology is Polymer Core Composite Conductors (PCCCs). PCCCs are comprised of a unidirectional carbon fiber composite covered by an insulating layer of electrically corrosion resistant (ECR) glass fiber composite. The hybrid composite rod is the load bearing component of the PCCC, and has several benefits [11-13], but primarily the design is conducive for greater amount of power to be transmitted. The current lines, aluminum conducting steel reinforced (ACSR), are temperature limited because they will sag significantly; a

problem the carbon in the PCCC has mitigated [14]. However, at these higher allowable operating temperatures, aging of the hybrid composite rod, and more specifically the matrix, is accelerated.

Aging is the result of polymers not being in thermodynamic equilibrium when below T_g. There are several ways to reduce the acceleration of polymer aging: change resins, reduce operation temperature, or reinforce the polymer (i.e. nanofillers). Changing resins is potentially costly and may result in manufacturing problems, reducing operation temperature may not be possible, and therefore the use of nanofillers is a tempting alternative. There are several considerations to be made with the implementation of nanofillers albeit. One such consideration is dispersion. For true isotropy, the nanofiller must be uniformly distributed. It is not trivial to mix nanofillers into a polymer with uniform distribution, nor quantify the degree of dispersion or uniformity. In literature, microscopy has been used to qualify dispersion: SEM [15-17], AFM [18], TEM [16, 17, 19-24], Fourier Transform Infrared Spectroscopy (FTIR) [25] and XRD [15, 22-24, 26, 27]. It should be noted that these techniques can subjective.

With the introduction of nanofillers, it is possible to increase the T_g and mechanical performance of polymers [26-28], but the resulting properties are not solely dependent on the type of nanofiller used. In addition, the amount of nanofiller, or weight percent (wt%), can have a significant impact on the nanocomposite's properties. Too much nanofiller can have a detrimental effect on the nanocomposite properties, instead of a positive effect. Li *et al.* showed that combining two different nanofillers can

significantly improve the performance of a diglycidyl ether bisphenol A (DGEBA) epoxy. At 3 wt% the nanocomposite displayed a peak in material performance. The T_g was increased approximately 14°C, and mechanical performance was significantly increased. However, at greater weight percents, a reduction in the nanocomposite's performance was observed [29]. A team in Singapore studied the effects of adding a nanoclay into DGEBA. With the addition of 1 wt% of nanoclay, an improvement in T_g and mechanical properties was seen. This team also observed a reduction in mechanical properties when the nanocomposite contained greater weight percents than 1 wt% [22].

1.3.1 THERMAL

Thermal, or physical aging, has been widely studied. Struik [4] did an extensive study on the aging of several different polymers. Creep tests were performed on polymers to measure the relaxations based on aging time and temperature and a master curve was developed to predict the creep compliance behavior. Equation 1.12 generally describes the physical aging of polymers

$$J_{t_e}(t) = J_{0_{te}} + \int_0^\infty f_{t_e}(\tau)\left[1 - e^{-\frac{t}{\tau}}d\tau\right] \tag{1.12}$$

in which τ is the relaxation time, $J_{te}(t)$ denotes the creep compliance of the material at a given aging time t_e, t is the creep time, J_{0te} is the limiting compliance for when t goes to zero, and finally the $f_{te}(\tau)$ is the retardation spectrum for an aging time t_e [4].

It should be noted here that a horizontal shift implies that a change in aging time from t_e to $t_{e'}$ is given by:

$$J_{t_{e'}}(t) = J_{t_e}(at) \tag{1.13}$$

$$f_{t_{e'}}(t) = af_{t_e}(a\tau) \tag{1.14}$$

Where a is the shift factor [4].

Since Struik, aging has been widely studied over quite a variety of polymers. L. Barral *et al.* [30] studied the enthalpy relaxations of a bisphenol A epoxy with a cycloaliphatic hardener. The authors used a differential scanning calorimeter to measure the specific heat capacity as a function of temperature. Viscoelastic properties were characterized as a function of temperature through the use of dynamic mechanical analysis (DMA). It was found that the enthalpy relaxations gradually increased with increased aging time. The DMA showed that the chains' stiffness increased with increased aging time.

Kapur *et al.* [31] studied the effects of aging quenched polypropylene on diffusion and mechanical properties. A strong dependence on aging time was observed for the transport properties. The transport properties of particles the size of helium and neon were affected, but particles the size or argon were not. It was also found that the yield strength increased after aging attributed to the quench process which results in thermal gradient due to low thermal conductivity, which in turn creates nonuniform plastic flow. Consequently there is a residual stress which puts the polymer in a state of compression

at the surface and tension at the center. As aging takes place and the polymer tends towards equilibrium and the chains are rearranged. This in effect relaxes out the stress and results with an increase in yield strength. The structural change of the polymer can not only explain the increase in yield stress, but it can explain the enhanced performance in all mechanical properties, i.e. the chain mobility decreases thereby stiffening the polymer [31].

Akay and Spratt studied the aging of a bismaleimide CFC and displayed that aging postcured the composite which raised T_g and simultaneously decreased the damping of the material. This is due to the fact that post curing can create more crosslinks, react any unreacted constituents, and allow the polymer to become more thermodynamically equilibrated. This results with an increase of T_g, and an increase in stiffness thereby reducing the bismaleimide's ability to damp out energy [6].

Post curing is not always beneficial. In some cases the mechanical properties are reduced instead of improved. This is especially true concerning composites where there is mismatching CTEs in the materials. Work done by Akay and Spratt showed that post curing leads to an increase in microcrack density and a reduction in flexural strength and interlaminar shear strength (ILSS) (6). Chandra, Rao and Kishore studied post curing on glass-phenolic composites. They found that post curing increased the impact values, but reduced the ILSS. This was attributed to the difference in CTE between the resin and the glass. As the composite was cooled back down to room temperature from the aging temperature, the difference in shrinkages between the two materials leads to residual

stresses that were strongly oriented in the direction perpendicular to the laminate face [32].

Chandra *et al.* studied the post curing effects of a glass fiber reinforced phenolic composite. The compressive, ILSS, and impact energy were studied after the composite was cured including a postcure of 2 hours at 110^{o}C and 160^{o}C. It was found that the ILSS and the compressive strength of the composite decreased after postcure. The effect was more pronounced with a higher postcure temperature. As the composite was postcured then brought back to room temperature the shrinkage difference between the polymer and the glass created residual stresses that can cause debonding among the plies. This in turn reduces both the shear and compressive strength of the composite. On the contrary, an increase in impact energy was seen and attributed to the debonding of the composite resulting from shrinkage differences creating crack detouring. In addition, crosslinking could have played a part in the increase in impact energy. Post curing increases the chance for main chain diffusion which in turn decreases the crosslink density, resulting in an increase in ductility and impact energy [32].

A team in Taiwan studied the effects of processing pultruded glass fiber reinforced polyurethane. This included the effect of pulling rate, the effect of die temperature, the effect of filler and the effect of postcure. In general it was found that slower pulling rates led to an increase in flexural performance. When the die temperature was increased albeit, slower pulling rates would lead to a degradation of the polyurethane matrix, and actually end up degrading the flexural properties. The die temperatures used

were 170, 180, 190, and 200^{o}C, and it was found that the optimum pulling rates were 20, 50, 120, and 160 cm/min respectively. There were two different types of fillers studied: calcium carbonate and mica. 10, 20, 30, and 40 parts per hundred of filler was added to the polyurethane composites. The flexural strength increased with increasing amount of filler, and was more significant with the calcium carbonate fillers. Lastly the effect of post curing was studied using five different temperatures: 100, 120, 130, 140, 150 and 160^{o}C. The results were similar to that of the die temperatures; generally as postcure temperature increased, the flexural performance increased as well and can be seen in **Figure 1.10**. However, at 160^{o}C, performance decreased due to degradation of the polymer. It can be seen that post curing at 130^{o}C for about 100 hrs results in the most significant increase in flexural strength. It can also be seen that after a given amount of time of postcure, the polymer would start to degrade in all temperatures except 100^{o}C [33].

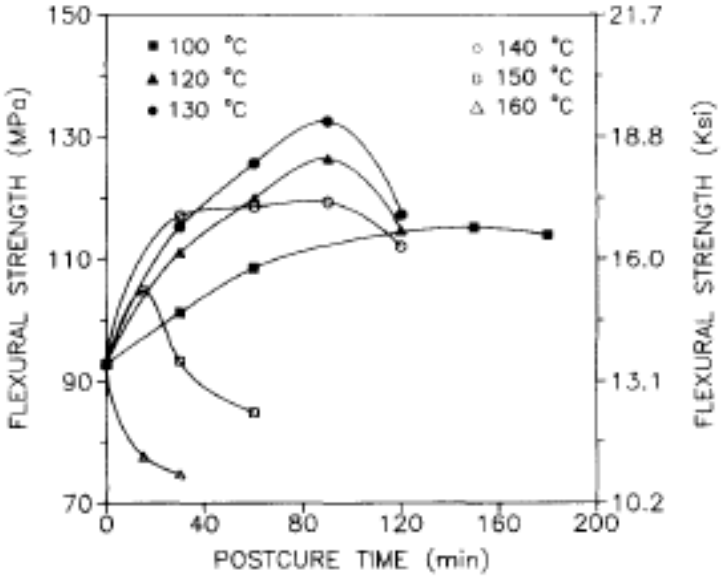

Figure 1.10: Flexural strength as a function of postcure temperature and time.

A paper presented in the 18th International Conference on Composite Materials reviewed a research team's findings on thermal aging of a carbon fiber/bismaleimide composite. The composite laminates were aged at several atmospheric temperatures: 150, 180 and 200°C. At each temperature, the laminates were aged for several thousand hours (1,500-10,000 hrs). After aging, there was a decrease in compression strength and thermo-oxidation had occurred, thereby degrading the initial 0° ply. Weight loss and FTIR analysis confirmed thermo-oxidation had taken place and therefore was indeed a mechanism in the degradation of the composite. Due to the thermo-oxidation, the matrix began to crack (seen through the use of an SEM). Aging also resulted in the reduction of toughness, and a modest decrease in off-axis tensile modulus [34].

1.3.2 CHEMICAL

In the case of PCCCs there are two major sources of aging that are of primary concern. The first is thermal aging [14, 35-37] and the second one is exposure to ozone. Heating a polymer in air can degrade it due to thermo-oxidative effects, especially when aging near the glass transition temperature (T_g) [14, 35, 36]. Both thermoset and thermoplastic polymers are susceptible to oxidation which breaks down polymer chains and crosslinks. This can damage the polymer, weakening its mechanical and electrical properties. Epoxies with high T_g are more resilient to this effect, albeit not much aging research has been done in this area. Oxidation occurs due to various sources, e.g. thermo-oxidation [38-40], UV oxidation [41], or ozone. Ozone is highly reactive and in the case of transmission lines, is constantly present since ozone can be created from air and an electrical discharge, although it dissociates at elevated temperatures (above ~100 ^{o}C) into O_2 and atomic oxygen [42].

O_2 can react with many different groups within the polymer. However, there is one dominant reaction that takes place and can be seen in **Figure 1.11**.

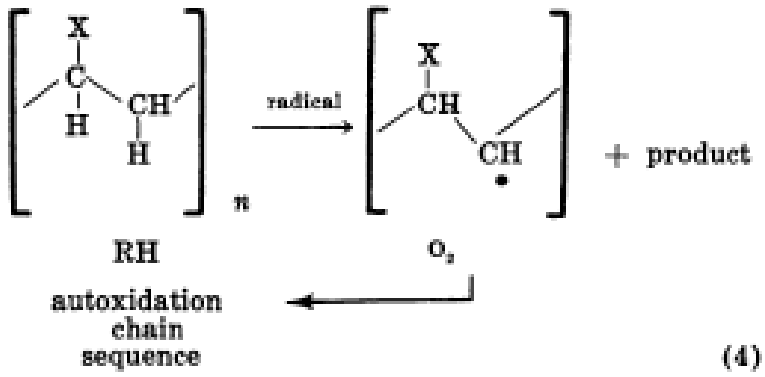

Figure 1.11: Most common form of oxidation in polymers.[6]

Due to the free radical nature of the C-H bond, the O_2 easily reacts and replaces the hydrogen. Obviously there are other bonds that can be oxidized such as the C=C, but the C-H bond is overwhelmingly prevalent. As this oxidation progresses to more functionalizable sites along the back bone of the polymer chain the chain will break in a process called chain scission. This is essentially the breaking of a long polymer chain into a shorter one, thereby increasing free-volume and chain mobility, and can be accelerated with the absorption of light energy i.e. photons [43].

Themo-oxidation has been found to alter the chemical structure of epoxy resins by chain scission, recombination and elimination reactions [44]. Pei *et al.* found that the oxidation of diglycidyl ether bishpenol A (DGEBA) occurs to the carbonyl group. Pei also demonstrated that the chain scission reaction occurs between the C-N bond in the amide group and in the C-C bond between the carbonyl and benzene, forming saturated aldehyde, ketone or acid [45]. Guo *et al.* studied a phenolic resin with similar results:

[6] From [43].

chain scission occurred at the C-N bond and carbonyl groups were formed after oxidation [46]. The formation of carbonyl groups has been shown to even take place in an aerospace grade epoxy by Tian and Hodgkin [47].

The degradation due to thermo-oxidation has been well studied [9, 11, 39, 48-50]. Parvatareddy *et al.* studied the aging of a composite in three different environments: ambient air, reduced pressure (13.8 kPa) air, and nitrogen. It was found that the ambient air environment resulted in the most substantial degradation of the composite due to the presence of oxygen diffusion processes. A 42% reduction in three point bending was found after six months of aging in ambient air, while nitrogen environment resulted only in a 14% reduction in bending strength. A similar trend was observed in strain to failure with the ambient air showing the greatest reduction of 58% and only a 22% reduction in the nitrogen environment. In all cases the partial pressure air environment showed a greater reduction than the nitrogen environment, but a less substantial reduction than that of ambient air [51].

Along with atmospheric aging, ozone is an oxidation mechanism and has been investigated for polymer degradation [52-57], and as a functionalizer [58, 59]. However, the degradation of epoxy due to ozone has received less attention [60]. Peng showed that for a bisphenol A epoxy cured with methyl anhydride and 2-methyl-4-ethyl imidazole, degradation by ozone at room temperature (RT) with ozone concentrations up to 100 ppm originates from the hydroxyl and methyl groups forming ozonide and carbonyl groups. It was also shown that after exposure to ozone for 500 hours the pencil hardness went down

from 2H to 1H. Moreover, it was found that by adding 50% of carbonyl iron by weight the degradation process slowed down significantly [60]. Aliphatic resins are an alternative of carbonyl iron to increasing resistance to oxidation degradation.

Aliphatic epoxy resins, with their fully saturated molecular structure can minimize oxidation due to atmosphere and ozone [11]. Aliphatic resins have unique properties: high resistance to ultraviolet degradation and arc tracking, and can have a high T_g when coupled with an anhydride. All of which makes them ideal for high voltage applications and great candidates for the PCCC matrix [61].

An interesting problem that arises from oxidation is the measurement of the oxidized layer that is produced on the surface of a polymer. A research team from Osaka, Narisawa *et al.* used Auger spectrum analysis to obtain elemental concentration as a function of depth in the material [62]. Several other groups used scanning tunneling microscopy (STM) to measure the depth of oxidation. Liao *et al.* used STM along with x-ray photoelectron spectroscopy (XPS) to study the topology of graphene and the oxygen signal (62), while Lee *et al.* used STM to study the depth of defects in graphite [63]. Lenkor *et al.* used infrared (IR) spectra to evaluate oxidation layers through absorbance of a common constituent found in each specimen [64], and Tandon *et al.* used dark-field photomicrographs to measure the oxidation layer [65].

Mailhot *et al.* did a two part study on the chemical changes that occur when an epoxy hardened with an amine resin is aged in ultra-violet (UV) radiation. Samples were aged in 60^{o}C with UV at wavelengths above 300 nm with the presence of oxygen.

Thermo-oxidative experiments were performed in a ventilated oven at an isothermal temperature of 100^{o}C. FTIR showed that after one hour of irradiation there was a decrease in absorbance that corresponded to the epoxy and amine reactions. The carbonyls albeit showed an increase in absorbance, which has been seen before [44-47, 66]. After 30 hours of aging, the spectrum becomes nearly invariant. In other words, a pseudo-steady state has been achieved. Aging results in a disappearance of the isopropylidene, which can lead to reactions that decompose and cause chain scission thereby degrading the polycarbonate. Photo-oxidation takes place to almost the entire DGEBA chains, including those pertaining to the crosslinks. The reactions resulting from thermo-oxidation were similar to those present from photo-oxidation [67]. In the second part of the study the depth of penetration was measured using nanoindentation. It was found that after thirty hours of aging, oxidation had taken place to a depth of 300 μm from the exposed edge. This was also the case for specimens aged for 110 hours. In both cases, there was significant stiffening towards the surface, and as distance from the exposed edge increased, the local stiffness reduced [68].

1.3.3 HYGROTHERMAL

Allara provides a brief overview of the chemical reactions that can take place from environmental (hygrothermal) aging which includes air, UV, water vapor and other environmental pollutants. Degradation of the polymer from hygrothermal aging can be described by the introduction and absorption of ultraviolet radiation and/or thermal

energy in general, which can melt or destroy weak bonds. The strong covalent bonds can be cleaved as well, provided there is enough energy supplied. This can give way to the formulation of new bonds which alters the structure of the original polymer (**Figure 1.12**).

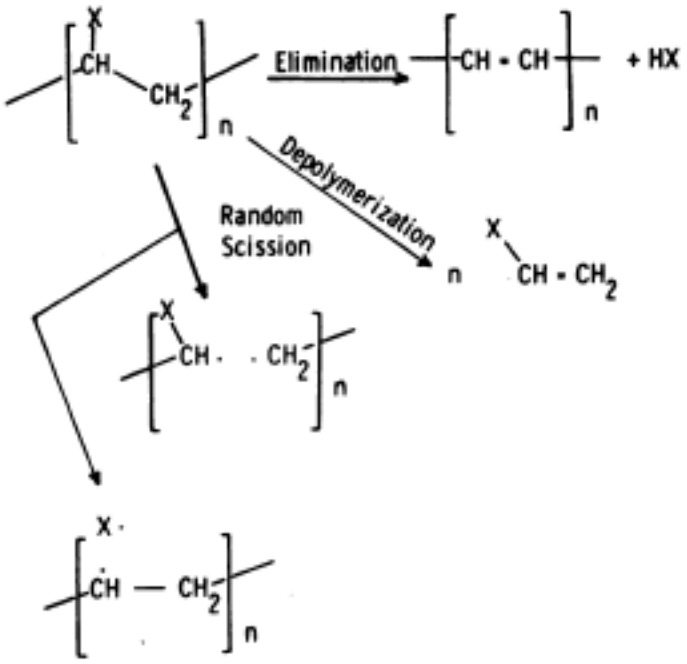

Figure 1.12: General reaction of polymers when different types of energies are introduced.[7]

Polymers with functional groups that include esters, amines and acetals can undergo hydrolysis and get attacked by water which leads to the formulation of parent acids or aldehyde groups.

[7] From [44].

As in the case of previously described aging sections, hygrothermal aging causes irreversible structural changes to the polymer. These changes in the structure, chain scission and introduction of carbonyl groups, lead to higher water absorption and weight loss irrevocably decreasing the glass transition temperature. Xiao *et al.* studied the degradation of DGEBA in water at several different temperatures. The authors aged the epoxy in 50, 70 and 90^{o}C. Through the use of FTIR, the introduction of carbonyl groups was observed in the spectra along with loss in functional groups that contain nitrogen. It was concluded that the loss in nitrogen groups was due to chain scission. When aged in the presence of water, the water reacted with the polymer chains creating oxygen containing groups and chain scission. Initially, these reactions yield an addition of chemically introduced water that is unable to leave upon drying resulting in an increase in weight. In later stages however, as more reactions take place, especially in the case of chain scission, chains get segmented and are much more readily leached into the water solution the polymer is submerged in leading to a weight loss [69].

The aging in different temperatures of water had a negative effect on T_g. After aging in 90^{o}C water, the specimen showed a decrease in T_g of 20^{o}C. It was concluded that this was due to chain scission, as a higher T_g is related to the amount of crosslink density. This decrease in T_g was also observed to be swelling dependent, and the temperature was a mere accelerant for water diffusion and swelling [69].

Guo *et al.* studied bisphenol A blends with a high degree of crystallinity in hygrothermal conditions. The molar fraction of novolac epoxy resin was varied and aged

in boiling distilled water. It was found that the resin with a molar fraction of 0.67 novolac resin absorbed more than the pristine bisphenol A dicyanate ester. Specimens with a molar fraction of 0.5 or less on the other hand, absorbed less water than the pristine ester. The hydrophobicity of lower epoxy molar fractions was attributed to the free-volume. The pristine ester has more free volume than the lower epoxy molar fractions due to the intramolecular triazine bicyclophane cage structures, and therefore can absorb more water [70].

The change in T_g was shown to be dependent upon the amount of epoxy molar fraction. In general, the lower the epoxy molar fraction the more aging had an effect, and the more the T_g was reduced [70].

Miller *et al.* performed hygrothermal cycling on epon 862 epoxy. The thermal cycling can be found in **Figure 1.13** [71].

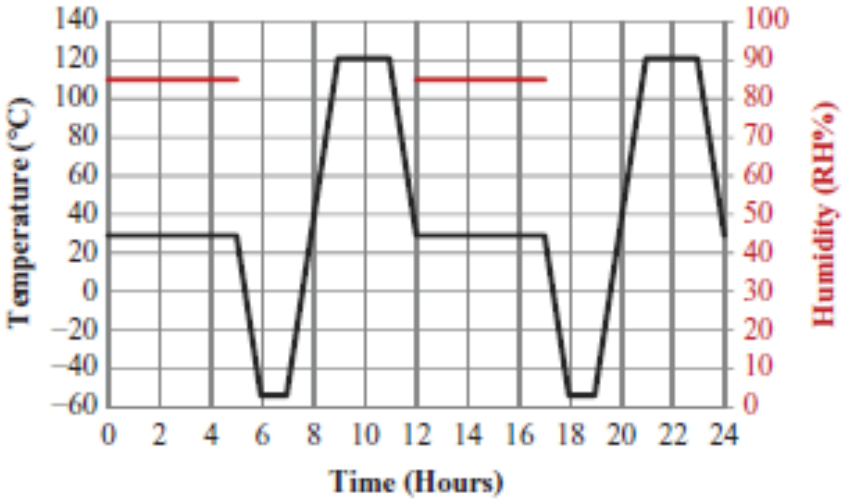

Figure 1.13: Hygrothermal cycles of aged epon 862.[8]

After aging FTIR analysis was done on the specimens to observe the chemical changes. For the first 217 cycles of aging the epoxy showed a gradual loss in the absorbance at 907 cm^{-1} which suggests an increase in crosslinking. Or in other words, postcure. After 108 cycles of aging, growth in the bands at 1653 and 1601 cm^{-1} was observed. This could be due to the formation of amide functionality resulting from the crosslink degradation of the epoxy and amine [71].

During the early aging cycles the polymer went through initial postcure increasing T_g. After the first hundred or so cycles, the T_g plateaued and no more increases were observed. A reduction however, was observed for the failure strain. As the number of hygrothermal cycles increased, the polymer became more brittle to the point where after 581 cycles the specimens were too brittle to be tested. Failure occurred upon loading the

[8]From [71]

specimens into the test fixture. After aging for 54 cycles, the strength of the specimens was increased, but after 54 cycles the polymer started to degrade and the ultimate strength declined [71].

Meiser *et al.* studied the effects of DGEBA in three different environmental conditions: dry air at 120^{o}C for 200 hundred days, dry air at 60^{o}C for 300 days and wet (90% relative humidity) air at 60^{o}C for 300 hundred days. It was found that after aging in dry air at 120^{o}C, autoxidation was the dominant form of oxidation. Lower dry air temperature followed the same oxidation process, albeit it was noted that the chemical reactions are temperature dependent, or in other words the reaction ranking and character of aging changes with temperature. Therefore, when making lifetime predictions based on accelerated chemical aging tests, caution is encouraged as the predictions can lead to false results.

Polymers have been shown to absorb water in accordance with Fick's law [72-74]. That is to say that the water absorption will increase linearly with the square root of time up to a certain point where absorption starts to slow down. Eventually the process will come to a steady state and the water absorption will equilibrate. However, some polymers, epoxies for instance, can deviate from Fickian behavior. Jana and Zhong reconcile this discrepancy by suggesting relaxations of the polymer. If the equilibrium relaxation process is slower than the diffusion process, the diffusion process is no longer Fickian. However, Jana and Zhong point out that since diffusion is thermally activated,

increasing the temperature will also increase the rate of water absorption and it is possible to achieve equilibrium states. This has been achieved in the past [75-77].

1.4 Computational Modeling

1.4.2 Finite Element Analysis

For this study, finite element (FE) modeling was performed through the use of a representative volume element (RVE). The concept of an RVE is that, when modeling small scales (i.e. micro scale), a snap shot of the material is taken such that it can represent the overall bulk material. In this way, the volume modeled is said to be an element of the overall macroscopic bulk material, hence the representative volume element. For this document, all boundary conditions are antiperiodic unless otherwise specified. That is to say that the displacements on one boundary of the RVE are equal and opposite of the displacements on the exact opposite boundary.

$$u_{dst} = -u_{src} \tag{1.15}$$

where u_{dst} is the displacement of the destination node, and u_{src} is the displacement of the source node.

CHAPTER 2: MATERIALS

2.1 INTRODUCTION

This section will describe the materials and manufacturing processes used for the studies performed in this document. The two materials used were: a hybrid composite rod that was the driving mechanism of this study, and a high temperature epoxy resin that could potentially be the matrix material for the hybrid composite rod. The composite rods were used to validate the research performed using the neat resin specimens. The motivation behind studying the neat resin and not just the composite rods was for complete research independence. Any type of specimen, composite, nanocomposite, neat resin etc could potentially be manufactured by using the neat resin specimens. The composite rods on the other hand are manufactured by an outside source as an actual implemented product. Therefore any manipulation of the composite rod was not possible. This document will contain a section on the hybrid composite rods and a section on the neat resin for each chapter.

2.2 MATERIALS

2.2.1 HIGH TEMPERATURE ALIPHATIC EPOXY

The neat epoxy tested in this research was supplied by Lindau Chemicals Inc. (Lindau). According to Lindau, the epoxy is a cycloaliphatic epoxy resin and has the chemical structure shown in **Figure 1.12B**. This type of epoxy could be an outstanding candidate for the use in the PCCCs. The chemical composition of the epoxy is: 3,4-Epoxycyclohexylmethyl-3',4'-epoxycyclohexane-carboxylate, trade name Lindoxy-190 (190). The hardener is specified as methyl-5-norbornene-2,3-dicarboxylic anhydride, or product name LS-252 (252). Using the cure cycle described in section 2.2.1, Lindau reports T_g values of 222 °C.

The mix ratio for the epoxy to hardener resin composition was 100:160 by mass. These constituents were massed out and then poured into a container and mixed at 198 RPM for two minutes. The resin was then degassed under vacuum for four hours. The degassing chamber averaged 23.33 Pa. After degassing, the resin was poured into a mold made of two steel plates. To ensure flatness and the correct thickness, shims were used between the steel plates. In between the two steel plates was silicon rubber cut out in a rectangle. This mold was then put into an oven and the manufacturer recommended cure cycle was employed. The first step of the cure cycle was two hours at 90^{o}C, followed by two hours at 150^{o}C, with the final step being four hours at 200^{o}C. Two things should be

noted here: first, according to the Lindau cure cycle, in the first step the resin should be "gelled" at 90°C without specifying the time period, and second, between these time steps there is a one hour linear ramp up to each temperature, and a final one hour linear ramp back down to room temperature. The manufacturing of the neat resin specimens was done at Composite Technology Development (CTD) in Lafayette, Colorado.

After curing, the specimens were cut using a Buehler ISOMET 1000 diamond saw. Two types of specimens were made: one type was prepared for the material properties and nanoindentation, and the other type was made for the flexure testing. The specimens made for material property measurements were cut to 6.35 mm x 6.35 mm x 13.97 mm ± 0.254 mm. The flexure specimens were prepared according to ASTM Standard D 790-07 and cut to the following dimensions: 60.96 mm long, 3.175 mm thick and 12.7 mm wide ± 0.254 mm. The test fixture had an inner span of 50.8 mm allowing for a 10% overhang [93].

To test for void content, samples were cut using a diamond blade, then placed in potting epoxy to cure for twenty-four hours, and then polished to a 0.05 μm finish. D.E. Light Software was used to measure the size of voids, and the total void content was calculated through equation 2.1 where $\sum A_{void}$ is the sum of the area of voids, assumed to be circular, and A_{total} is the total area of the micrograph.

$$Void\ Volume\ Fraction = \frac{\sum A_{void}}{A_{total}} \tag{2.1}$$

2.2.2 PCCC RODS

In addition to the neat resin tests, unidirectional hybrid composite rods based on ECR-glass and T700 carbon fibers with a HT epoxy (manufactured by a PCCC producer) were also tested after aging. The composite rods were supplied for this research by the Western Area Power Administration (WAPA). The name of the rod manufacturer may be obtained from WAPA. The volume fractions of fibers in the glass and carbon portions of the rod (**Figure 1.11B**) are 64% and 69%, respectively [94].

The T_g for the PCCC rods tested in this project was evaluated in another study using Dynamic Mechanical Analysis (DMA) and was found to be 205.5 °C and 208.1 °C [95]. The manufacturer did not agree to release the chemical structure of the resin; therefore, considering the high values of T_g and the type of application, it can only be speculated that the resin in the composite rods has the cycloaliphatic structure illustrated in **Figure 1.12B**.

The composite rods were cut to 355.6 mm length using a diamond blade chop saw and aged in an aluminum chamber 304.8 mm long. The motivation behind making the rods longer than the chamber was to ensure that axial diffusion was not present during aging. Axial and transverse diffusions in unidirectional composites behave differently [65], with transverse diffusion more closely representing in-service conditions imposed on PCCC rods. When aging the rods at temperature, to ensure axial thermo-oxidation did not occur, a silicon sealant was placed on the ends of the composite rods. After aging the rods were cut to their final test length of 279.4 mm.

CHAPTER 3: EXPERIMENTAL METHODS

3.1 INTRODUCTION

It has been shown that polymers will age, and will degrade over time when exposed to high temperatures. In the case of a PCCC, temperature is always present due to the flow of electric power through the aluminum strands. Therefore, the PCCC will be always exposed to elevated or even high temperatures. Another ever present aging mechanism is ozone. Ozone is created when an electrical discharge occurs in the atmosphere on a transmission line. Therefore this section presents the aging conditions for this study, and the experimental methods and tests performed.

3.2 AGING CONDITIONS

The neat resin and hybrid composite rods were aged in several conditions: atmospheric high temperature of 140 and 180^{o}C, and 1% ozone at RT. Two different 140°C aging conditions were applied, namely: (1) atmospheric and (2) 1% ozone (10,000 ppm). The 180°C rod aging data was taken from (85). The temperature conditions for the

neat resin and the rods were chosen to simulate aging below their glass transition temperatures, but temperatures that could be achieved in-service. The T_g's were about 248°C and about 205°C for the neat resin and hybrid composite rods, respectively. Aging of polymers in high temperature or ozone has been studied before, as previously shown. However, the combination of both high temperature and ozone has never been investigated before. Since the hybrid composite rods of the PCCC will constantly be exposed to both, this study incorporates the actual aging condition where both ozone and high temperature are present.

For each aging condition, specimens were aged for seven, fourteen, thirty, and ninety days. Aging in atmospheric 180°C specimens was performed in a Precision Scientific EconoTherm Laboratory Oven. This oven was also used to age specimens in 1% ozone at 140^{o}C. The ozone was generated by flowing industrial grade dry oxygen into two 12 kV dischargers connected in parallel at a flow rate of 20 mL/min. The neat resin specimens were placed in a desiccator inside the oven and aged for the appropriate time. The composite rods aged at 140°C were placed in an aluminum tube with the sealed ends containing holes to support the rods (**Figure 3.1**). The CE140C composite rod specimens were aged in a Blue M Single-Wall Transite Oven.

A  B

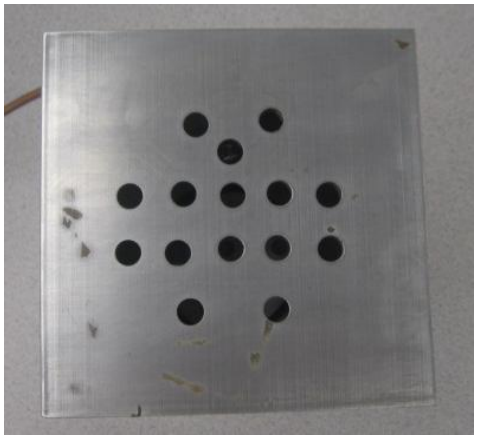

Figure 3.1: Chamber in which the hybrid composite rods were aged.

3.3 Mass Loss, Density Change and Volumetric Shrinkage

Mass loss and density change in the neat resin specimens were measured at each time interval. From these two parameters, volumetric change was calculated. An Ohaus Voyager scale with a range from 0-200 g and repeatability of 0.3 mg was used. The scale calculates density using Archimedes' principle, by taking the ratio of weight in air and weight in a known liquid

$$\rho = \left[\frac{A}{(A-B)}\right] Q_0 \tag{3.1}$$

where ρ is the specimen density, Q_0 is the density of the known liquid, in this case water, B is the weight of the specimen in the known liquid, and A is the weight of the specimen in air.

3.3 Flexure Strength

The four point bend configuration established in ASTM Standard D4476 results with transverse crushing. This can result with erroneous data by yielding a lower load at failure. Therefore Burks *et al.* developed a test in which the transverse crushing is eliminated [85]. The test deviates from ASTM Standard D4476 (96) by enlarging the saddled loading pins to 17.46 mm in diameter. In addition, the composite rod is lightly wrapped in Teflon® tape at locations where the specimen makes contact with the loading pins. These modifications create a test in which transverse crushing is absent, and therefore a true failure is tested. A linear variable differential transducer (LVDT) was used to measure the mid-span deflection and acquired data at a rate of 20 Hz (**Figure 3.2**). The test was performed in displacement control and the loading rate was 3 mm/min.

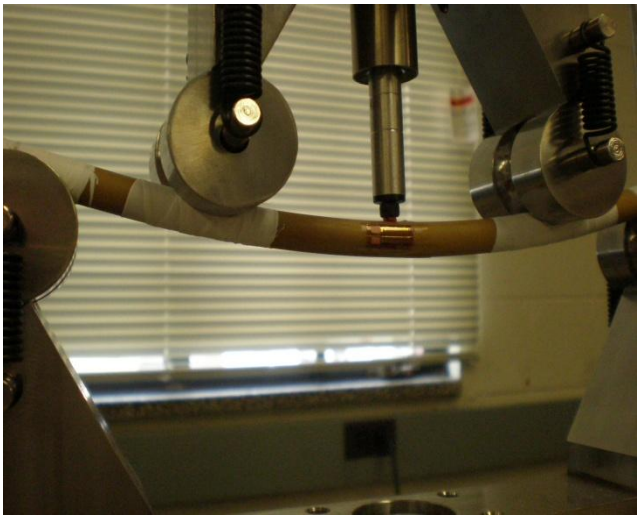

Figure 3.2: 4 point loading configuration with modified saddled loading pins and Teflon® tape at points of contact.

Flexure tests were performed in the three point bend configuration on the aged neat resin specimens using an MTS 858 in displacement control. The loading rate was 1.346 mm/min based upon the ASTM Standard D 790-07 [93]. The loading pins were first aligned, and then the specimen was loaded and set square with the test fixture using a "1-2-3 block". A preload of 1 N was applied to each specimen.

The flexural modulus (E) was calculated using the following relation [93]

$$E = \frac{L^3 m}{4bd^3} \tag{3.2}$$

where L is the support span, m is the slope of the linear portion of the load versus displacement curve, b is the width of the beam tested, and d is the depth of the beam tested.

3.4 Dynamic Mechanical Analysis

The storage modulus, loss modulus, and damping of the material were characterized through dynamic mechanical analysis (DMA). DMA is a common way to test viscoelastic materials. It allows a material to be characterized as a function of temperature, frequency or both in many different set ups (**Figure 3.3**).

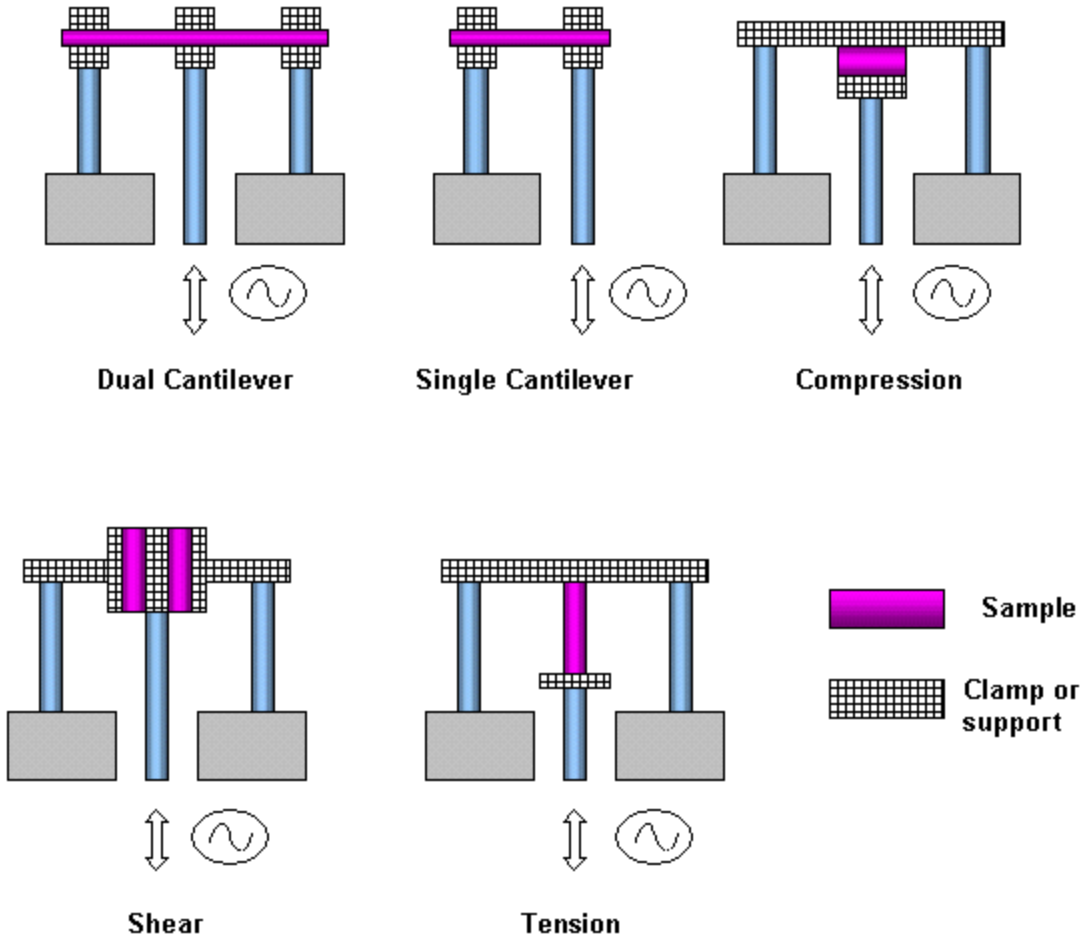

Figure 3.3: Schematics of DMA set ups available[9].

There are three major properties acquired from DMA: storage modulus, loss modulus and the material damping, *tanδ*. The concept behind DMA is if a periodic stress is applied within the polymer's linear elastic region, the stress can be calculated by:

$$\sigma = \sigma_0 \sin(\omega t) \tag{3.3}$$

[9] Google Images

where σ is the stress at time *t*, σ_0 is the maximum stress and ω is the frequency of the periodic stress. To get the stress rate, the derivative of equation 3.3 can be taken which yields

$$\frac{d\sigma}{dt} = \omega\sigma_0 \cos(\omega t) \tag{3.4}$$

The strain wave that results will be dependent on two things: the amount of viscous behavior and the amount of elastic behavior. The two extreme cases are all viscous or all elastic. Looking at these two extreme cases allows for the limits to be calculated, that when added together yields the strain wave. The viscous behavior will be proportional to the strain rate. Therefore, the dashpot model discussed earlier is applicable and the equation becomes

$$\varepsilon(t) = \eta \frac{d\sigma_0}{dt} = \eta\omega\sigma_0 \cos(\omega t) \tag{3.5}$$

where η is the viscosity. The elastic response will behave Hookean and the strain at any time can be calculated by

$$\varepsilon(t) = \frac{\sigma_0}{E} \sin(\omega t) \tag{3.6}$$

where the new terms $\varepsilon(t)$ and E are the strain at any time *t*, and the modulus respectively. Using Hooke's law, the σ_0/E term can be eliminated and equation 3.6 becomes

$$\varepsilon(t) = \varepsilon_0 \sin(\omega t) \tag{3.7}$$

where ε_0 is the maximum strain at the maximum stress.

Equations 3.5-3.7 deal with the limits of the viscoelastic response of the material. But in reality the true behavior is somewhere in between those limits. The difference between the stress and the resulting strain is a phase angle, δ, changing equation 3.7 to

$$\varepsilon(t) = \varepsilon_0 \sin(\omega t + \delta) \tag{3.8}$$

Using a trigonometric identity equation 3.8 can be written as

$$\varepsilon(t) = \varepsilon_0[\sin(\omega t)\cos(\delta) + \cos(\omega t)\sin(\delta)] \tag{3.9}$$

This is a convenient form, because now the equation can be broken up into two different parts: the in and out of phase parts.

$$\varepsilon' = \varepsilon_0 \sin(\delta) \tag{3.10}$$

$$\varepsilon'' = \varepsilon_0 \cos(\delta) \tag{3.11}$$

Taking the vector sum of these two equations allows the complex strain to be calculated

$$\varepsilon^* = \varepsilon' + i\varepsilon'' \tag{3.12}$$

This approach allows a single modulus to be broken up into two parts, namely the ability for the material to store energy, and the ability to lose energy. In other words, how much the polymer will respond in an elastic manner (spring-like response), and how much it will respond in a viscous manner (dashpot response).

From the stress and strain waves, the aforementioned three important parameters can be calculated. The first is the storage modulus, which is a quantitative measure of the elasticity of the polymer. The storage modulus can be calculated by

$$E' = \left(\frac{\sigma_0}{\varepsilon_0}\right)\cos(\delta) = \left(\frac{f_0}{bk}\right)\cos(\delta) \tag{3.13}$$

where δ is the phase angle, f_0 is the force at the peak of the sine wave, b is a sample geometry term, and k is the sample displacement at the sine wave peak. The amount of energy lost by the material is the loss modulus and is calculated in a similar fashion

$$E'' = \left(\frac{\sigma_0}{\varepsilon_0}\right)\sin(\delta) = \left(\frac{f_0}{bk}\right)\sin(\delta) \tag{3.14}$$

with all the terms as the same for equation 3.13. As with the strain, there is a complex modulus that can be calculated as well.

$$E^* = E' + iE'' \tag{3.15}$$

Taking the tangent of the phase angle δ, results in one of the most basic material properties: damping. This material property reveals how efficiently the material loses energy to internal processes such as molecular rearrangement and friction. The calculation of *tan(δ)* is easier to imagine if the calculation of the complex modulus E^* is pictured as a right triangle with the two sides as E' and E'' and the hypotenuse as E^*. Then the damping factor *tan(δ)* is the angle between the loss modulus and the complex modulus. The diagram representation of this can be seen in **Figure 3.4**.

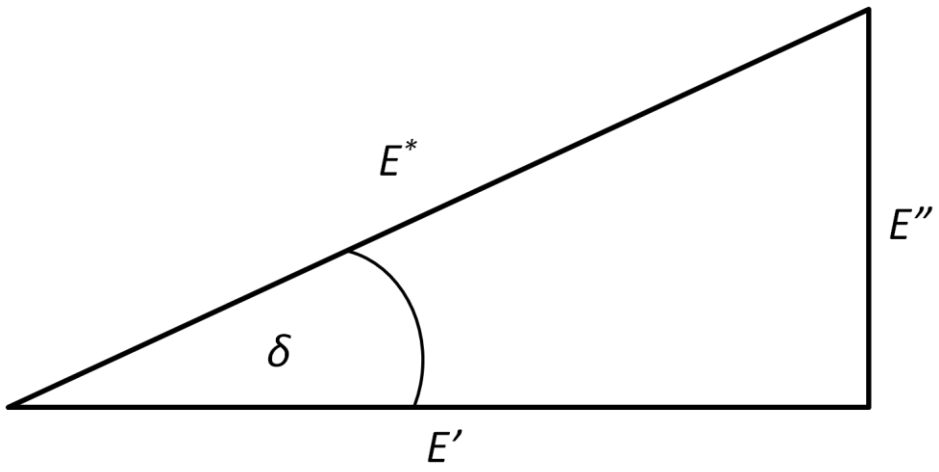

Figure 3.4: Schematic of the material properties calculated from DMA.

From **Figure 3.4** it is clear that *tan(δ)* can be calculated as such

$$\tan(\delta) = \frac{E''}{E'} = \frac{\eta'}{\eta''} = \frac{\varepsilon''}{\varepsilon'} \tag{3.16}$$

where η' is the energy loss portion and η'' is the storage portion of the viscosity [105].

For this study, DMA was used to study *E'*, *E''*, and *tan(δ)* as a function of frequency and as a function of temperature. Characterizing the aforementioned properties as a function of temperature allows for a T_g to be measured, as well as a qualitative measure of polymer chain damage.

3.5 NANOINDENTATION

Nanoindentation was used to characterize local hardness of the material, which in turn can provide useful information on depth of oxidation. The principle behind

nanoindentation is to extract some material properties, such as elastic modulus and hardness, at a nanoscale. The properties are calculated from a load applied from the indenter and the depth of penetration (97).

Hertz developed an equation that relates the radius of the circle from contact *a*, the indenter load *P*, indenter radius *R*, and the elastic properties of the material and indenter E^*.

$$a^3 = \frac{3}{4}\frac{PR}{E^*} \tag{3.17}$$

E^*, or the reduced modulus, incorporates the elastic properties of both the indenter and the material being indented by

$$\frac{1}{E^*} = \frac{(1-\nu^2)}{E}\frac{(1-\nu'^2)}{E'} \tag{3.18}$$

where ν is Poisson's ratio and E is the elastic modulus. The primes in the above equation refer to the indenter properties [97].

3.6 Fourier Transform Infrared Spectroscopy

Fourier transform infrared spectroscopy (FTIR) was used to track chemical changes after aging of both the composite rods and the neat resin. All FTIR spectra were recorded with a Digilab (Randolph, MA) FTS 7000 FTIR spectrometer equipped with a liquid nitrogen-cooled mercury cadmium telluride (MCT) detector and a SensIR

Technologies (Danbury, CT) DurasamplIR II outfitted with a Dicomp Duradisk and a torque limited pressure device. Spectra were collected over a range 4000–600 cm^{-1} with a resolution of 1 cm^{-1}. The spectra were produced by averaging data collected at four distinct sites on the sample. Measurements of each site comprised 48 coadded scans.

3.7 Dimensional Relaxations

If a polymer is thermorheologically simple (TRS), then the dimensional relaxation can be modeled using a stretched exponential function [98]. When normalized, the function has the form

$$\frac{L(t)}{L(0)} = e^{\left[-\left(\frac{t}{\tau}\right)^{\beta}\right]} \tag{3.19}$$

where *L(t)* is the length of the specimen at a given time *t*, *L(0)* is the initial specimen length, τ is the relaxation time associated with the given isothermal temperature, and β is a fractional exponent associated with the dimensional relaxation and is between 0 and 1. If β is constant between aging temperatures, then the material is said to be TRS, and the dimensional relaxation curve will be dominated by only one relaxation time, τ. With τ known, the activation energy can be calculated from the linearized Arrhenius equation:

$$\ln(\tau) = \frac{\Delta H}{RT} + \ln(\tau_0) \tag{3.20}$$

where ΔH is the activation energy, R is the universal gas constant, T is the isothermal temperature, and τ_0 is a material constant.

A Netzsch© DIL 402C dilatometer running DIL402C 414/4 software was used to perform the thermal aging. There were four different isothermal aging temperatures: 140, 160, 180 and 200^{o}C. The specimens were aged under ambient air and pressure to allow for a more accurate representation of in-service conditions. The specimens were first brought to ~15^{o}C (265^{o}C) above T_g for ten minutes to erase any previous thermal history, then quenched at 5^{o}C/min to the aging temperature. Data was collected at 2 points/min for this step and for one hour at the isothermal aging temperature. Then data was collected once every two minutes for the duration of the aging time of 30,000 minutes.

3.8 Representative Volume Element Models

3.8.1 Representative Volume Elements and Repeating Unit Cell Modeling

Micromechanical analyses typically make use of two geometric implementations of an overall macro model. These are the concepts of either a representative volume element (RVE), or a repeating unit cell (RUC). According to Drago and Pindera, an RVE "characterizes heterogeneous materials with macroscopically or statistically homogeneous microstructures at an appropriate scale…[99]". RVE's are based on the

boundary conditions of equivalence of homogeneous tractions and displacements. An RUC on the other hand characterizes a periodic heterogeneous material. The boundary conditions for RUC's implement a combination of periodic displacements and tractions. These two geometric representations have been used interchangeably in literature. There are a few possible reasons for this, one of which is unidirectional fiber composites being represented by a fiber array with either square or hexagonal fiber packing arrangements that could be represented by a single RUC. Not differentiating can lead to inaccurate boundary conditions, e.g. displacements or symmetry conditions. For this study, two different models were developed. The first was an RVE of a fiber array. The second model was an axis symmetric model involving one layer of fiber, one layer of matrix.

3.8.2 RVE MODEL

The stress within the matrix of a PCCC was characterized through finite element (FE) modeling via the use of a representative volume element (RVE) using the COMSOL software package. RVEs are developed such that, when modeling small scales (i.e. micro), a snap shot of the material can be representative of the overall bulk material when proper boundary conditions are applied. The RVEs developed for this study were both the CFC and GFC portions of the hybrid composite rod. The RVE geometry was a 2-D plane strain 5X5 fiber array with two symmetry planes to model a 10X10 fiber array; similar to the RVE by Drago and Pindera [99].

There are two commonly observed fiber packing arrangements in unidirectional fiber composites: square and hexagonal. The RVEs developed in this study include both packing types, and the volume fractions (v_f) of the GFC and CFC were 64% and 69% respectively. Perfect bonding between the fibers and the matrix was modeled. It is understood that the bonding and packing arrangements of the RVEs modeled are idealized, but they provide useful information on stress distributions and trends.

For the carbon fiber material properties, the anisotropic CTE was taken from [83] and [84], the elasticity matrix was taken from [100], and all other properties were taken from the Toray data sheet. The isotropic glass fiber material properties were taken from [83], with the properties found in **Table 1**. The matrix material properties can also be found in **Table 1**.

Table 1: Glass fiber material properties used for RVE model.

Property	**E-Glass**	**Matrix**
E (GPa)	76	2.1
v	0.22	0.4
ρ (kg/m^3)	2560	1200
k (W/m K)	13	0.819
α (*10^{-6} K^{-1})	4.9	100

With TRS materials, a transformation from a change in temperature to a change in time can easily be modeled. Thus the relaxation times are modified by a shift function. The Williams-Landel-Ferry (WLF) shift function was employed (equation 2.1), where α_T is the shift factor, C_1 and C_2 are material constants, T_{ref} is a reference temperature, typically T_g, and T is some temperature. C_1, C_2 and α_T were calculated using the process described in the Ferry text (101).

$$\log(\alpha_T) = \frac{-C_1(T - T_{ref})}{C_2 + (T - T_{ref})} \tag{3.21}$$

A five step FE model was used in which the first step is a stress free high temperature equilibration at 200°C. This is to establish the state of stress ($\sigma \approx 0$) at the curing temperature with curing stresses neglected. The next step was a cool down from 200°C to room temperature (RT), or 23°C, at a rate of 5°C/min, simulating the quench from curing after the pultrusion process. The next step was a temperature ramp up to the isothermal temperature at a rate of 5°C/min. This was to simulate when the conductor has been strung up and recently energized. The next step was an aging step at the specified isothermal temperature for a given aging time to simulate a specific continuous operating temperature (COT). The COTs chosen for this study were 140, 160, 180 and 200°C. At this step the physical aging was applied by calculating the volumetric shrinkage via equation 3.21 with the fit data. This shrinkage was then converted to a strain and applied at the beginning of the aging step. The final step was a cool down back to RT at the same 5°C/min ramp rate. Aging time lengths were chosen to coincide with previous studies the

authors have performed [11, 113], or seven days, fourteen days, thirty days, ninety days, six months, nine months and one year.

Benedikt *et al.* has previously shown that viscoelasticity must be considered when modeling [98, 102-104]. Therefore, to model the viscoelasticity of the matrix, a three term Generalized Maxwell Model was fit to the dimensional relaxation data (equation 3.22).

$$\Gamma(t) = G_0\left[\mu_0 + \sum_{m=1}^{N} \mu_m exp\left(-\frac{t}{\tau_m}\right)\right] \tag{3.22}$$

In the above equation, G_0 is the instantaneous shear modulus, the τ_m terms are the *m*th relaxation time, and the μ_m terms are material constants that should sum to 1, and *t* is time. The raw dilatometer data was fit with equation 3.22 using a nonlinear least squares regression. The matrix constants can be found in **Table**. It should be noted here that the μ_m terms for the matrix do not sum to exactly 1. This is because with the values obtained, the correlation coefficient was very close to 1, and it was decided to have a greater correlation coefficient (more representative of the data) than μ_m terms that summed perfectly to 1.

3.8.3 Axis Symmetric Model

The axis symmetric model was developed as a model to represent a composite in aging in a simplified manner. The model consisted of alternating layers of fiber and

matrix. There were two variations of the geometry, one with a constant fiber radius, and one with a constant matrix radius. This was to keep the volume fraction at the correct percentage, in the case of CFC 69%. Rings (i.e. ring of fiber and ring of matrix) were added and the stress was characterized as a function of number of rings to check for convergence. The stresses were characterized in the innermost fiber and matrix layers. It should be pointed out here that, with this model, if only one fiber and one ring of matrix is considered, the model would be a single fiber in an infinite matrix.

CHAPTER 4: AGING IN OZONE AT ROOM TEMPERATURE

4.1 INTRODUCTION

This section will describe the results from aging the neat resin and hybrid composite rods at room temperature in 1% ozone. As previously discussed, polymers are susceptible to oxidation, and ozone (a strong source for oxidation) is present around high voltage transmission systems. Therefore, the primary goals of this study were to investigate (1) the effects of aging in ozone at room temperature of a high temperature epoxy, and (2) the effect of ozone exposure on a hybrid polymer matrix composite rod presently used in-service. Most of the work done in this study was performed on the neat resin specimens. The neat resin results are therefore presented first, and make up most of the results. There is also a section on the chemical validation of the neat resin.. Or in other words, the section describes whether the neat resin used was an accurate representation of the hybrid composite rods.

4.2 Mass, volumetric, density, and Void Content Changes in Aged Neat Resin

The changes in mass and density with aging time are illustrated in **Figure 4.1**. It can be seen that after about one month of aging the quantities begin to stabilize without further reductions. The mass loss could be caused by the release of volatiles. The mass and density changes resulting from ozone exposure are dependent on the rate of diffusion into the specimen. It appears that somewhere between one and three months the diffusion process reached its limit. The void content was obtained using equation 2.1 and was found to be less than 2% on the unaged specimens.

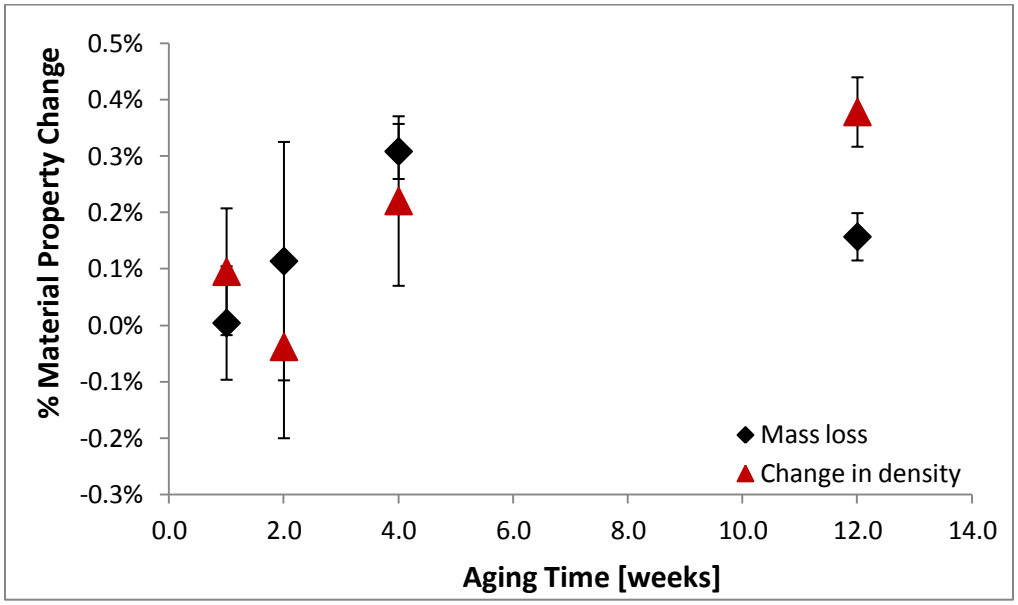

Figure 4.1: Mass loss and density change as a function of aging time. A negative value here represents an increase in the property, while a positive value represents a decrease in the property.

4.3 NANOHARDNESS

The reduced modulus and nanohardness were used to evaluate the depth of oxidation in the neat resin specimens. As an example, the unaged, one month and three month aged data are shown in **Figure 4.2** and **Figure 4.3**. Several observations can be made in **Figure 4.2**. First, the reduced modulus on the surface of the specimens increased after aging from about 3.8 GPa for the unaged sample to about 4.1-4.2 GPa for the three month aged specimen. Second, the modulus decreased after aging for one and three months up to a depth of about 60-80 μm. At that point the diffusion layer becomes a type of transition layer. Finally, at a depth of about 100-120 μm the moduli of the unaged and aged specimens became very similar.

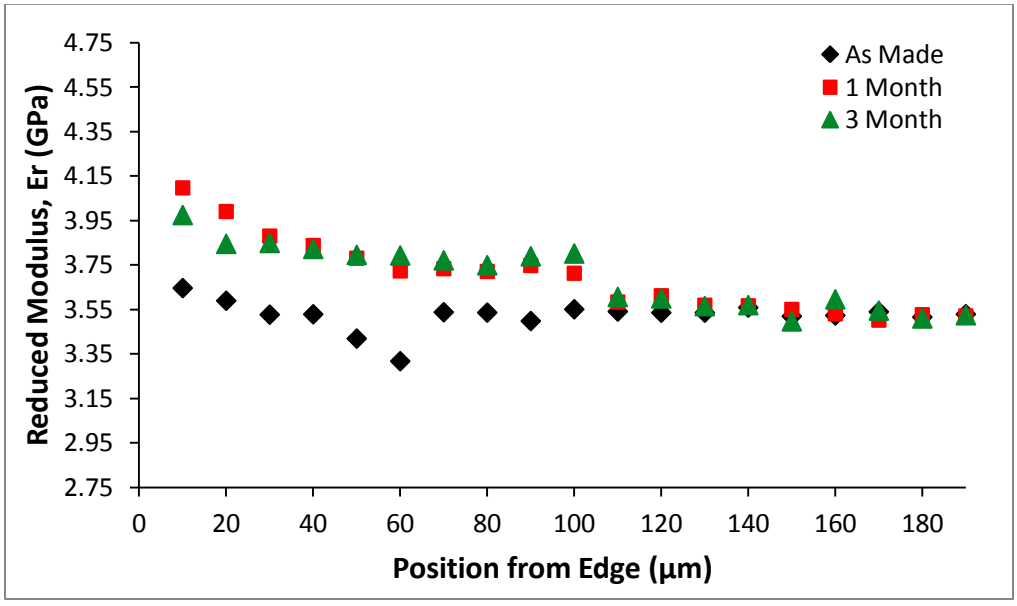

Figure 4.2: Reduced modulus profiles for unaged and aged neat resin specimens.

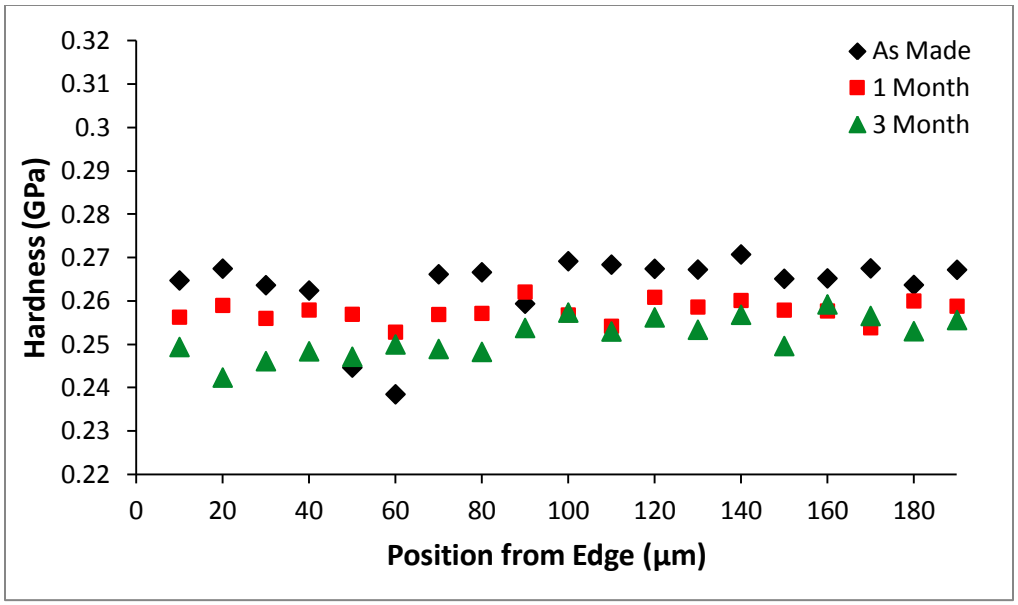

Figure 4.3: Nanohardness profiles for unaged and aged neat resin specimens.

No obvious oxidation layer could be observed in the nanohardness profiles. However, within the entire range of measurements, up to 190 µm, the nanohardness data for the three month aged specimen was about 10 to 15% below the values for the unaged specimen. The nanohardness for the one month specimen was always somewhere in between the unaged and three month aged profiles. The fact that nanohardness was reduced on the surface of the aged specimen could indicate chain damage in the polymer caused by the ozone exposure.

4.4 Mechanical Properties of Neat Resin and Rod Specimens

Three point bend tests were performed to evaluate the change in flexural strength due to aging of the neat epoxy specimens. Three specimens were tested for each

condition. The load and displacement at failure were plotted against exposure time (**Figure 4.4** and **Figure 4.5**). The load and displacement at failure data, in addition to the flexural moduli, are summarized in **Table 2**.

Table 2: Mechanical properties of aged resin specimens as a function of aging time.

t (weeks)	Load at failure (N)	σ (N)	Displ. at failure (mm)	σ (mm)	E (MPa)	σ (MPa)
0	156.7	6.4	7.593	0.654	2268.05	0.09
1	178.4	3.7	8.769	1.869	2277.97	21.00
2	152.2	13.7	8.031	1.939	2293.43	3.12
4	152.9	6.5	10.719	2.992	2231.64	19.48
12	150.8	19.7	12.100	1.987	2314.21	18.19

An increase in load to failure was observed for specimens subjected to 1 week of exposure to ozone, followed by a substantial decrease back to the unaged material property magnitude at subsequent exposure times.

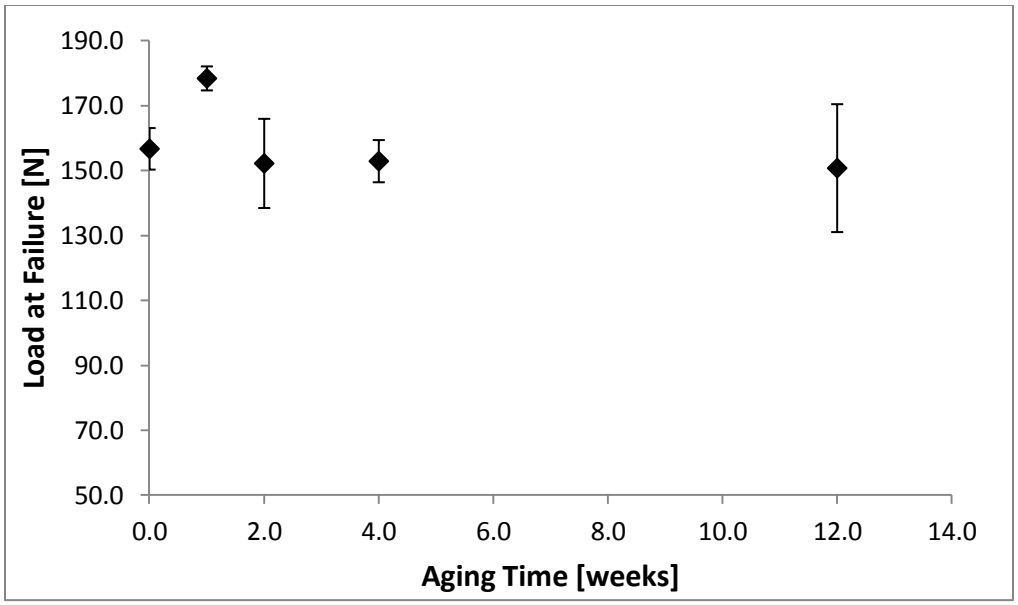

Figure 4.4: Loads at failure of aged resin specimens as a function of aging time with 1 σ error bars.

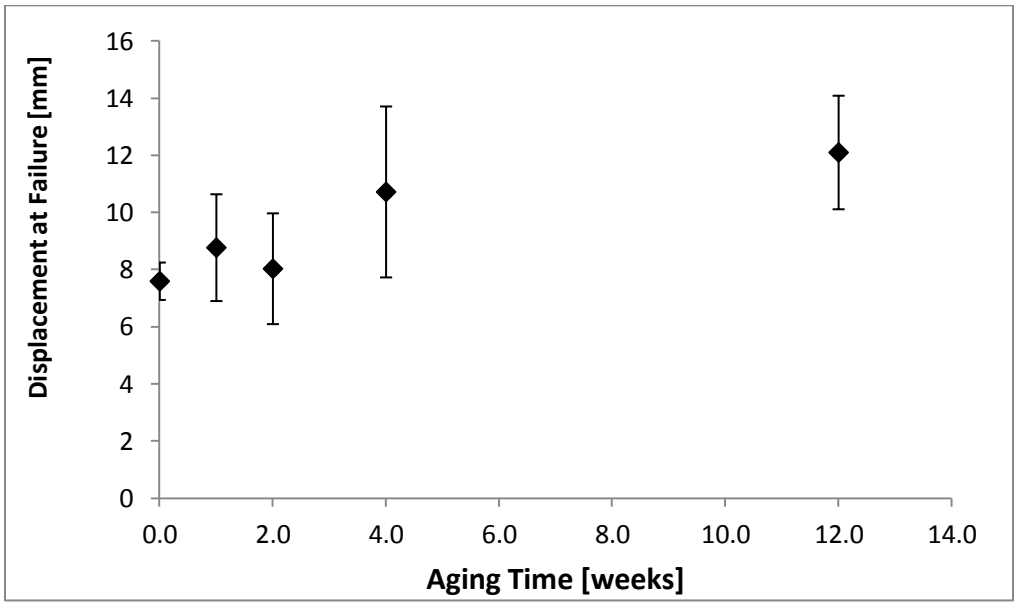

Figure 4.5: Displacements at failure of aged resin specimens as a function of aging time with 1 σ error bars.

Five unidirectional composite rod specimens were tested for their flexural strength for each aging condition. **Figure 4.6** and **Figure 4.7** show the loads and mid-span deflections at failure as a function of aging time. Unlike in the neat resin specimens, it can be seen that as aging time increased the load to failure also increased in the composite rod specimens (**Figure 4.6**). For the specimens aged for one month, the loads to failure increased by about 11%. There was also a substantial increase of mid-span deflection for specimens aged up to one month, as seen in **Figure 4.7**.

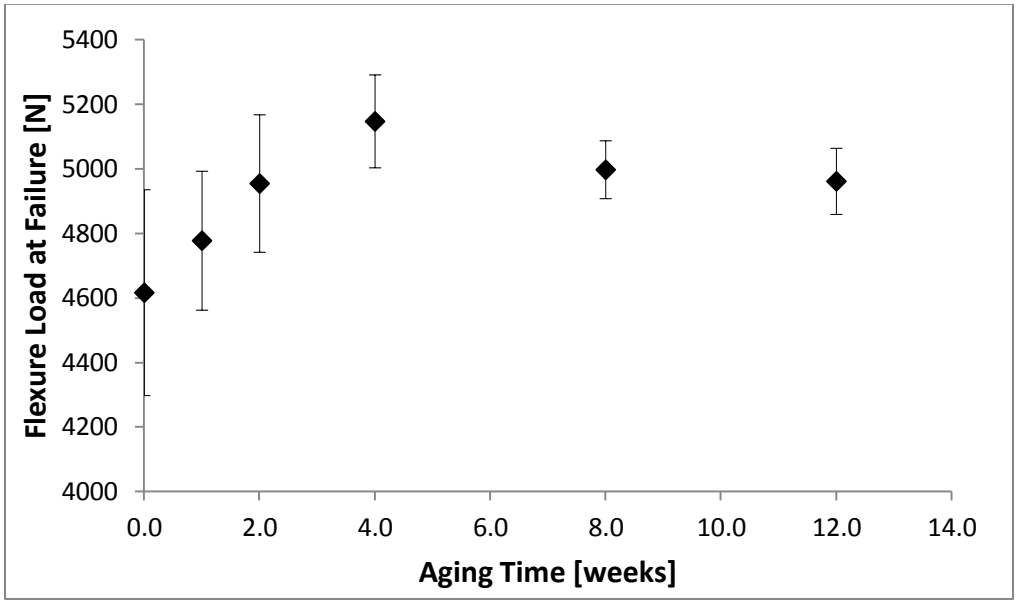

Figure 4.6: Loads at failure for aged ACCC rods as a function of aging time with 1 σ error bars.

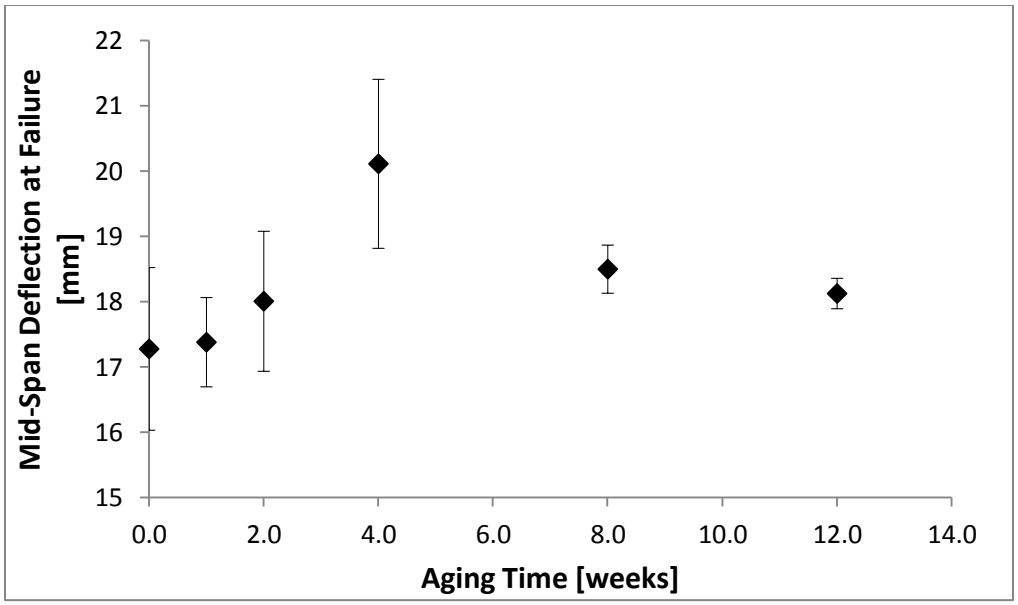

Figure 4.7: Mid-span deflections at failure for aged ACCC rods as a function of aging time with 1 σ error bars.

A good measure of aging of the polymer is the change in the damping of the material, or tan δ (105). The tan δ is defined by tan δ = E''/E' where E'' is the loss modulus and E' is the storage modulus. The storage and loss moduli for the aged neat resin specimens as a function of frequency are shown in **Figure 4.8** and **Figure 4.9**, respectively. The change in the damping of the neat resin as a function of temperature and aging time can be seen in **Figure 4.10** when the T_g peak areas are analyzed.

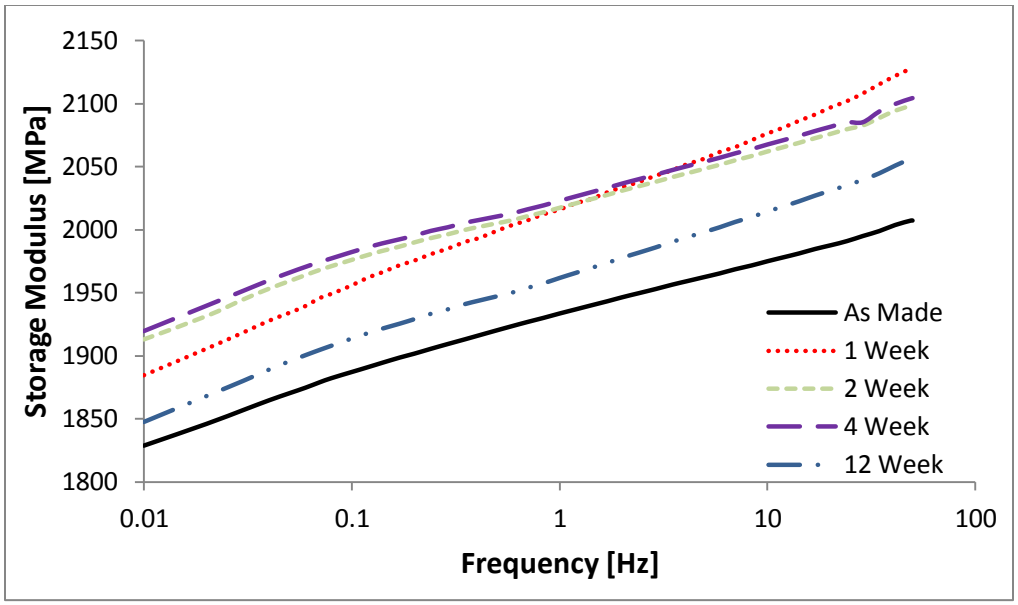

Figure 4.8: Storage modulus of aged resin for varying aging times as a function of frequency.

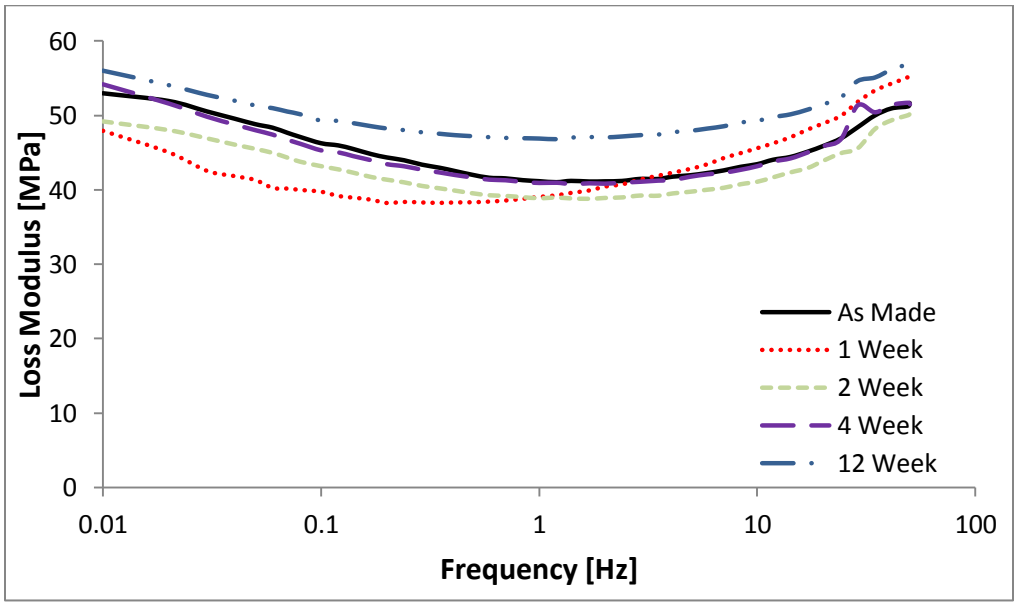

Figure 4.9: Loss modulus of aged resin for varying aging times as a function of frequency.

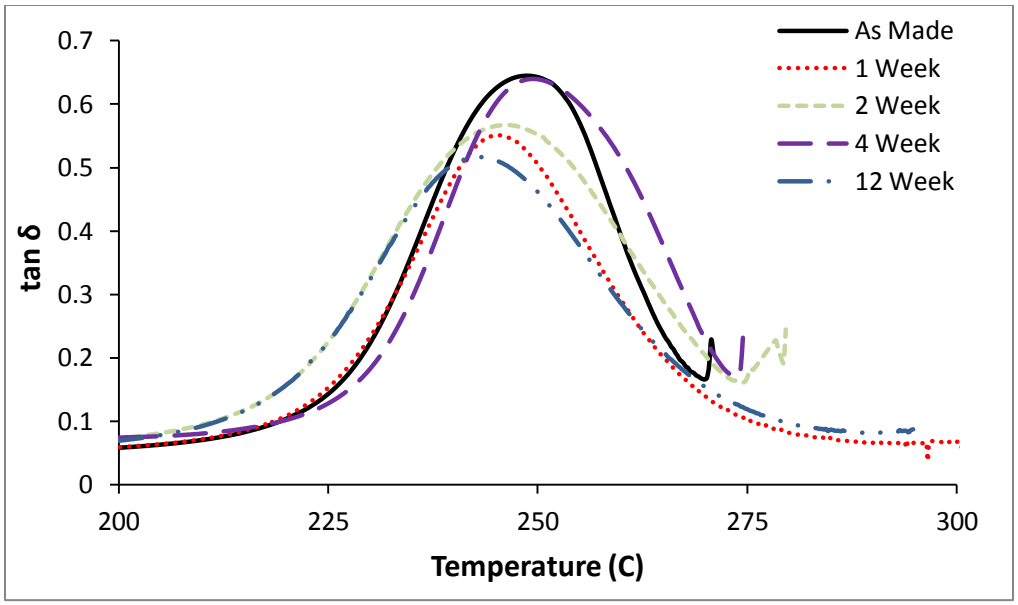

Figure 4.10: Damping (tan δ) of aged resin for varying aging times as a function of temperature at 1Hz.

4.5 Glass Transition Temperature

Figure 4.11 shows T_g as a function of aging time for the neat resin specimens. The uncertainty in **Figure 4.11** represents the uncertainty in the measurements. Since the T_g values for up to one month were all within the uncertainty, the effect of ozone on T_g within this time period can be assumed to be insignificant. This is evident by the fact that after three months of ozone exposure, only a 3% reduction in T_g was observed. The peak of the tan δ curve was chosen as T_g, following [4].

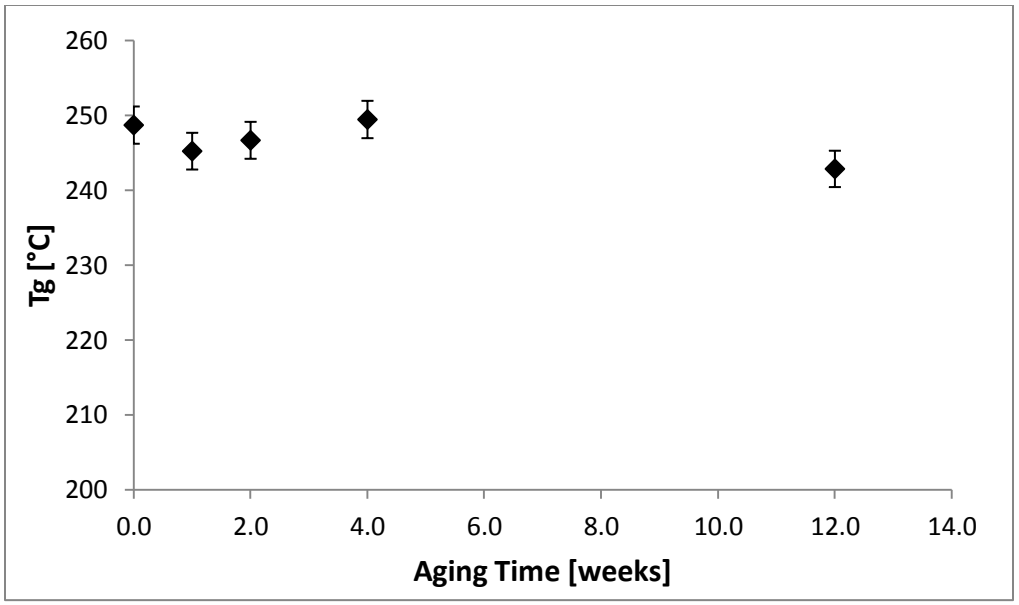

Figure 4.11: Tg as a function of aging time for neat resin specimens.

4.6 FTIR ANALYSIS

The impact of ozone on the neat resin samples is evident in the FTIR spectra shown in **Figure 4.12** and **Figure 4.13** following only one week of exposure. The bands in the 1000-1050 cm^{-1} region shown in **Figure 4.12** typically contain ozonides, esters, and ethers. Contributions from esters and ethers can also be observed between 1100-1300 cm^{-1}. Between 1620-1670 cm^{-1} unsaturated carbonyls and aromatic carbonyls are typically found [31, 106].

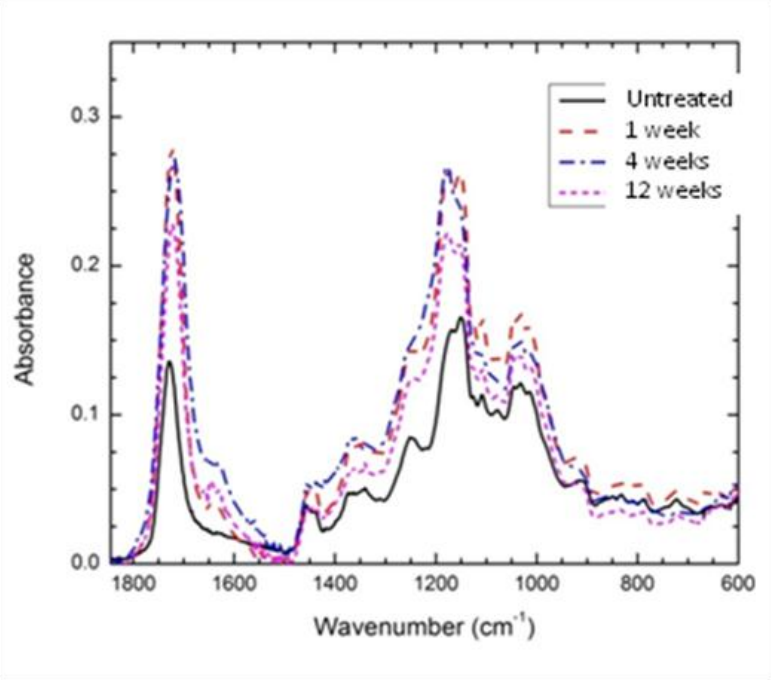

Figure 4.12: FTIR spectra of aged neat resin samples for varying time lengths.

The band at 1725 cm^{-1} may include contributions from ketones, aldehydes and aliphatic esters. Increase in the –OH stretching region is also observed (**Figure 4.13**) at 3250 cm^{-1} (carboxylic acids, phenols, and hydroperoxides) and 3450 cm^{-1} (alcohols and phenols) [107].

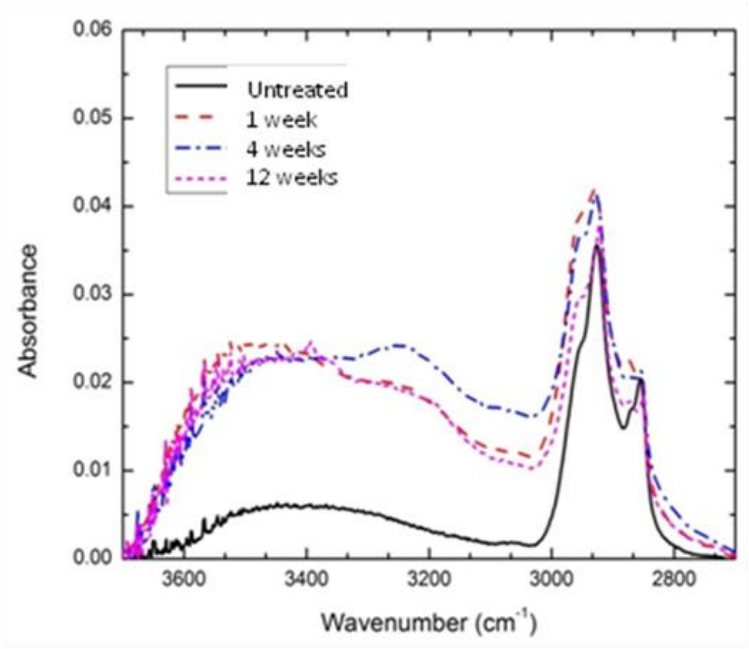

Figure 4.13: FTIR spectra of aged neat resin samples for varying time lengths.

While similar chemical changes were observed for the composite rods, absorbance increases continued after one week of exposure (**Figure 4.14** and **Figure 4.15**). Some variations in the spectra of the rods may be due to non-reproducibility in positioning the curved surface of the rod on the attenuated total reflectance crystal. An attempt was made to minimize these differences by normalizing to the symmetric -CH stretch, because this region showed little change in the neat resin samples. Other differences between the composite rod and neat resin samples (i.e. the more pronounced peak between 900-950 cm^{-1} in the rods) may be due to different additives and the presence of glass fibers in the rod samples. Both types of specimens showed maximum changes for two weeks and one month of ozone exposure.

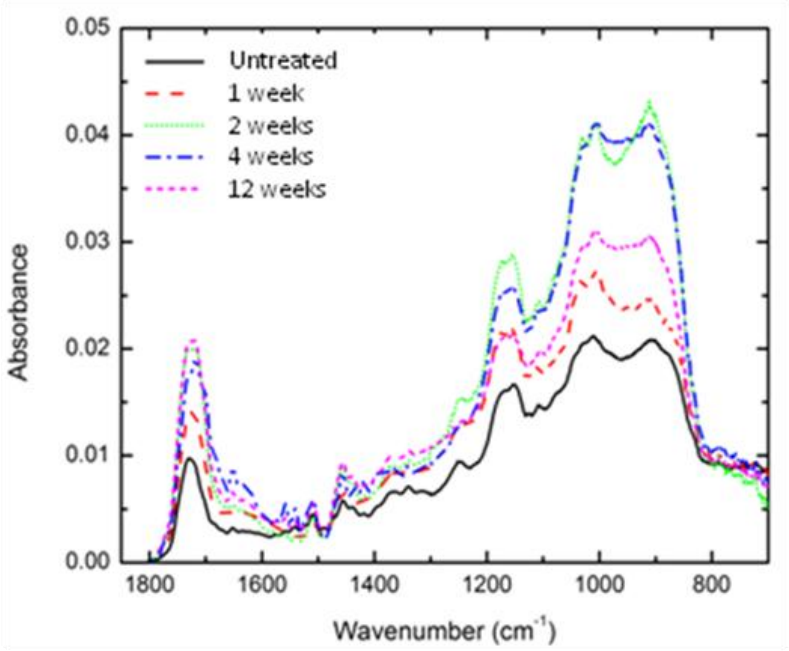

Figure 4.14: FTIR spectra of an aged composite rod for varying time lengths.

Ozone reacts with unsaturated aliphatic compounds resulting in the development of ozonides [108]. Evidence for ozonide formation can be seen as the increase in the bands between 1000 and 1050 cm^{-1}. Eventual decomposition of the ozonides should result in cleavage at the position of the double bond, potentially forming ketones, aldehydes, and carboxylic acids (1725 cm^{-1}, 1620-1670 cm^{-1}, and 3250 cm^{-1}, respectively shown in **Figure 4.14** and **Figure 4.15**).

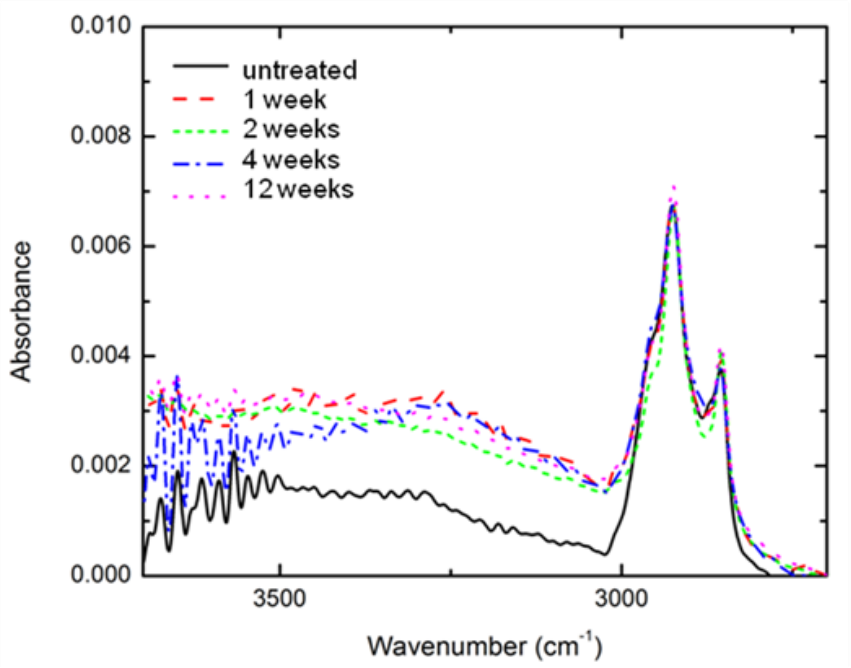

Figure 4.15: FTIR spectra of an aged composite rod for varying time lengths.

Ozone reacts with saturated hydrocarbons significantly slower at room temperature. This reaction yields peroxides, ketones, aldehydes, alcohols, and acids [109]. Regardless of whether the site of initial ozone attack is an aliphatic double bond, an aromatic double bond or a saturated aliphatic chain, the growth of peaks indicative of carbonyls and carboxylic acids suggest ozone exposure results in scission events.

4.7 Overall Effect of Chemical Changes on Mechanical Properties of Neat Resin and Composite Rod Specimens

The data presented in this work clearly demonstrate that the overall resistance of the neat resin and the rod composite specimens to 10,000 ppm ozone exposure for up to three months was high considering the very strong oxidizing nature of the aging environment. Surprisingly, no catastrophic effects in the neat resin and composite rod's behavior during bending tests were observed. Moreover, the neat resin and rod specimens exhibited similar behavior in response to ozone exposure. Also, the FTIR spectra of the unaged neat resin and rod samples were found to be comparable. The broadening of the spectrum at about 800 cm^{-1} to 1100 cm^{-1} can be explained by the presence of glass fibers. Therefore, one of the possible conclusions from this work is that the polymer systems (epoxy and hardener) in the neat resin and the composite specimens are quite similar. Going further, it could be suspected that the B type epoxy monomer was used in the rod manufacturing.

The slight increase in the loads to failure and in the displacement to failure of both the resin and rod specimens could be explained by two competing factors: the crosslinking of the epoxy chains and their subsequent scission. The initial increase in storage modulus can be attributed to an increase in crosslink density [50]. On the other hand, the increase in displacement at failure and a drop in the loads at failure for longer exposure times can be explained by chain scission. The evidence of polymer degradation by chain scission is clearly corroborated by the FTIR analysis showing an increase in

absorption around the 3500 cm^{-1} wavenumber associated with the formation of carbonyls and carboxylic acids.

The two competing mechanisms of crosslinking and chain scission can also be observed in the viscoelastic data for the neat resin specimens. For the first week of aging, the crosslinking mechanism dominated, thereby creating a smaller value for tan δ. However, after one week the chain scission mechanism started becoming dominant. Evidence of this can be seen particularly well in **Figure 4.8**, where initially there is a significant increase in the storage modulus, and a decrease in the loss modulus (**Figure 4.9**). This effect is also evident in **Figure 4.10**, where the T_g peak area initially decreases after one week and then increases to a maximum at four weeks. After twelve weeks the peak area decreases again. This decrease could indicate a radical change in the polymer structure.

As the chains break, free volume and chain mobility increase allowing for greater deflection to failure. After one to two weeks of aging for the neat resin, and about one month for the rod specimens, chain degradation and scission had increased to an extent that the specimens started losing their strength. The effect of chain scission has been studied numerically by Stowe *et al.* (110). Using Molecular Dynamics they showed that the stiffness of a high density polyethylene rapidly decreased with the amount of chain fragmentations by scission.

Another very important comment needs to be made here: the testing conditions selected were very aggressive. The 1% ozone concentration could be possible on a HV

transmission line, but not necessarily for long periods of time. Therefore, the fact that the resin tested in this research was found to be so resistant to highly concentrated ozone should be good news for the rod manufacturers. On the other hand, the PCC conductors have been designed to work under high temperature conditions. Under those conditions, ozone is not stable and dissociates into atomic oxygen and O_2 [42]. So, caution should be observed when attempting to extrapolate the data presented in this research to the combined HT and high ozone concentration in-service situations.

4.8 CONCLUSIONS

Aging of a moderately HT epoxy in 1% ozone for up to three months created two competing mechanisms, namely crosslinking and chain scission. Initially, in exposures of up to one week, the crosslinking mechanism dominated, resulting in an increase in the load to failure of the resin under three point bending, and a slight stiffening of the polymer. As aging continued the chain scission mechanism becomes dominant, initially causing an increase in deflection to failure. However, at some point, the chains of the epoxy were damaged so much by scission that they could no longer bear as much load, resulting in a reduction of the load at failure. The PCCC rods exhibited similar mechanical behavior as seen in the resins after aging in 1% ozone. The loads and deflection at failure of the rods were found to increase under four point bending with increasing aging time up to one month. This was attributed to the matrix material's ability to bear more load, caused by an increase in crosslinking. However, contrary to the neat

resin behavior, only small reductions in the loads and displacements at failure of the rods were observed at 3 months aging time. This might suggest that the scission mechanism was hindered by the inert glass fibers on the surface of the composite specimens. The viscoelastic and FTIR analyses performed on the epoxy resin as a function of aging further corroborated the presence of the transition from crosslinking to chain scission as the dominant mechanism. Most importantly, both the epoxy and the rods were found to be quite resistant to aging in 1 % ozone at room temperature for up to three months.

CHAPTER 5: AGING OF NEAT RESIN AND PCCC IN ATMOSPHERIC HIGH TEMPERATURE

5.1 INTRODUCTION

This section presents the results of aging the neat resin and the PCCC rod in atmospheric high temperature. There were two temperatures chosen: 140 and 180°C. These reason for the temperatures chosen was previously discussed (section 3.2), but briefly they are low enough to be below the glass transition temperatures, but high enough to cause accelerated aging. The aging was conducted in atmosphere and not under vacuum in order to be more representative of in-service conditions. This chapter is broken up into sections based on the hybrid composite rods, and then on the neat resin.

5.2 AGING OF THE HYBRID COMPOSITE RODS

Temperature had a dramatic effect on the flexure strength of the hybrid composite rods. It can be seen from **Figure 5.1** that aging specimens in atmosphere at 140°C had no detrimental effect, even after a full year of aging. In fact, the load showed a slight increase due to slight post curing. **Figure 5.2** and **Figure 5.3** show the displacement at

failure and the flexural modulus respectively. It can be seen from these figures that aging at 140°C had very little effect. The displacement at failure showed a very slight increase, as did the flexural modulus. Atmospheric 180°C albeit, showed a dramatic decrease in load at failure. With only three months of aging, there already was a measurable decrease in load at failure. After a full year of aging in atmospheric 180°C, there was about a 75% reduction in flexure load at failure. The displacement at failure showed a large reduction as well of a little over 50%. This trend continued with the flexural modulus, although even less dramatic than the displacement at failure. After 1 year of aging at 180°C, the modulus only showed about a 15% reduction.

With increasing temperature, physical aging is increased, and therefore the amount of reduction in free volume is greater. This reduction in free volume increases the residual stresses in the hybrid composite rods (see section 3.2). In other words, at higher temperatures the hybrid composite rod is in a higher state of stress, thereby weakening the composite rods and reducing the flexural strength. On a micro level it is possible that the stress is high enough to create micro cracks and even fiber matrix debonding. The debonding of the fibers could be the reason that there is an observed drop in stiffness.

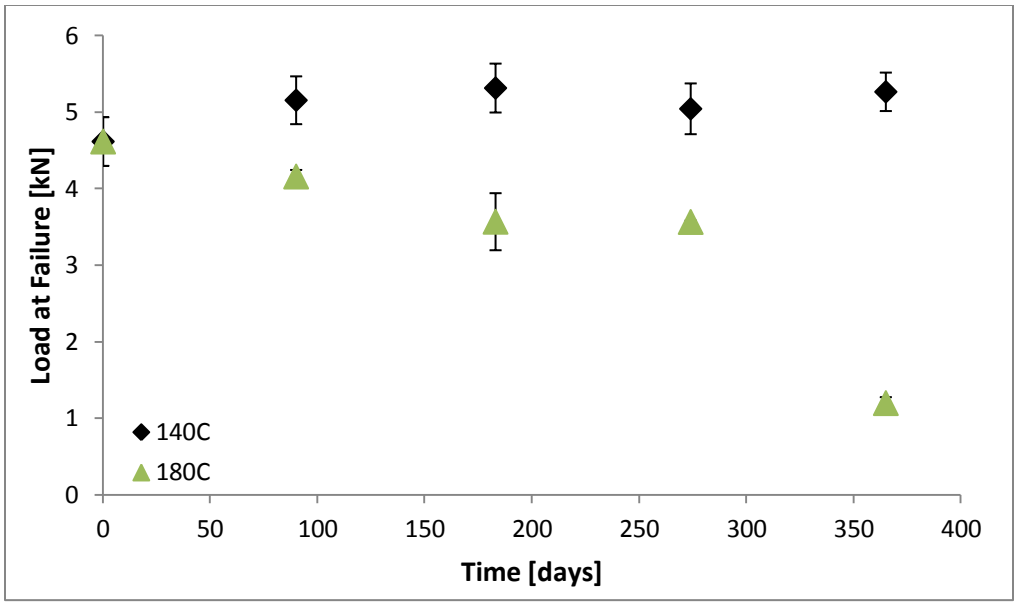

Figure 5.1: Load at failure of hybrid composite rods in 4 point flexure as a function of aging time.

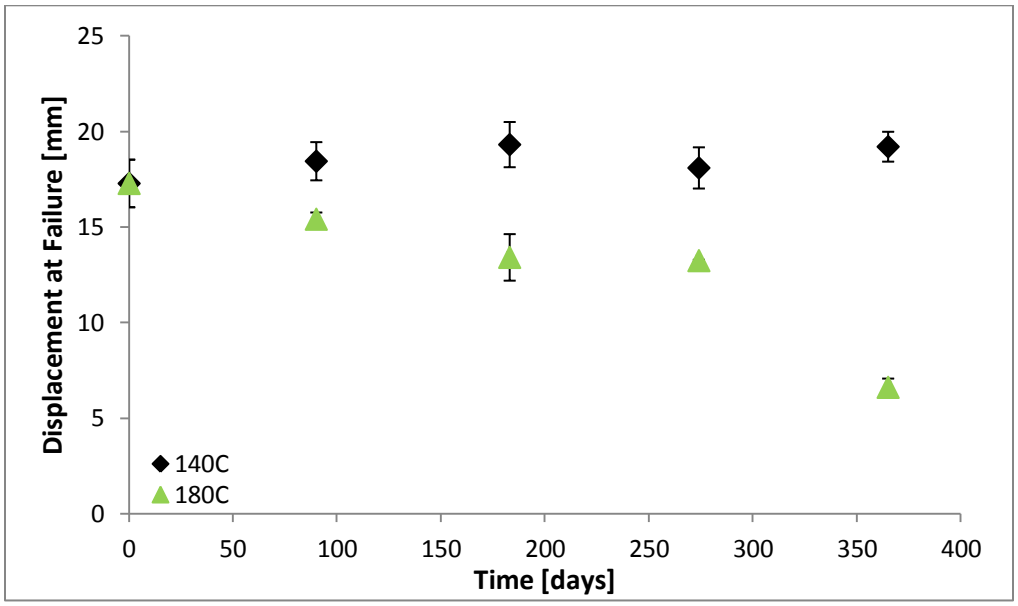

Figure 5.2: Displacement at failure of hybrid composite rods as a function of aging time.

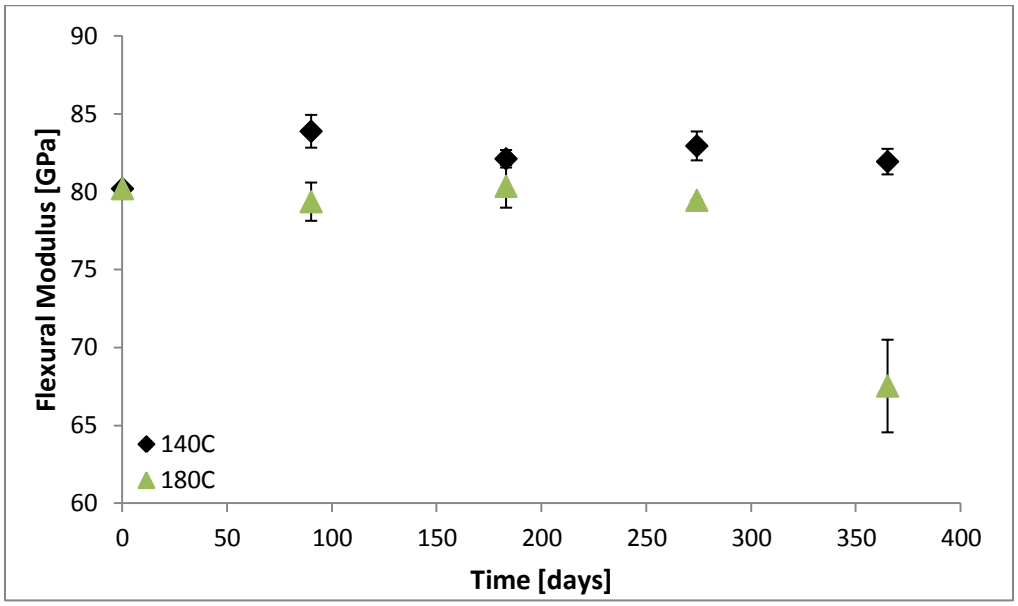

Figure 5.3: Flexural modulus of hybrid composite rods as a function of aging time.

Aging of the hybrid composite also revealed a significant amount of post curing due to unreacted constituents. This is a result of the pultrusion process used to manufacture the hybrid composites. Pultrusion is a process in which tows of fibers are pulled through a resin bath into a die where the composite is shaped. After exiting the die, the composite is cured along a long oven starting at a high temperature and ending at a low temperature (i.e. RT). Pultrusion has relatively short curing time lengths to make it viable for mass production in industry, but can leave the matrix of the composite under cured. Therefore when the composite is aged in high temperature, curing of the unreacted constituents occurs resulting in an increase in strength and stiffness due to better fiber/matrix interactions. This can be seen in **Figure 5.1** where the load at failure

increases for specimens aged at 140 ^{o}C. Aging at a temperature of 180^{o}C on the other hand, accelerates aging of the hybrid composite rod to the point where, within 3 months, physical aging is the dominant mechanism. This results in the observed slight reduction in load at failure and stiffness.

Aging of polymers can result in oxidation (as previously discussed) which can be detrimental to the composite. Its progression over time is important to characterize, and therefore was studied as a function of aging time. For this study, the oxidation created after aging at both 180 and 140°C was characterized using dark field microscopy. The composites were cut using a Buehler wafering blade, then put into a potting epoxy and cured for 24 hours at RT. The specimens were then polished down to a 0.05 μm finished and inspected using an Olympus BX51M Microscope and D.E. Light software. Dark field photomicrographs were taken which allow a distinct oxidation layer to be seen. The thickness of the oxidation layer was then measured. The results for specimens aged at 180 ^{o}C were done in a previous study by Burks *et al.* [85].

The dark field photomicrographs revealed the transverse oxidation was self-limited **Figure 5.4**. The photomicrographs show that the progression of the oxide layer was consistent with literature [38]. The self-limiting process can be seen in **Figure 5.4** as up to 9 months of aging shows a continual observable increase in oxidation. However, between 9 and 12 months there is no observable difference in oxidation layer thickness. It should be noted here albeit; the measurement of the oxidation layer was inexact due to the glass fibers becoming loose on the surface due to thermal oxidation after aging. Thus, the edge becomes obscure, requiring an estimation of the oxidation layer, and not an

exact measurement. This suggests that the matrix is being lost at the surface of the hybrid composite rods. **Figure 5.5** shows scanning electron microscopy (SEM) micrographs of aged specimens. It is clear from the SEM micrographs that there is a substantial amount of matrix being lost at the surface of the aged hybrid composite rods. The actual amount of polymer lost was not measured in the study by Burks, but from a qualitative stand point, with increasing aging time, more polymer matrix was lost, and therefore more glass fibers exposed [14].

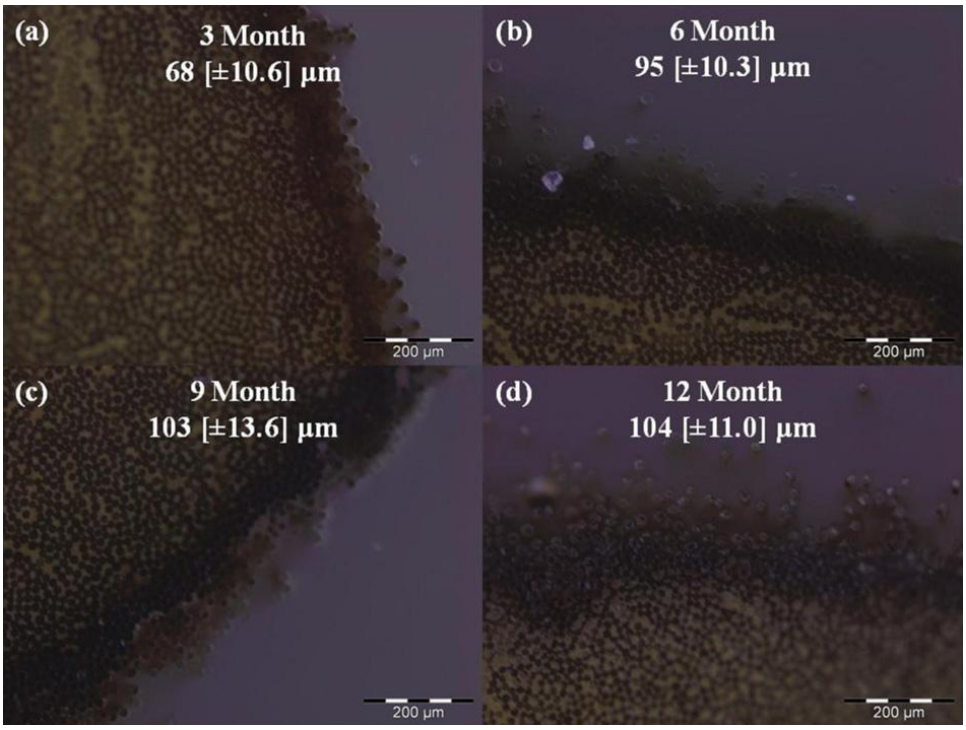

Figure 5.4: Dark field micrographs showing the oxidation layer of A180C specimens aged for (a) 3 months (b) 6 months (c) 9 months and (d) 12 months. The dark layer between the potting epoxy and the bulk composite is the oxidation layer with mean [± standard deviation][10].

[10] From [87]

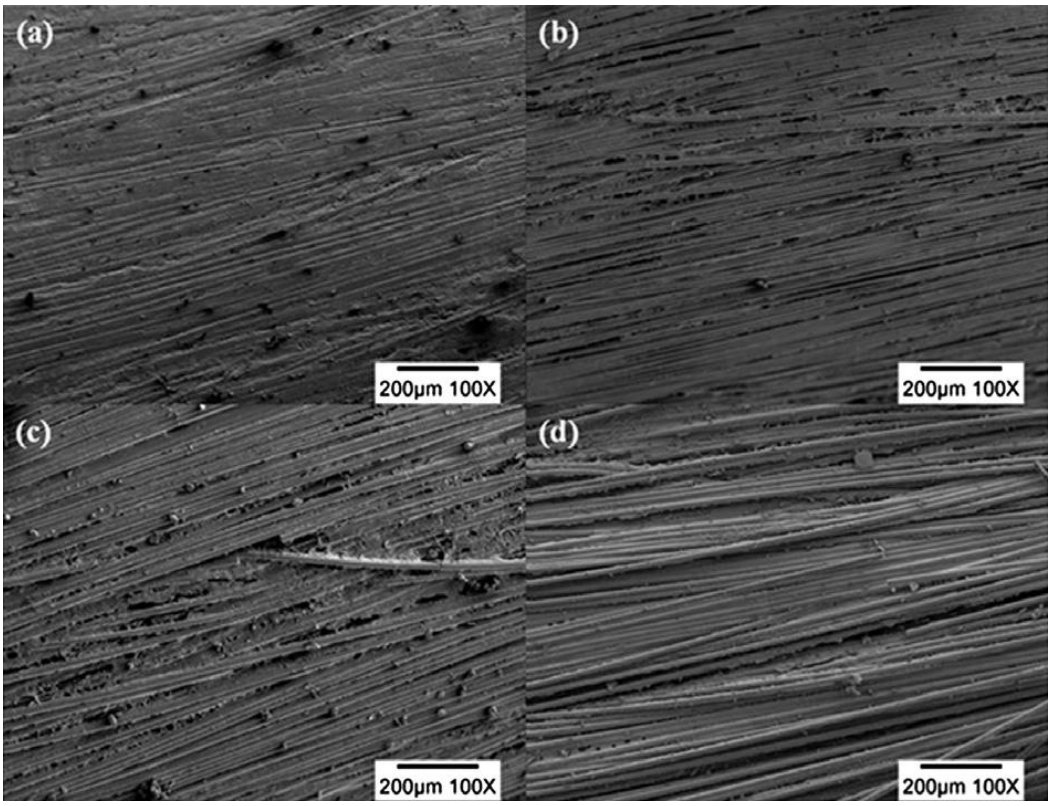

Figure 5.5: SEM surface micrographs of A). 0 months, B). 3 months, C). 6 months and D). 12 months aged hybrid composite rods[11].

Hardness testing was performed using a Rockwell Hardness Tester on specimens aged at 180°C. Due to the cylindrical geometry of the specimens, a fixture was manufactured to ensure the indenter made contact with the specimen's apex (**Figure 5.6**). A 3.175 mm indenter was used and the preload was applied for two minutes to account for the viscoelastic nature of the polymer matrix. The final load was then applied, and the measurement was taken.

[11] From [87]

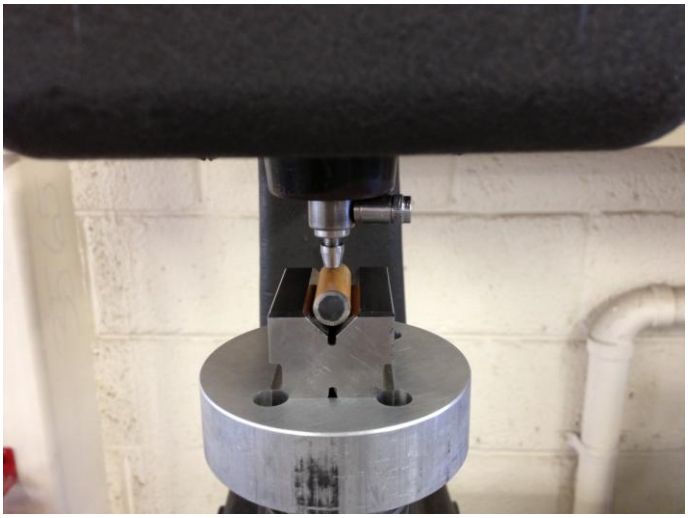

Figure 5.6: Schematic of hardness test set up. The cylindrical aluminum cap was designed to house a V-block and be placed over the built in stage.

The hardness of the hybrid composite rods showed an initial decrease after aging for seven days, but showed no conclusive trend at longer aging times (**Figure 5.7**). As aging time increased, as already discussed, the matrix at the surface began to disappear. This made measurements of hardness difficult, because at longer aging times more and more fibers became exposed (**Figure 5.4**). As more fibers became exposed, less and less matrix was present during the test. Therefore hardness tests were performed on exposed fibers more than the aged matrix, yielding erroneous data. This would help explain why no conclusive trend could be found.

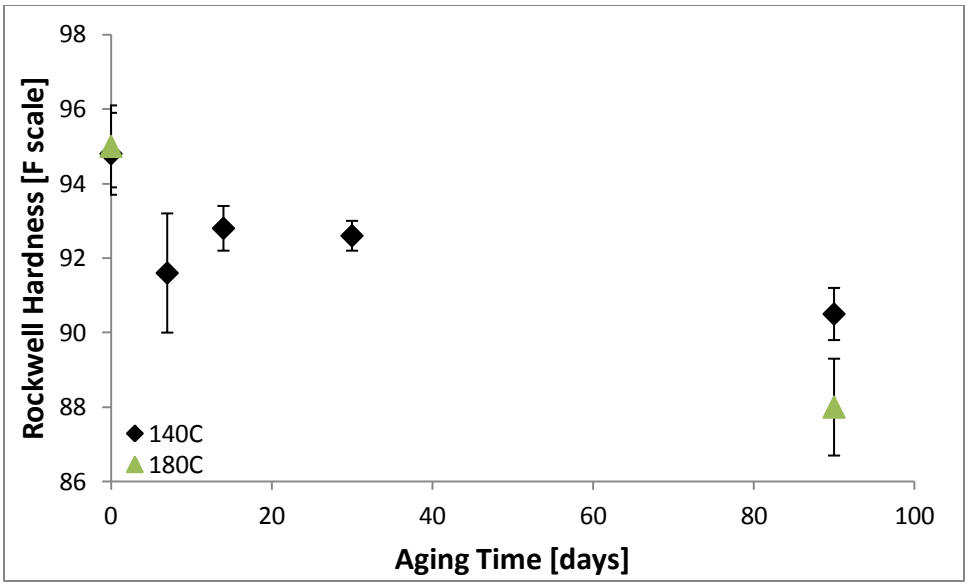

Figure 5.7: Rockwell hardness of hybrid composite rods aged in high temperature.

The dimensional relaxations of the hybrid composite rods were performed earlier in a different study by Burks and Kumosa [85]. Essentially, the transverse dimensional relaxation was measured using a Netzch© 402C dilatometer. The relaxations of the hybrid composite rod are associated with the polymer matrix and not the fibers; therefore the transverse relaxation was measured. The specimens were first heated to 240^{o}C, which is approximately 15^{o}C above T_g, to erase any previous thermal history. Next the specimens were cooled at a rate of 5^{o}C/min to the specified isothermal temperature and held for 500 hrs. For the first 60 minutes, 2 data points per minute were collected, and for the remainder of the aging time a data point was collected once every two minutes.

Relaxation curves were fit using equation 3.19 in Section 3.7, using a non-linear least squares regression and can be seen in **Figure 5.8**. The relaxation increased with increasing isothermal temperatures. A β of 0.58 was found to describe each relaxation

curve well, indicating that the hybrid composite rod could be treated as thermorheologically simple. The activation energy of the aging process was found to be 130.5 kJ/mol.

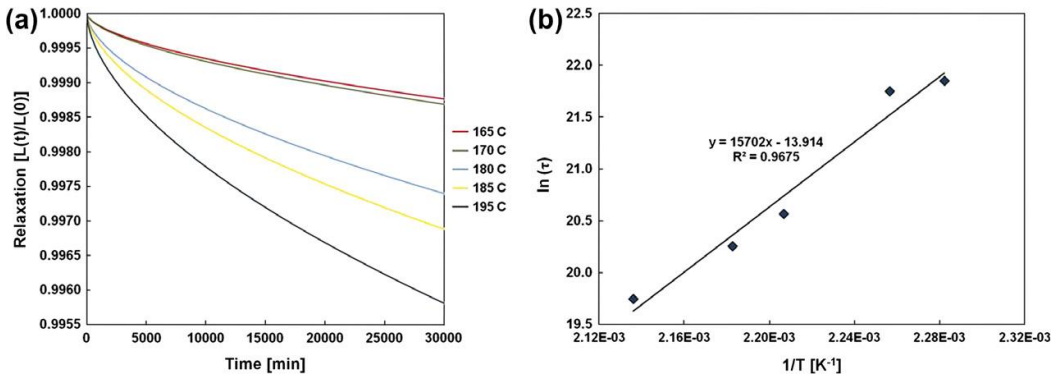

Figure 5.8: (a) Dimensional relaxations curves for various isothermal aging temperatures and (b) linearized Arrhenius plot for activation energy determination.

5.3 Aging of the Neat Resin

The impact of isothermal aging temperature on the neat resin is apparent in **Figure 5.9**. After ninety days of aging the flexural load was reduced over 20% for specimens aged at 140°C, and over 60% for specimens aged at 180°C. After the initial reduction in load at failure, there was no subsequent reduction up to three months of aging for specimens aged at 140°C. Aging at 180°C on the other hand showed a large decrease initially, then a general decrease in load at failure for longer aging times. The displacement at failure showed a large initial decrease for both aging temperatures at the first aging time (**Figure 5.10**). At the next aging time length (14 days), 180°C showed another decrease in displacement at failure, but specimens aged at 140°C did not. This

could be because 140^{o}C is a low enough temperature that the oxidation process is slower, and more time was required to further oxidize and therefore embrittle the polymer. This is evidenced by a reduction in displacement at failure at the next aging time length. However, after one month of aging, the self-limiting oxidation process has reached its asymptotic behavior, and the displacement at failure was not further reduced for specimens aged at 140^{o}C. The oxidation process is faster for specimens aged at 180°C due to the proximity to the activation energy at this temperature. This means it only required fourteen days of aging to reach asymptotic behavior, and no further reductions in displacement were observed.

Despite being put through a rigorous cure cycle, there is evidence of post curing which can be seen in **Figure 5.11**. An increase of the modulus is indicative of post curing. In **Figure 5.11**, there is a modest increase in flexural modulus up to one month of aging at 180^{o}C. After one month of aging at 180^{o}C, there is no more evidence of post curing. This is the opposite of what occurred in specimens aged at 140^{o}C. At 140^{o}C, there is no observable post curing occurring during the first two weeks of aging. Only at one month of aging does the process of post curing appear to happen. This continues up to three months of aging where there is another increase in flexural modulus. Again, 180°C is closer to the activation energy than 140°C, thus the slower start to post curing in the specimens aged at lower temperatures.

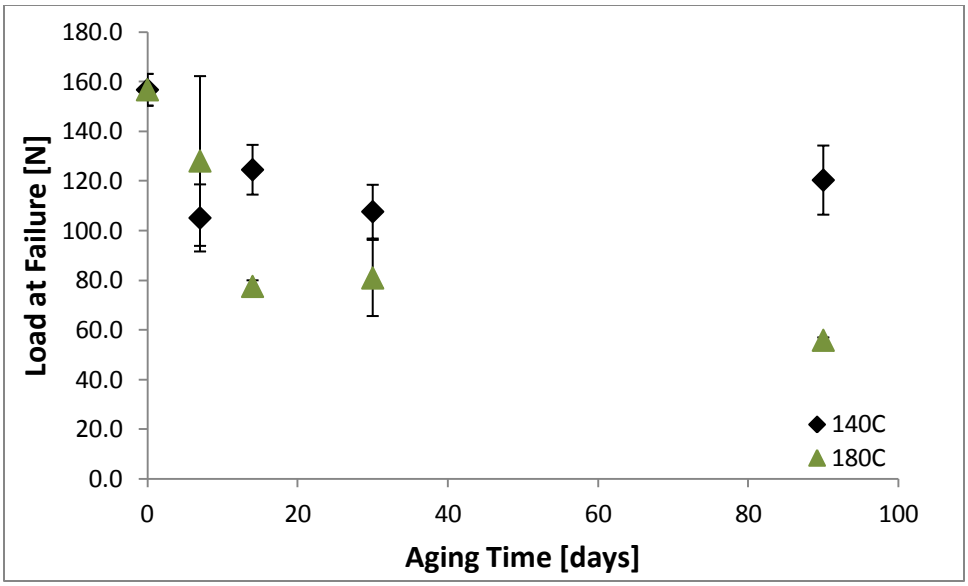

Figure 5.9: Load at failure of aged neat resin specimens with ±σ.

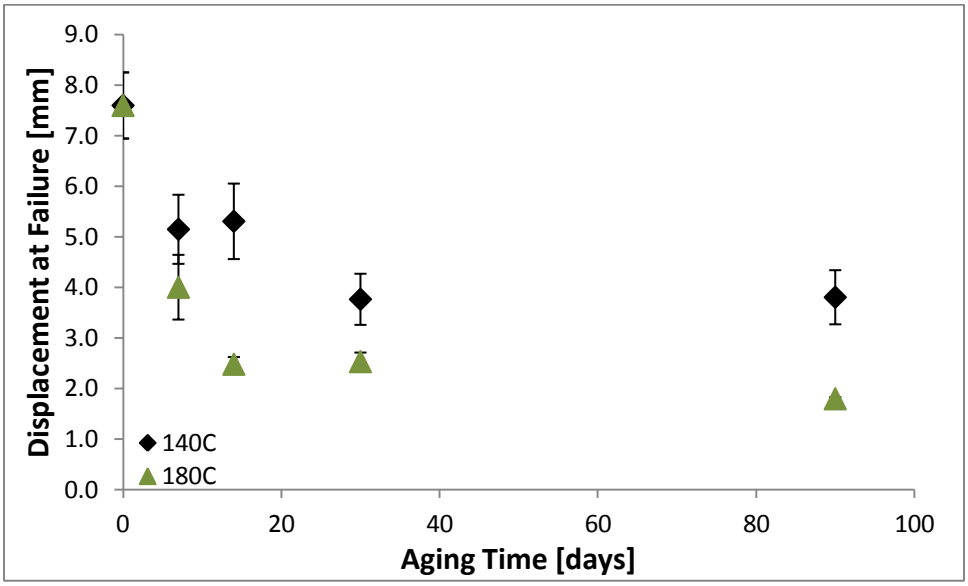

Figure 5.10: Displacement at failure of neat resin specimens aged at high temperature with ±σ.

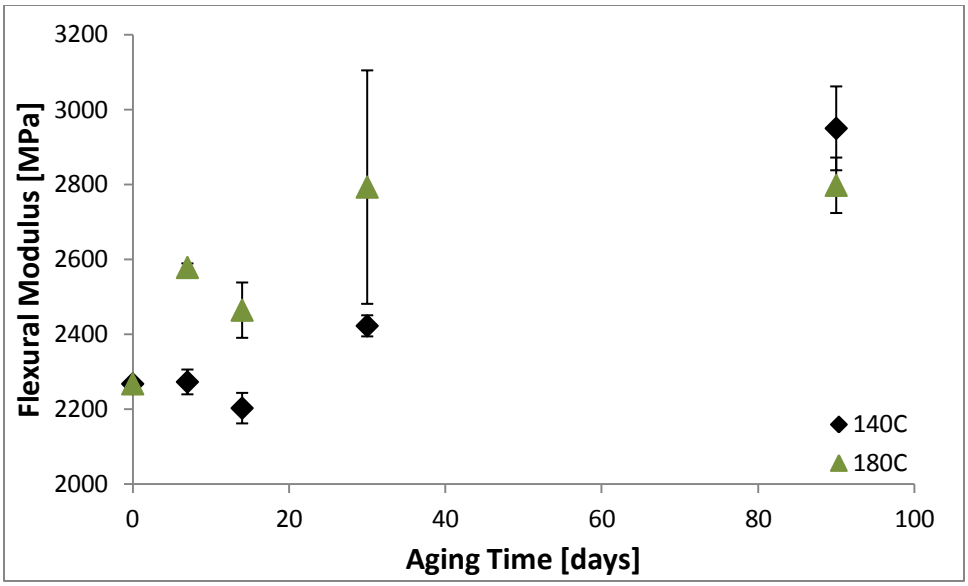

Figure 5.11: Flexural modulus of neat resin aged at high temperature with ±σ.

5.4 CONCLUSIONS

The aging in atmospheric high temperature of 140°C and 180°C of a polymer core composite conductor and neat resin was performed. At the higher temperature, the reduction to load at failure was greater. In fact, after a full year of aging the flexural load at failure was reduced by 75% for the composite rod when aged at 180°C. When aged at 140°C, there was post curing present and the load was not reduced at all for the hybrid composite rod. Thermo-oxidation was shown to reduce the amount of resin on the surface of the hybrid composite rods, in turn creating loose fibers on the surface for specimens aged at 180°C. This was shown through photomicrographs and confirmed through scanning electron microscopy. Aging also resulted in a reduction of hardness of the hybrid composite rods after the initial aging time. However, it was difficult to

characterize hardness at longer aging times due to the fibers being exposed on the surface. The activation energy was found through the use of dimensional relaxations and was found to be 130.5 kJ/mol. The neat resin was put through a rigorous cure cycle and post curing was minimal. Therefore, only after three months of aging at 180°C the neat resin load at failure was reduced by over 60%. Aging the neat resin at 140°C only had a moderate effect which reduced the load at failure by a little over 20% after three months of aging.

CHAPTER 6: THE COMBINED EFFECT OF HIGH TEMPERATURE AND OZONE

6.1 INTRODUCTION

In this section the results for specimens aged in 1% ozone at 140^{o}C are presented. For clarity and comparison, specimens aged in 1% ozone at RT, atmospheric 140^{o}C, and atmospheric 180^{o}C are included in the results. For specifics on how the specimens were aged please see Section 3.2, but briefly specimens were aged in an oven for the appropriate time length. The specimens were not under vacuum, but in atmospheric conditions. As with the last section, this section will be broken up into sections based on the hybrid composite rods, and then the neat resin. From this section on, for ease the aging conditions will be designated as seen in **Table 3**:

Table 3: Aging condition designations

Aging Condition	Designation
As Made (Unaged neat resin)	AM
As Received (Unaged hybrid composite rods)	AR
1% Ozone at RT	1ORT
Atmospheric 140^{o}C	A140C
1% Ozone at 140^{o}C	CE140C
Atmospheric 180^{o}C	A180C

6.2 HYBRID COMPOSITE RODS

6.2.1 MECHANICAL PERFORMANCE OF THE HYBRID COMPOSITE RODS

The hybrid composite rods showed significant postcure after aging. This can be seen from **Figure 6.1, Figure 6.2,** and **Figure 6.3**. The flexure loads at failure, mid-span deflection and flexural modulus all increase with increasing aging time, except for the A180C specimens tested after ninety days. This is due to postcure of unreacted constituents resulting from pultrusion. To make manufacturing viable for commercial use, pultrusion employs fast curing times at high temperature which can lead to a non-fully cured matrix. Therefore, as the composite rods are aged at elevated or high temperatures, postcure is taking place, potentially allowing for better fiber/matrix

interfaces. This results in more efficient load transfer between the matrix and the fibers producing a stronger and stiffer composite.

The A180C specimens showed a slight decrease in mechanical performance after ninety days of aging because the aging temperature was very close to the composite rod's T_g (205°C). Therefore, at this temperature aging was highly accelerated, and within ninety days the composite rods went through complete postcure and started to degrade by both physical and chemical aging. Volumetric shrinkage led to greater internal stresses decreasing the mechanical properties of the composite [85].

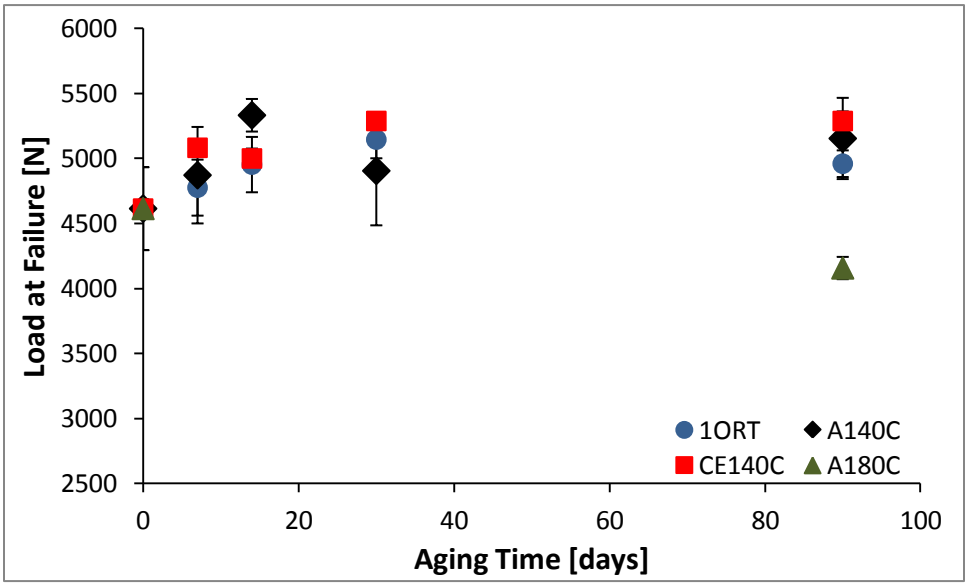

Figure 6.1: Load at failure of hybrid composite rods as a function of aging time with ± 1 σ.

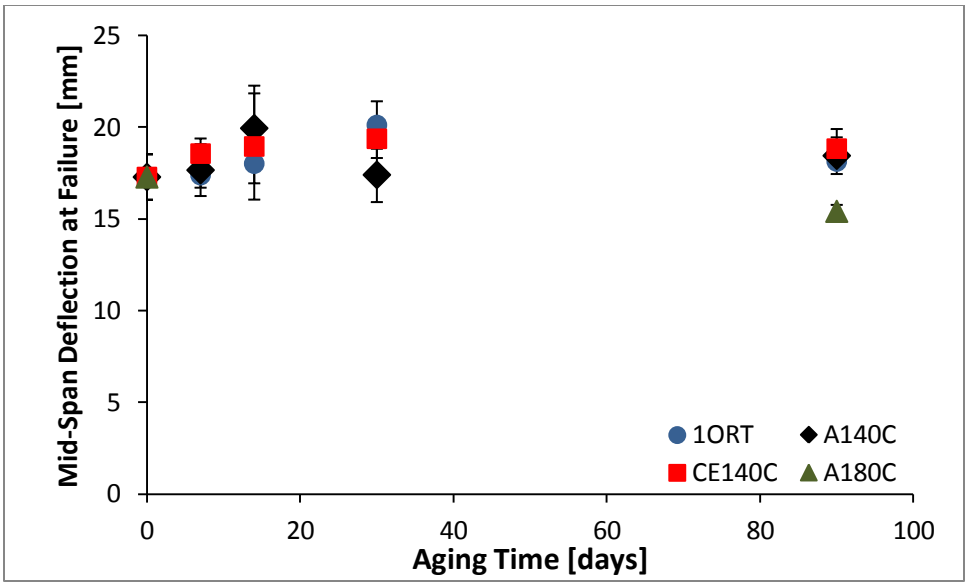

Figure 6.2: Mid-span deflection of hybrid composite rods as a function of aging time with ± 1 σ.

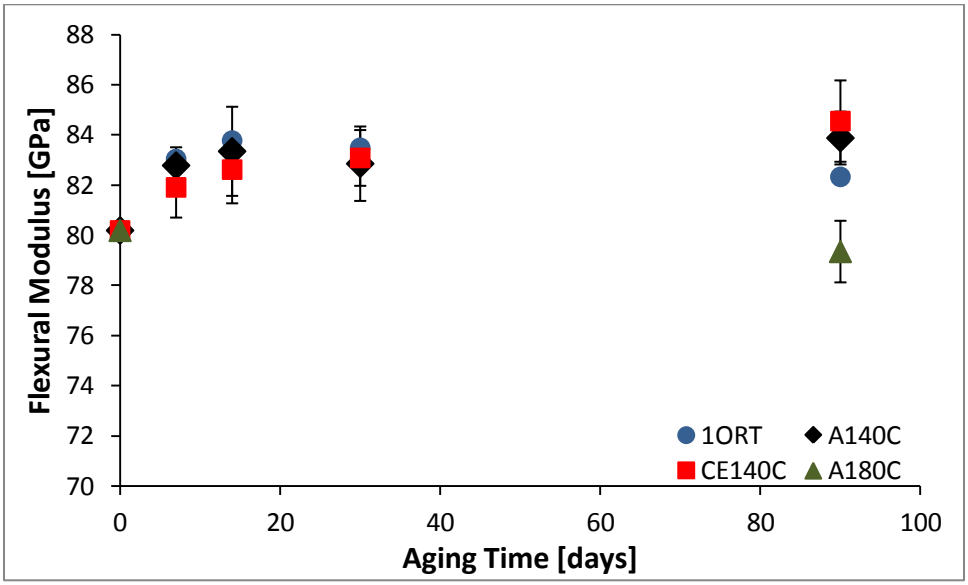

Figure 6.3: Flexural modulus of hybrid composite rods as a function of aging time with ± 1 σ.

6.2.2 OXIDATION OF THE HYBRID COMPOSITE RODS

Evidence of oxidation was very limited in all specimens except for the A180C specimens which have been already discussed. In **Figure 6.4** there is no apparent oxide layer in the photomicrographs of aged specimens, which is apparent in specimens aged at 180°C (**Figure 5.4**). The only evidence of oxidation is the surface discoloration observed from A140C, CE140C, and A180C specimens. This can be seen in **Figure 6.5** and **Figure 6.6** where photographs show the surface of each aged specimen. In **Figure 6.5** the surface of A140C specimens becomes slightly darker than the AR specimens. This indicates that the oxidation process has begun, but from **Figure 6.4** it is apparent that oxidation has not penetrated into the hybrid composite rod and is limited to the very surface. This is the same for A140C specimens, albeit the specimens have become significantly darker. Again, this oxidation is limited to the very surface of the hybrid composite rod as there is no evidence of penetration into the bulk from the photomicrographs.

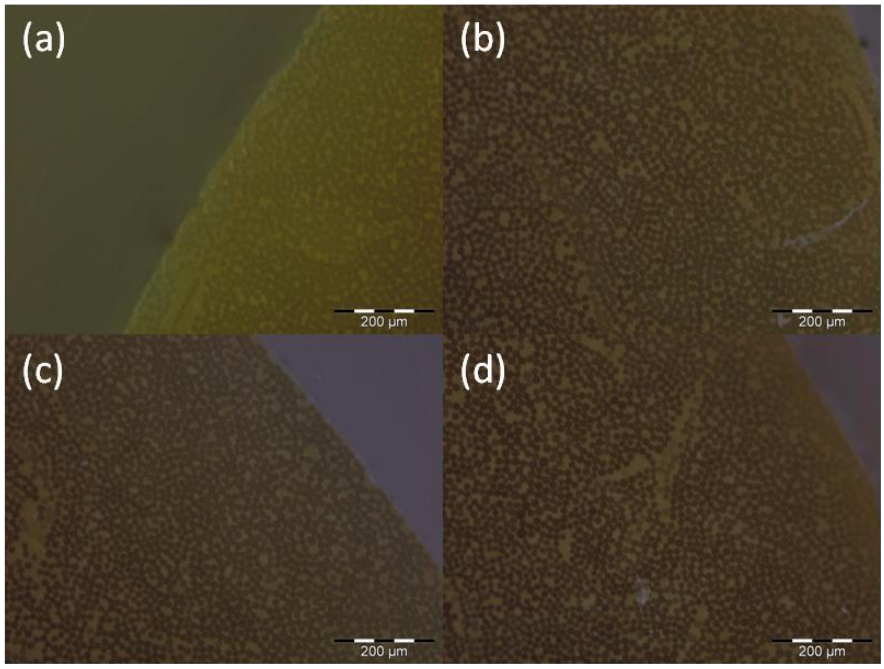

Figure 6.4: Photomicrographs of A). AR, B). 1ORT, C). A140C, and D). CE140C specimens aged for three months.

Figure 6.5: Comparison of surface discoloration in A). AR, B). 1ORT, C). A140C, and D). CE140C specimens aged for three months.

Figure 6.6: Surface damage of a specimen aged at 180°C for three months.

6.2.3 Hardness of Aged Hybrid Composite Rods

Hardness revealed no real trend as seen in **Figure 6.7**. There was a slight reduction in hardness after the initial week of aging for all specimens, but it then appears to remain constant. Because hardness tests were performed after flexure tests, a few specimens were split in half, which could have contributed to a lower hardness reading than true hardness. It should be noted, however, that the error bars of $\pm\sigma$ have been included, and there does not appear to be significant deviation between specimens. This suggests that the process used resulted in consistent results.

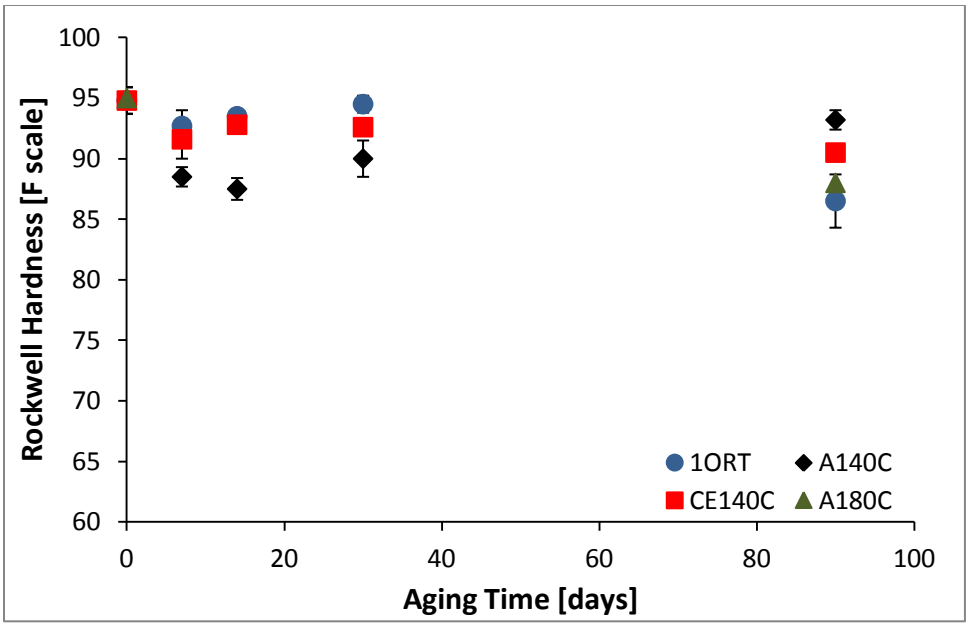

Figure 6.7: Rockwell hardness of hybrid composite rods aged in various conditions as a function of aging time. Error bars of ± 1 σ have been included.

6.3 Aged Neat Resin

6.3.1 Mass Loss and Volumetric Shrinkage

As aging time and temperature increased, the amount of mass loss and volumetric shrinkage of the neat specimens increased. **Figure 6.8** shows that after ninety days of aging the A180C specimens lost 8.64% mass, while the A140C and CE140C specimens lost only 0.90% and 1.09% mass, respectively. The A180C specimens also exhibited the most significant volumetric shrinkage (**Figure 6.9**). This is due to in part to the significant amount of mass loss and in part to the fact that polymers below T_g are not in equilibrium. Therefore, during aging the polymer will reconfigure its chains slowly to

reach equilibrium. The higher the chain mobility or higher the free volume, the faster the polymer can reconfigure its chain structure. Chain mobility increases with temperature and the polymer has more energy to reconfigure itself and equilibrate [4]. Therefore, at higher temperatures, the chains can reconfigure more readily and reduce the free volume, resulting in higher volumetric shrinkage.

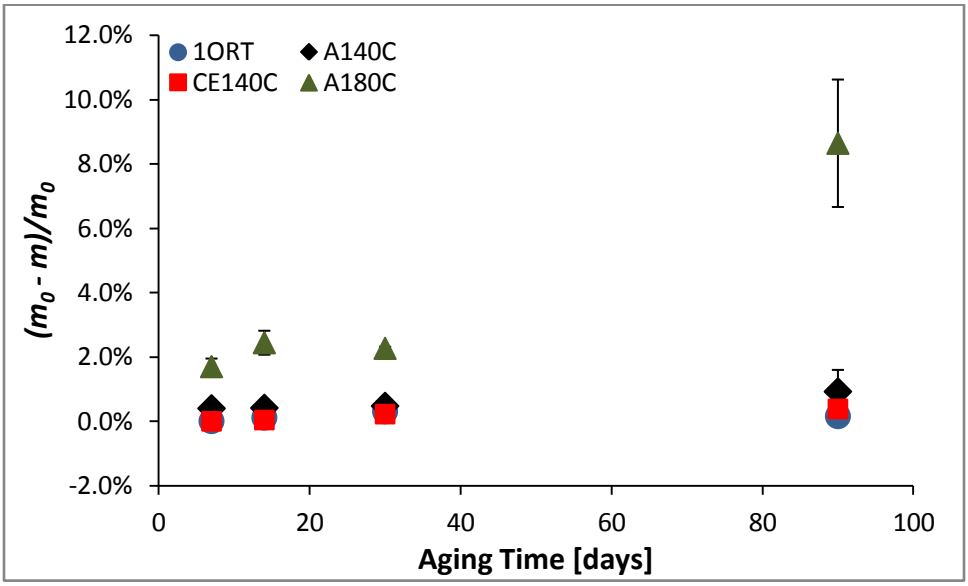

Figure 6.8: Mass loss of samples aged in various conditions as a function of aging time. For the y-axis m_0 is the original mass and m is the mass at the given aging time. Error bars of ± 1 σ have been included.

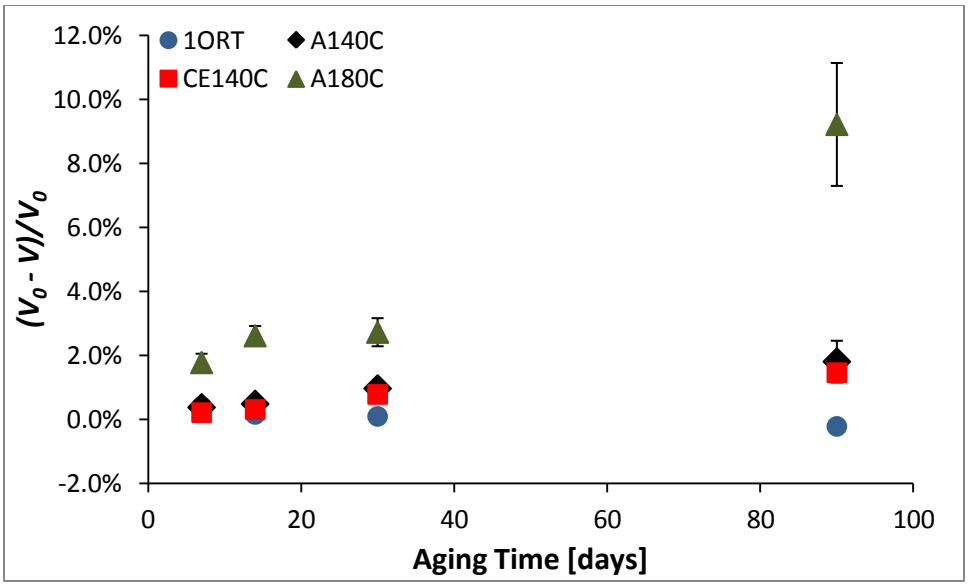

Figure 6.9: Volumetric shrinkage as a function of aging time of samples aged in various conditions with ± 1 σ. V_0 is the volume before aging, and V is the volume at a given aging time.

It can be seen in **Figure 6.8** and **Figure 6.9** that there appears to be very little observable difference between the A140C and CE140C specimens regarding both mass loss and volumetric shrinkage. Since the only difference between the A140C and CE140C specimens is the addition of 1% ozone at the same aging temperature, this is to be expected. The 1ORT specimens showed a 0.22% increase in volume due to the fact that there was no elevated temperature present which could accelerate the loss of volatiles and reconfiguration of the chains, and thereby reducing the mass and free-volume. Instead, aging in 1% ozone at RT resulted in chain scission events which increased the free-volume and ultimately the volume of the specimens [11].

6.3.2 Flexure Testing of Aged Neat Resin

All aged neat resin specimens showed significant reduction in loads at failure as aging time increased, as seen in **Figure 6.10**. After ninety days of aging, the most significant reduction in the load at failure was found in the A180C specimens, with a decrease of 64% from 156.7 N to 55.9 N. The A140C and CE140C specimens exhibited 23% and 44% reductions in loads at failure after ninety days, respectively. The initial increase of strength after aging for seven days of the 1ORT specimens resulted from the creation of crosslinks [11]. The subsequent reduction in the strength was attributed to chain scission [11]. After ninety days of aging, 1ORT specimens had a 3% reduction in loads at failure.

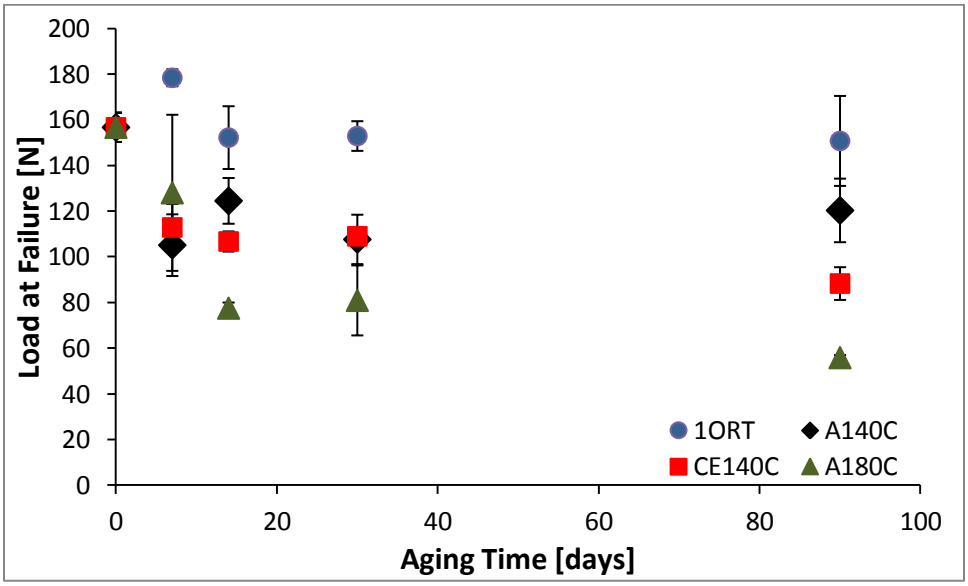

Figure 6.10: Loads at failure of neat resin specimens as a function of aging time with ± 1 σ.

Figure 6.11 shows that the displacement at failure of the epoxy is reduced as both the aging time and temperature increase. The A180C specimens displayed nearly an 80% reduction in the displacement at failure. The A140C and CE140C specimens exhibited a similar trend, with their displacements at failure being reduced after ninety days by 50% and 61%, respectively. The 1ORT specimens on the other hand, showed an increase in displacements at failure due to chain scission [11].

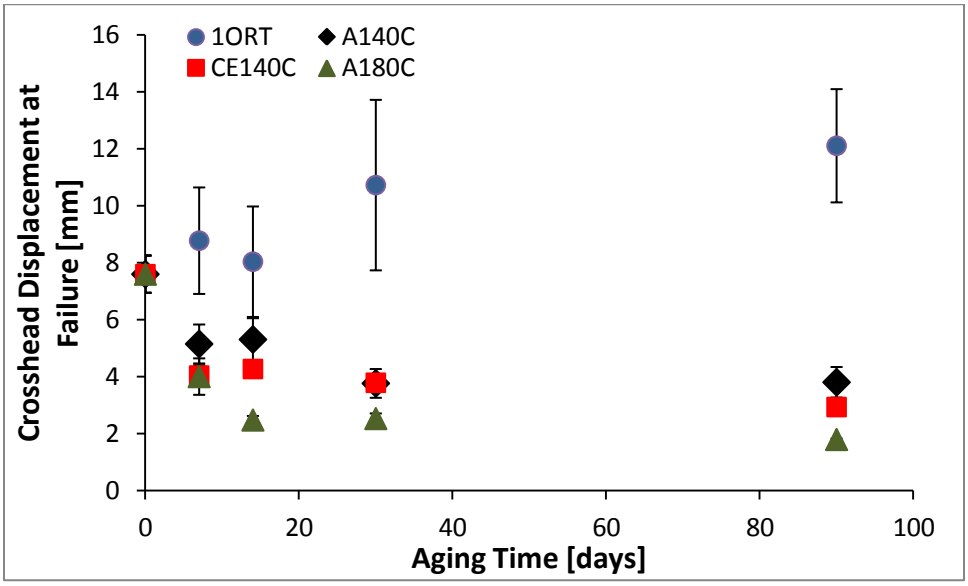

Figure 6.11: Crosshead displacement at failure of neat resin specimens as a function of aging time with ± 1 σ.

It can be seen from **Figure 6.12** that the stiffness of the neat resin increases modestly with increasing aging time. This could be partially caused by post curing [14, 71]. There can be unreacted constituents present after initial cure of the resin. Therefore aging can act as a postcure, giving rise to possibly more crosslinks, and allowing for the material to tend towards equilibrium, thereby producing a stiffer material [31]. It can be

seen from **Figure 6.12** that the stiffening phenomenon is slightly accelerated in the A180C specimens for shorter aging times. It was noted that the A140C specimens show no discernible difference in modulus from the CE140C specimens.

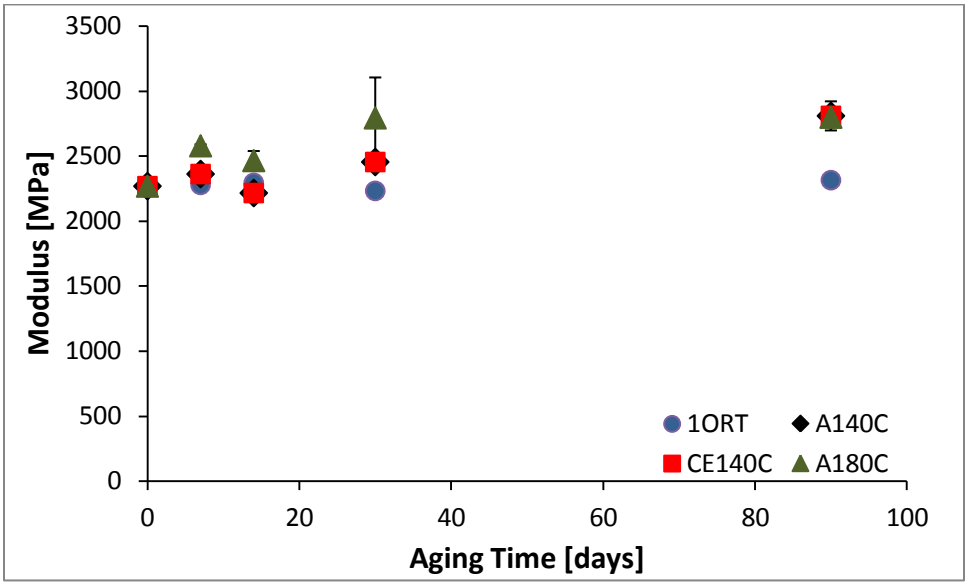

Figure 6.12: Flexure modulus of neat resin specimens as a function of aging time with ± 1 σ.

6.3.3 Dynamic Mechanical Analysis of Aged Neat Resin

Dynamic Mechanical Analysis (DMA) was used to evaluate the storage modulus as a function of frequency and aging time. It can be seen in **Figure 6.13** that aging caused the epoxy to embrittle with an increase in the aging time. The "As Made" specimen, not shown in **Figure 6.13** to allow for more clarity, has a significantly lower storage modulus. However, the "As Made" specimen data can be found in [11]. All specimens showed a significant increase in storage modulus when aged seven and ninety days. After

ninety days the CE140C exhibited the most significant increase in the storage modulus. This could be due the addition of 1% ozone, which enriched the environment with oxygen and consequently oxidized the polymer further.

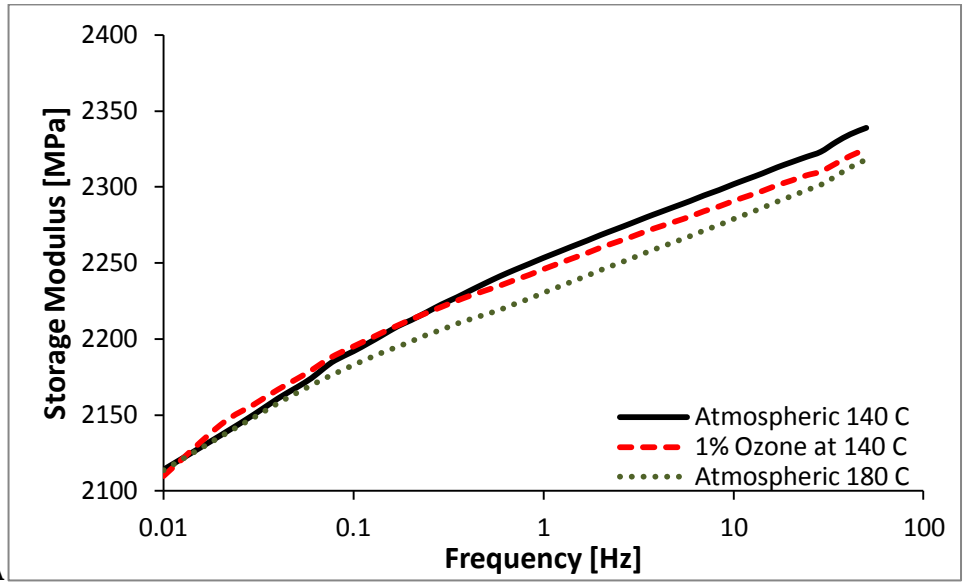

A

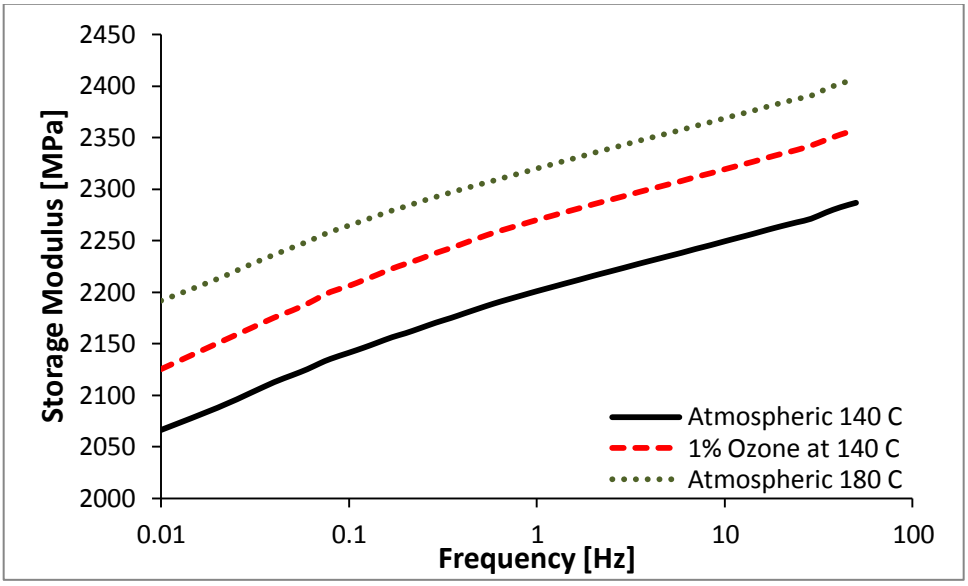

B

C

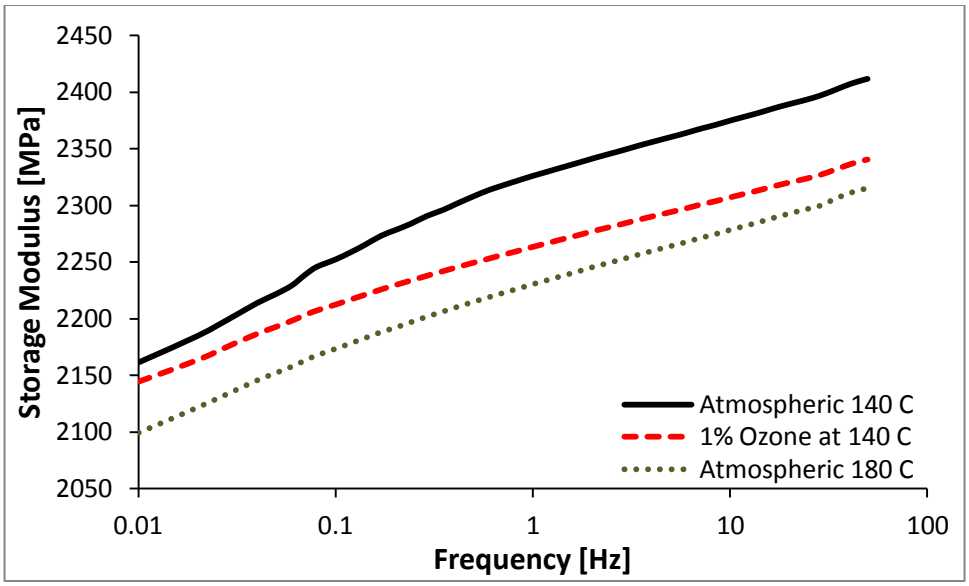

D

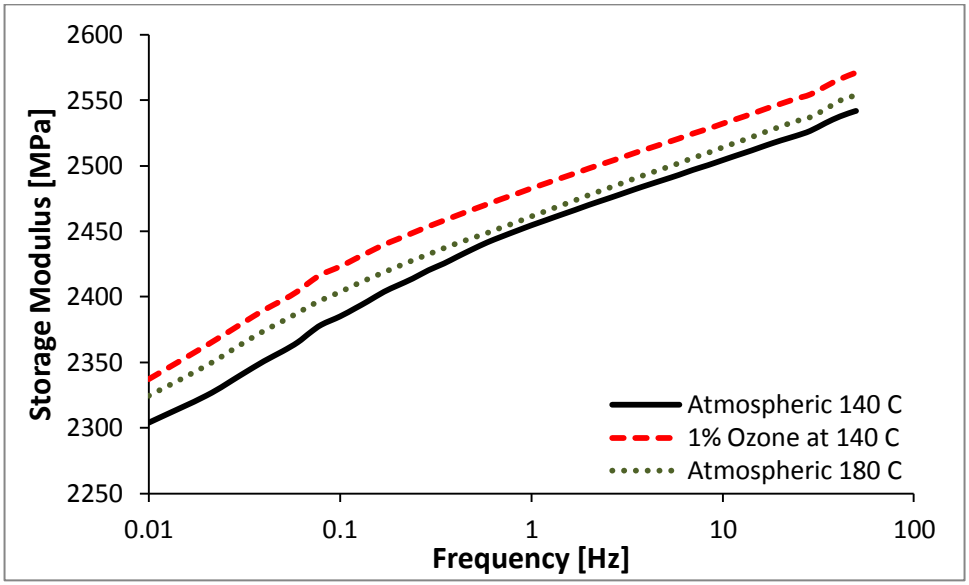

Figure 6.13: Storage modulus as a function of frequency at varying time lengths: (A) seven days (B) fourteen days (C) thirty days and (D) ninety days.

The damping of the material was also determined through DMA, but as a function of temperature. **Figure 6.14** shows the evolution of tan δ as aging time increased. An intense and thin peak typically corresponds to a highly crosslinked polymer with little chain mobility, while less intense and broader peaks represent chain damage i.e. chain scission, with high chain mobility. This is the case for all aged specimens, albeit the most pronounced effect was found in the A180C specimens. This can be seen in **Figure 6.14** where the dotted curves represent A180C specimens and are the broadest and least intense. The shift in the peak represents the change in glass transition temperature. Minimal changes in T_g were observed for all aged specimens (**Figure 6.15**), with the greatest shifts being in the A180C specimens with an increase of 10°C. The T_g for the A140C and CE140C specimens decreased by 7°C after ninety days of aging (**Figure 6.15**).

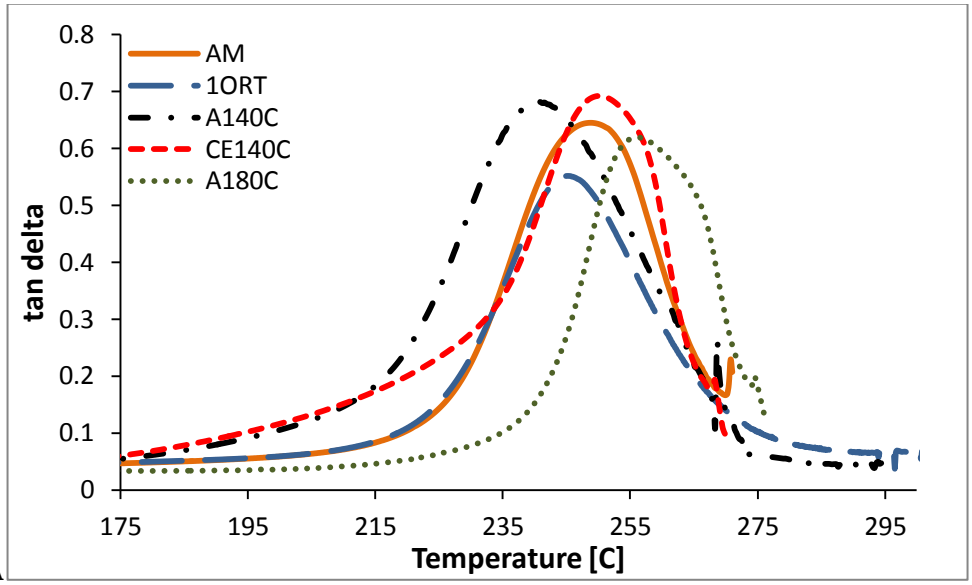

A

B

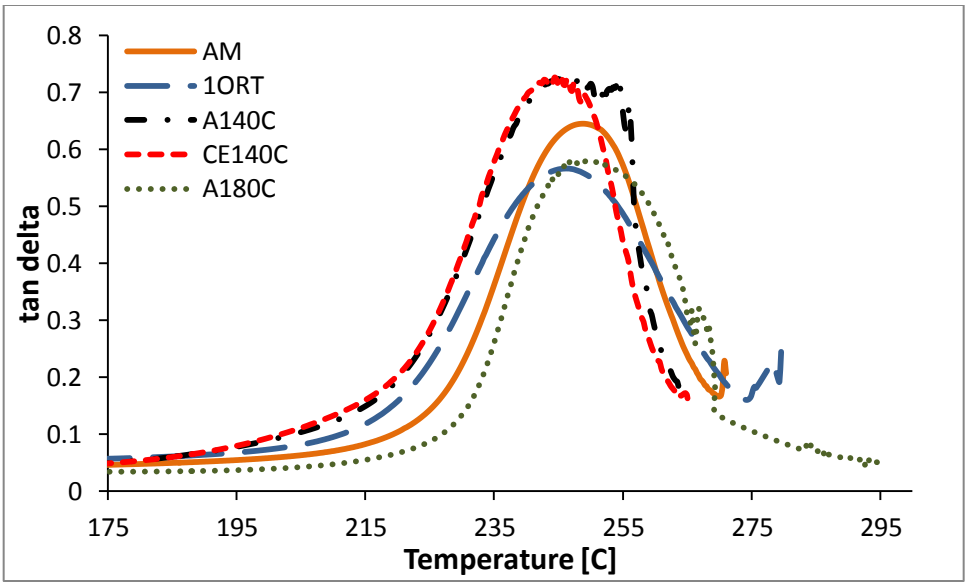
0.8
0.7
0.6
0.5
0.4
0.3
0.2
0.1
0
tan delta
AM
1ORT
A140C
CE140C
A180C
175
195
215
235
255
275
295
Temperature [C]

C

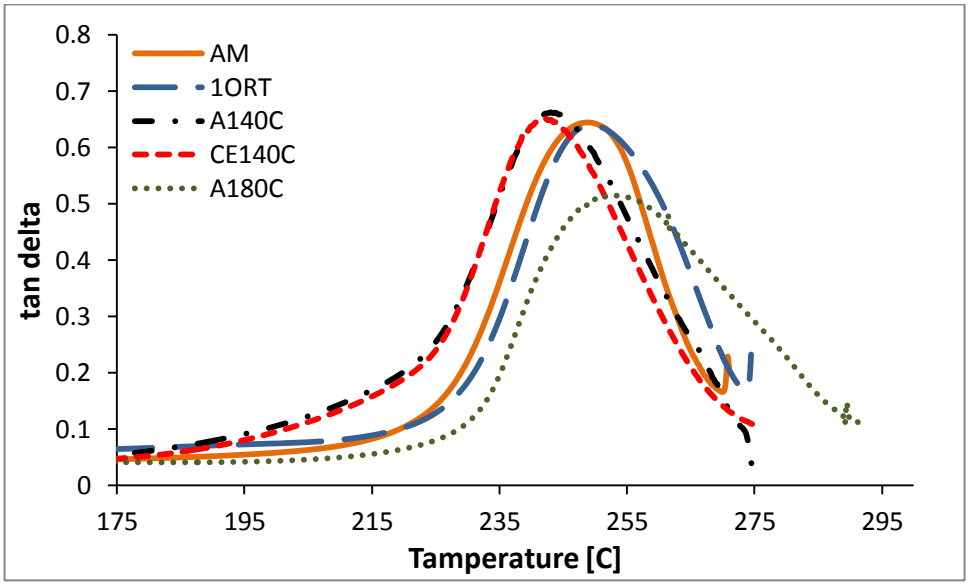
0.8
0.7
0.6
0.5
0.4
0.3
0.2
0.1
0
tan delta
AM
1ORT
A140C
CE140C
A180C
175
195
215
235
255
275
295
Tamperature [C]

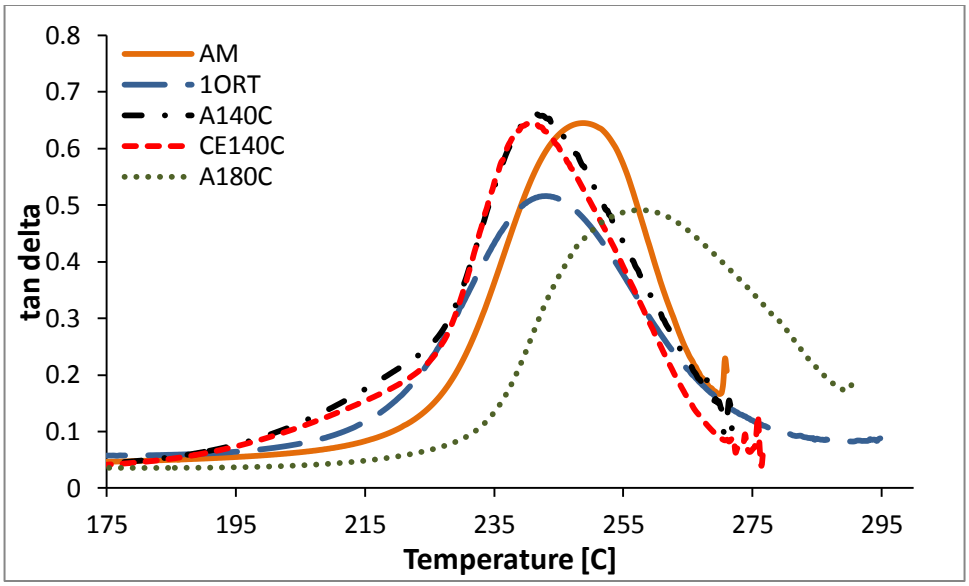

D

Figure 6.14: Damping (tan δ) as a function of temperature for various aging conditions and time lengths: (A) seven days (B) fourteen days (C) thirty days and (D) ninety days.

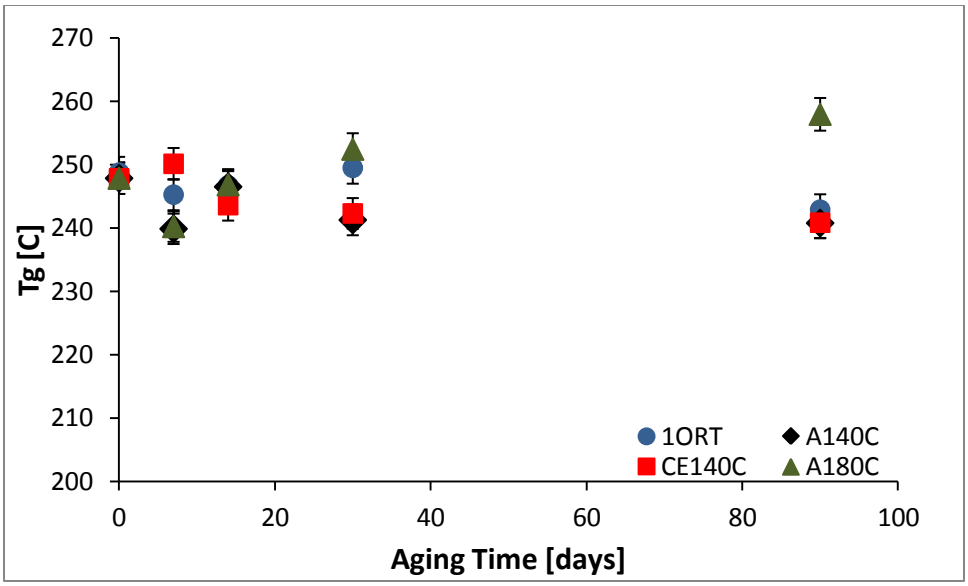

Figure 6.15: The evolution of Tg as a function of aging time and aging condition with ± 1 σ.

6.3.4 Nanoindentation of Aged Neat Resin

Thermo-oxidation of the neat resin was apparent after aging due to a local increase in stiffness, seen in **Figure 6.16**, where the reduced modulus is higher at the surface and then reduces as the depth from the edge of the specimen increases. Interestingly, this effect is most accelerated in specimens aged in atmospheric 180°C; despite the fact that the CE140C specimens have 1% ozone in the atmosphere, which increases the amount of oxygen available for oxidation. In fact, the A180C specimens exhibited the most significant stiffening effect after thirty days, which could be a result of post curing, but is most likely predominantly caused by thermo-oxidation. Such data suggest that for this resin system, temperature activation plays a greater role in the oxidation behavior, as compared to oxygen (e.g., diatomic oxygen, ozone, and atomic

oxygen). After ninety days of aging, the surface was damaged and degraded enough such that a reduction in reduced modulus was observed. The A140C specimens aged for seven days were similar to the "As Made" specimens because the time length was too short and the temperature was not high enough for any significant amount of oxidation to occur.

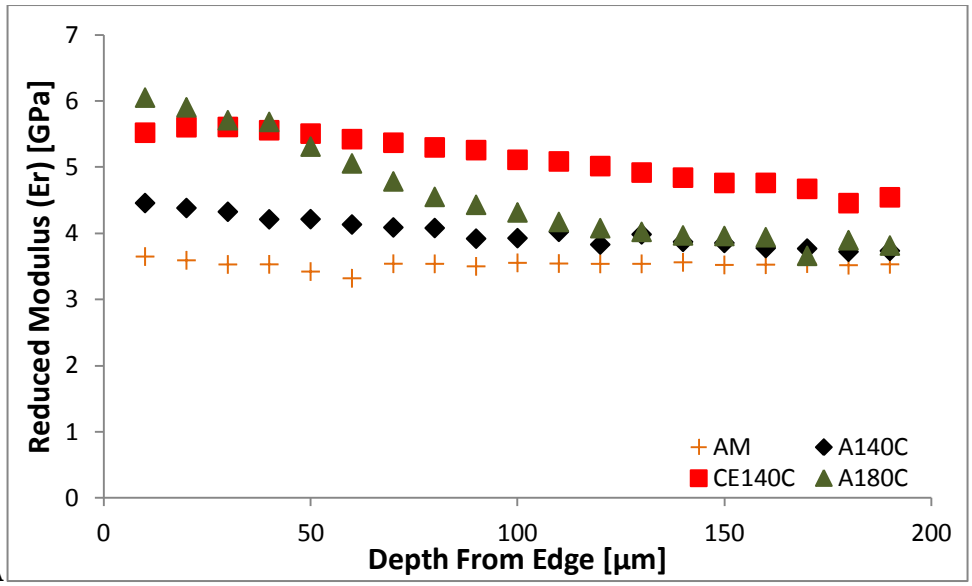

A

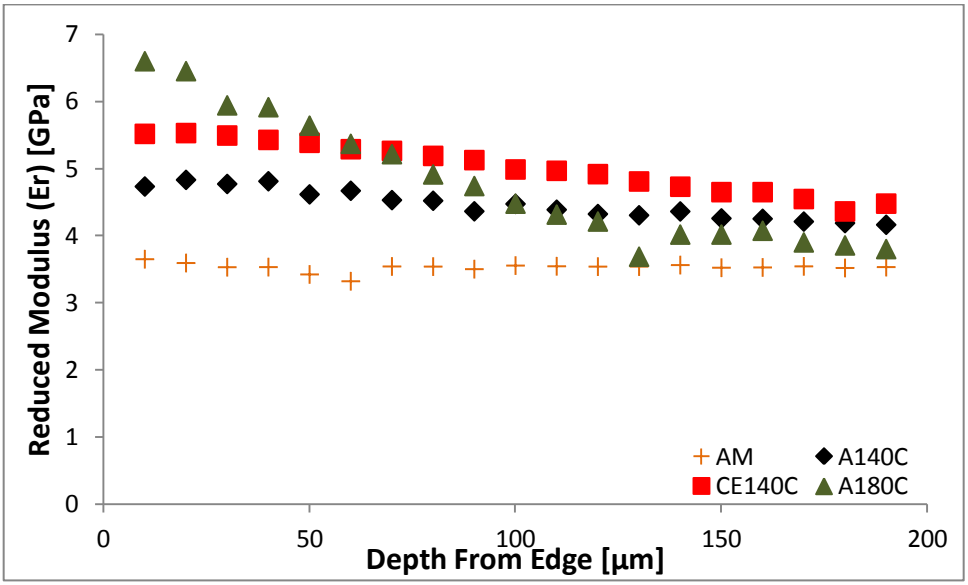

B

C

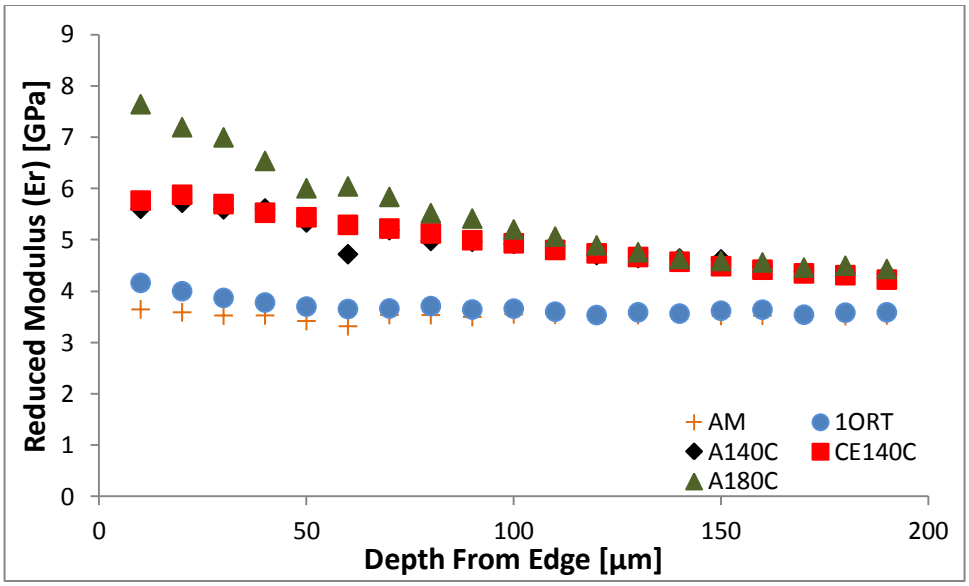

D

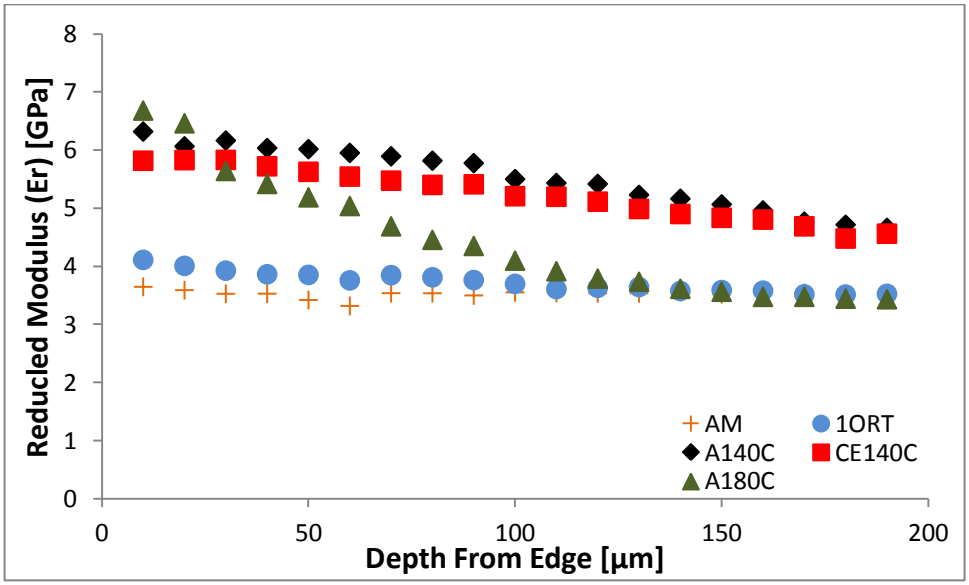

Figure 6.16: Reduced modulus of aged specimens for A). 7 days, B). 14 days, C). 30 days and D). 90 days. Values taken at the very edge of the specimen were not included because of edge effects.

The nanohardness revealed few conclusions. However, it can be seen from **Figure 6.17** that in general, A180C specimens were harder on the surface up until aged for 1 year **Figure 6.17D**. After one year of aging, it appears the surface of the neat resin was degraded such that there was not a constant reading of nanohardness. For clarity and comparison, the 1ORT samples have been included for the one month and three month time lengths. Even at three months of aging, the nanohardness of the 1ORT specimens is slightly higher than that of the AM specimen. Interestingly, the CE140C specimens are initially harder than the A140C specimens, but at fourteen days and longer aging times, the hardness becomes relatively equal. This again suggests that the temperature activation is more dominant than that of the presence of more oxygen.

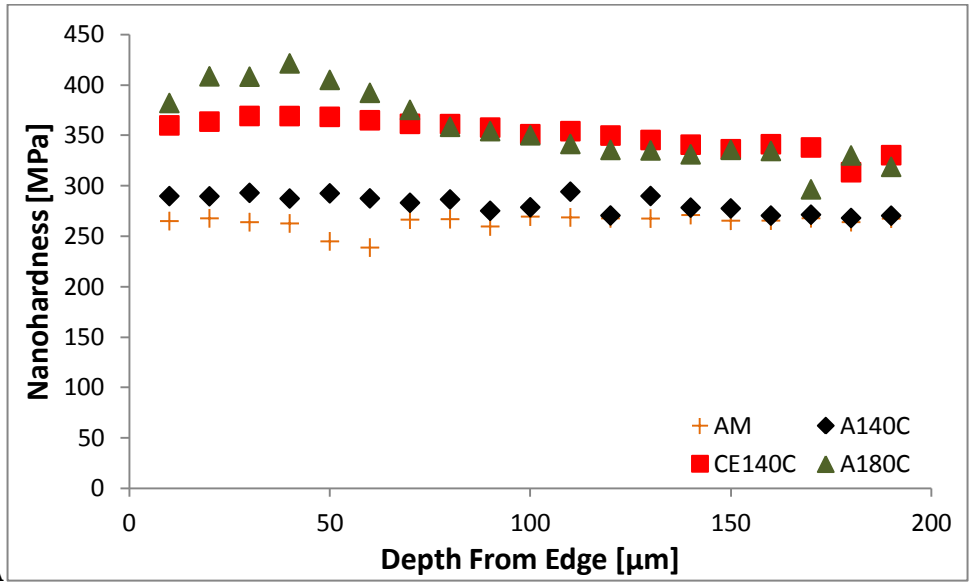

A

B

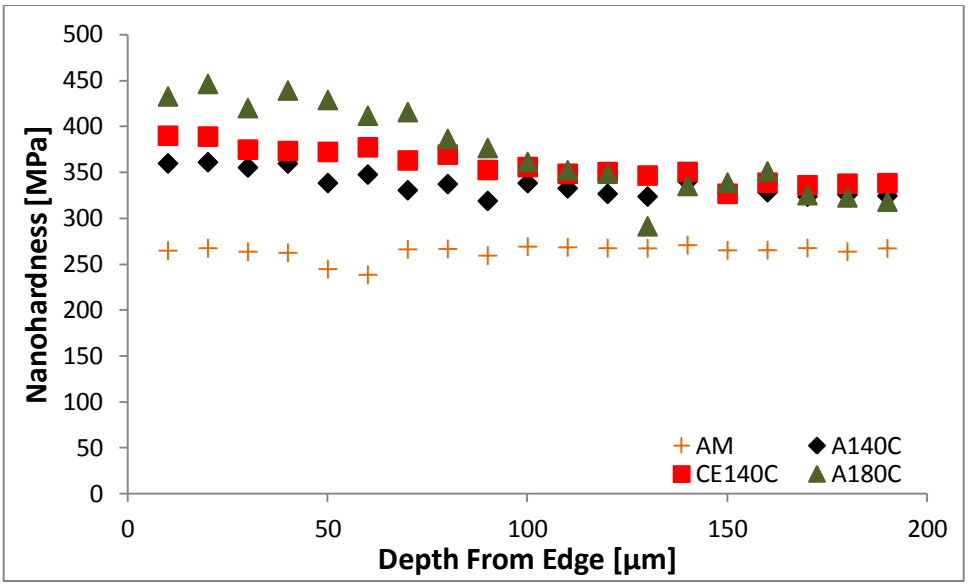
Nanohardness [MPa]
500
450
400
350
300
250
200
150
100
50
0
0
50
100
150
200
Depth From Edge [µm]
AM
A140C
CE140C
A180C

C

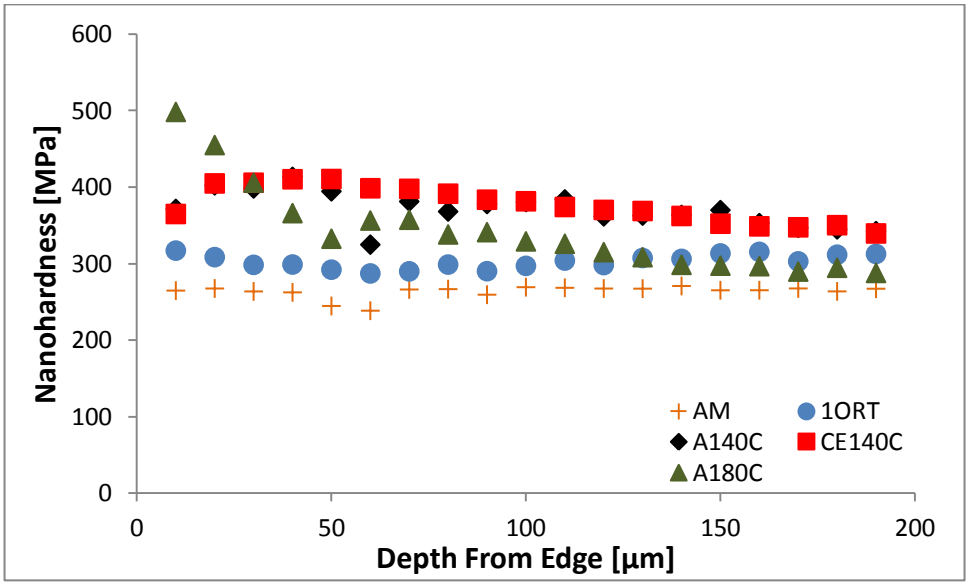
Nanohardness [MPa]
600
500
400
300
200
100
0
0
50
100
150
200
Depth From Edge [µm]
AM
1ORT
A140C
CE140C
A180C

D

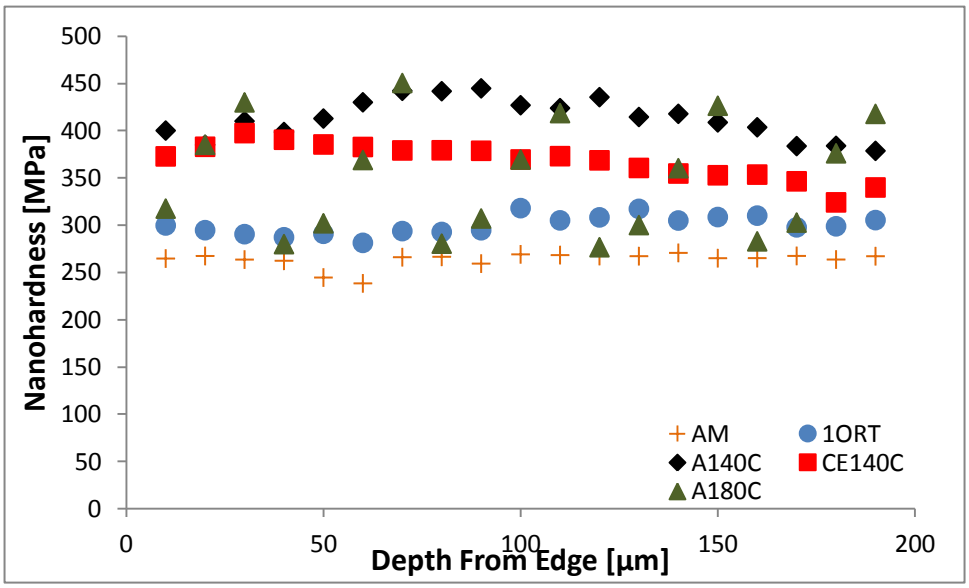

Figure 6.17: Nanohardness of specimens aged for A). 7 days, B). 14 days, C). 30 days and D). 90 days. The 0 µm depth data points were not included due to edge effects.

6.3.5 FTIR OF AGED NEAT RESIN

The A180C aged neat resin specimens exhibited the most dramatic chemical changes. This can be seen in **Figure 6.18**, **Figure 6.19**, and **Figure 6.20** where the absorption of broken double bonded sites is significantly higher for the A180C specimens. The broken double bonds potentially form ketones (1725 cm^{-1}), aldehydes (1620-1670 cm^{-1}), and carboxylic acids (3250 cm^{-1}) [11]. Carboxylic acids, along with carbonyls (1620-1670 cm^{-1}), are typically associated with chain scission [11, 31, 44, 46, 47, 106]. These regions show the most absorption in A180C specimens. Comparing **Figure 6.18** with **Figure 6.19**, it can be seen that there is not a significant difference in spectra absorbance between A140C and CE140C specimens.

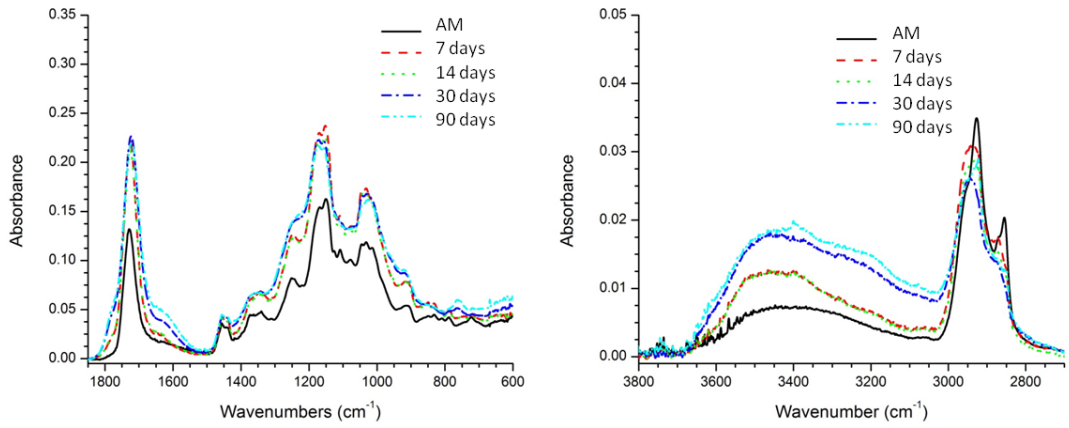

Figure 6.18: FTIR spectra of A140C aged specimens.

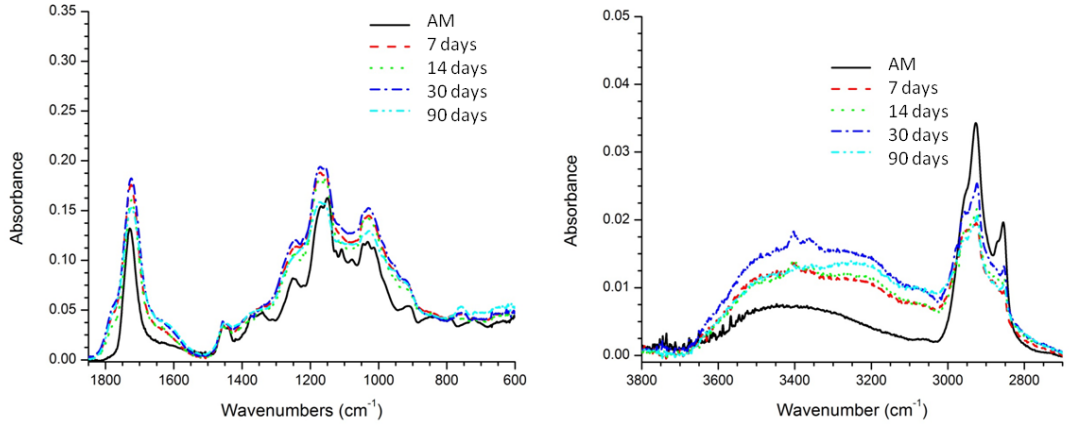

Figure 6.19: FTIR spectra of CE140C aged specimens.

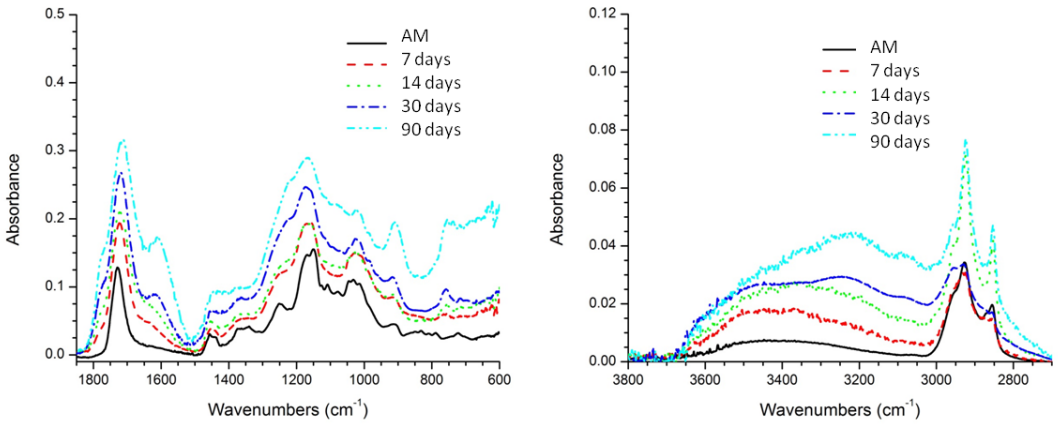

Figure 6.20: FTIR spectra of A180C specimens.

6.3.6 STATISTICAL ANALYSIS

Aging at 140°C with and without 1% ozone yielded little observable difference in the results for mass loss, volumetric shrinkage, flexure and change in T_g. Therefore, the t-Test was applied to these data sets to evaluate the statistical difference between the A140C and CE140C specimens. It was found that there was no statistical distinction between the A140C and the CE140C specimens regarding their behavior after aging in the aforementioned tests. Therefore, it can be concluded that up to ninety days of aging, the polymer degradation is thermally driven and the presence of 1% ozone at 140°C does not significantly affect the aging process. It should be noted that at ninety days of aging that there may be an observable effect of ozone starting to take place. This was never confirmed nor denied as longer aging time lengths would be needed to observe if ozone was starting to have an effect or not. Ozone did however have an effect on the polymer viscoelasticity. When 1% ozone was present, the storage modulus increased, which has not been explained in this research. It has been reported in the past that ozone will

disassociate into diatomic and atomic oxygen at about 100°C [42]. Atomic oxygen is highly reactive and could have a very detrimental effect on the polymer and composite properties. This, however, was not observed at 140°C for the materials tested in this research. To fully understand the effect the presence of 1% ozone has on the polymer degradation, longer time lengths must be employed.

6.4 CONCLUSIONS

Neat resin and hybrid composite rods have been aged in atmospheric high temperature and 1% ozone at 140°C. The loads at failure reduced in neat resin specimens, but increased in the hybrid composite rods. This was attributed to the fact that the neat resin was manufactured using a rigorous cure cycle that enabled a fully cured resin, while the composite rods were manufactured through pultrusion leaving unreacted constituents allowing for postcure during aging. Both neat resin and hybrid composite rods exhibited an increase in stiffness due to postcure. For the neat resin specimens, aging allows for equilibration creating a stiffer material. For the hybrid composite rods, aging creates improved fiber/matrix interfaces which allow for better load transfer. Aging degraded the neat resin specimens and indeed the higher the temperature the more degradation that took place. Chains were damaged on the surface of specimens through a thermo-oxidative process. Application of the t-Test showed there was no statistical difference between the specimens aged in atmospheric 140°C, and the specimens aged under both 1% ozone and 140°C with the exception of viscoelastic properties where the effect of

ozone at 140°C on the polymer was clearly visible. Aging of both the rods and neat resin specimens in 1% ozone at room temperature resulted in minimal effects in comparison with both the 140°C and 180°C aging. The 180°C aging in air was found to be especially damaging to both the rods and the neat resin specimens. Therefore, the mechanical degradation of the neat resin and rod specimens due to aging can be said to be thermally driven and not significantly affected by the presence of ozone both at room and elevated temperatures up to ninety days.

6.5 The Most Damaging Aging Condition

One of the goals of this study was to determine which condition, (i) extreme ozone, (ii) elevated temperature, or (iii) a combination thereof, would be most damaging to the hybrid composite rod used for PCCC applications. From the previous sections it is clear that temperature has the greatest influence on the performance of the hybrid composite rod and neat resin. However, this is limited to very extreme high temperatures. At lower temperatures, e.g. 140°C, there is no observed detrimental effect on the hybrid composite rods when aged up to one year. There was on observed reduction in load at failure for the neat resin, but that is because of the neat resin was put through a rigorous cure cycle. This results in little to no post curing; meanwhile the hybrid composite rod contains plenty of unreacted constituents and therefore goes through post curing. Eventually, the post curing process will finish, and degradation will start to take place in the hybrid composite rod. However, to characterize when that will occur, further studies

must be performed. It is interesting to note here that Burks had developed a way to use physical aging to predict the in service life of the hybrid composite rod. This method used the reduction in load at failure though, and therefore, this method could not be applied to the A140C specimens, as there was no observed reduction in load at failure. Also this method relied on only physical aging, and therefore does not account for chemical aging, or in this case oxidation.

The presence of ozone had no discernible effect on the hybrid composite rod, and only one discernible effect on the neat resin. After statistical analysis it was concluded the A140C and CE140C aging conditions results were statistically equivalent. Therefore the presence of ozone did not influence the aging process drastically. However, for the neat resin, there was an observed increase in storage modulus. This means ozone had an influence on the viscoelastic properties of the neat resin. This did not influence the mechanical performance of the neat resin though. The results of neat resin A140C specimens and CE140C specimens were statistically equivalent. Thus ozone was determined to have no real detrimental effect on the neat resin, the aging is purely thermally driven up to three months of aging. Further studies are needed to determine the effect on changing the storage modulus, and thus the viscoelastic properties of the neat resin have.

CHAPTER 7: RESIDUAL STRESSES FROM PHYSICAL AGING USING FINITE ELEMENT MODELING

7.1 INTRODUCTION

In this section the finite element models used to characterize the residual stress created from physical aging is presented. There are two models created. One is a 2-D plane strain fiber array representative volume element, and the other is an axis symmetric model with alternating layers of fiber and matrix. In the previous chapter it was concluded that the degradation of the hybrid composite rod was thermally driven, and ozone had little to no impact. Therefore, the finite element (FE) models developed were to characterize stresses induced by the worst condition, i.e. high temperature [111] and to predict life of a PCCC. The stresses found from the FE models are used to characterize and predict the experimental behavior of the hybrid composite rods.

7.2 REPRESENTATIVE VOLUME ELEMENT MODEL

The stress within the matrix of a PCCC was characterized through finite element (FE) modeling via the use of a representative volume element (RVE) using the COMSOL

v.4.3a software package. RVEs model materials at small scales (i.e. micro), and are representative of the overall bulk material when proper boundary conditions are applied. The RVEs developed for this study were developed for both the carbon fiber composite (CFC) and the glass fiber composite (GFC) portions of the hybrid composite rod. The RVE geometry used was a 2-D plane strain 5X5 fiber array with two symmetry planes to model a 10X10 fiber array (**Figure 7.1**); similar to the RVE geometry by Drago and Pindera [99].

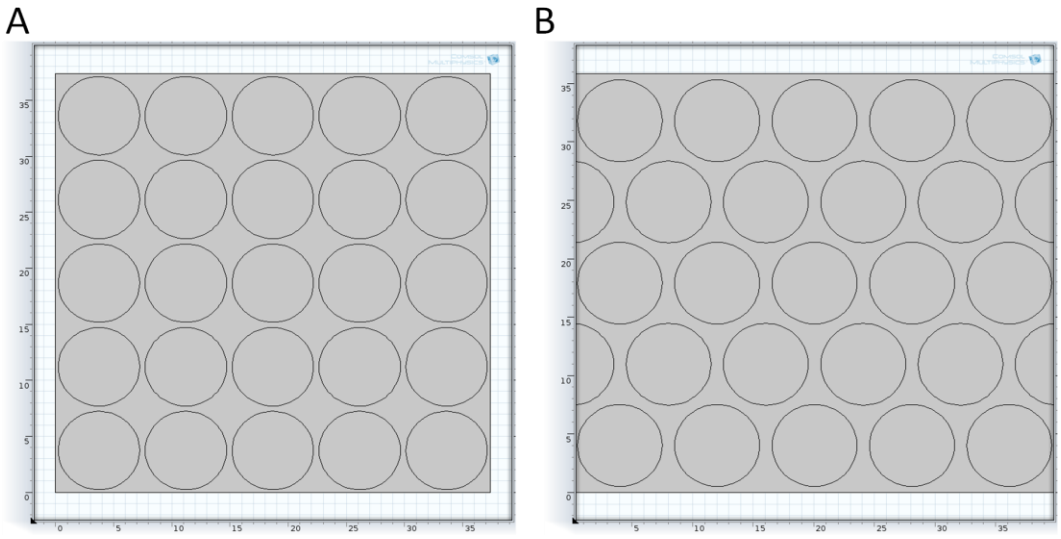

Figure 7.1: A). Geometry of square fiber array FE model B). hexagonal fiber array geometry.

There are two common fiber packing arrangements used in modeling for unidirectional fiber composites: square and hexagonal. The RVEs developed in this study included both packing types, and the fiber volume fractions (v_f) of the GFC and CFC were 64% and 69% respectively. Perfect bonding between the fibers and the matrix was

assumed for this model. It is understood that the bonding and packing arrangements of the RVEs modeled are idealized, but they provide useful information about stress distributions and trends.

For the carbon fiber material properties, the anisotropic coefficient of thermal (CTE) was taken from [83] and [84], the elasticity matrix was taken from [100] (seen in **Table 4**), and all other properties were taken from the Toray data sheet. For **Table 4**, the axial direction is in the global 1 direction, and all other values not reported are 0.

Table 4: Stiffness matrix components of carbon fiber.

Stiffness Matrix Component	Stiffness (GPa)
C11	235
C12	3.69
C13	3.69
C22	26
C23	3.32
C33	26
C44	5.52
C55	28.2
C66	28.2

The isotropic ECR glass fiber material properties were taken from (83), and are given in **Table 5**. The matrix material properties can also be found in **Table 5**, where E and ρ were measured from [11, 112], v came from [10], and the thermal properties came from [113].

Table 5: Material properties of the ECR glass fiber and epoxy matrix used for RVE modeling.

Property	E-Glass	Matrix
E (GPa)	76	2.1
ν	0.22	0.4
ρ (kg/m^3)	2560	1200
k (W/m K)	13	0.819
α (*10^{-6} K^{-1})	4.9	100

With TRS materials, a transformation from a change in temperature to a change in time can easily be modeled. Thus the relaxation times are modified by a shift function. The Williams-Landel-Ferry (WLF) shift function was employed (equation 3.21), where α_T is the shift factor, C_1 and C_2 are material constants, T_{ref} is a reference temperature, typically T_g, and T is the measured temperature. C_1, C_2 and α_T were calculated using the process described in the Ferry text [101], and the WLF constants were found to be: C_1 = -3.992 K^{-1}, and C_2 = -42.335 K.

A five step FE model was used in which the first step is a stress free high temperature equilibration at 200^{o}C. This is to establish the state of stress ($\sigma \approx 0$) at the curing temperature (curing stresses were neglected for this model). Step two was a cool down from 200^{o}C to room temperature (RT), i.e. 23^{o}C, at a rate of 5^{o}C/min, simulating

the quench from curing. Step three was a temperature ramp up to the isothermal aging temperature at a rate of 5°C/min. This was to simulate the temperature rise when the conductor was initially energized. Step four was an aging step at the specified isothermal temperature for a given aging time to simulate a specific continuous operating temperature (COT). The COTs chosen for this study were 140, 160, 180 and 200°C. At this step the physical aging was applied. Shrinkage obtained from the dimensional relaxation study was converted to a strain and applied at the beginning of the aging step. The final step was a cool down back to RT at the same 5°C/min ramp rate. Aging time lengths were chosen to coincide with previous studies the authors have performed [11, 113]: seven days, fourteen days, thirty days, ninety days, six months, nine months and 1 year.

7.3 THERMORHEOLOGICAL RELAXATIONS

Figure 7.2A shows the normalized dimensional relaxations as a function of aging time of the neat resin. The amount of relaxation increases with increasing isothermal temperatures. The raw data was fit using a nonlinear least squares regression with equation 3.19. A β value of 0.491 accurately described all relaxation curves, meaning the polymer can be treated as TRS. **Figure 7.2B** shows a linear Arrhenius plot from which the activation energy of the aging process was found to be 74.8 kJ/mol. This seems to be a relatively low activation energy compared with other polymer [114].

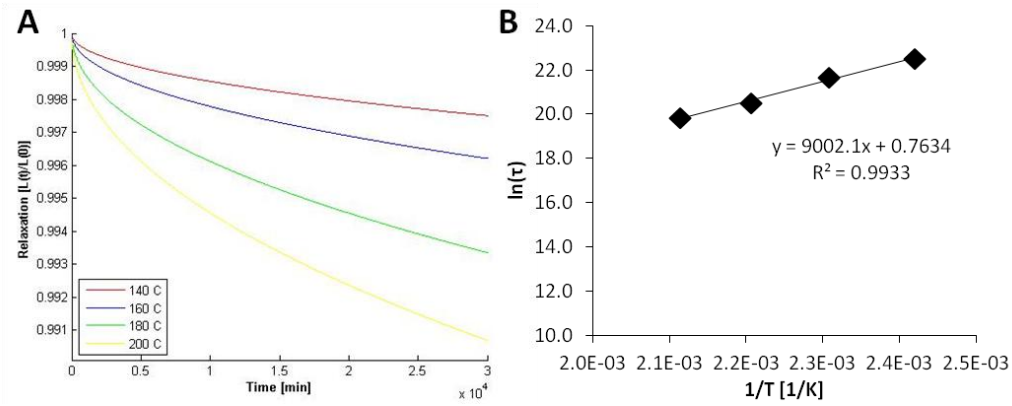

Figure 7.2: (A) Dimensional relaxations of aged neat resin specimens (B) plot of ln(τ) vs. 1/T for determining activation energy.

In a study by Gentz *et al.* [115], the activation energy determined by the dimensional relaxation and the shear relaxation were discovered to be equivalent. In other words, there exists an arithmetic shift between the two curves when plotted as a linearization of the Arrhenius equation. This arithmetic shift was calculated for the curves found by Gentz, and applied to the dimensional relaxations in this study. The result was a line below and parallel to the dimensional relaxation curve and can be seen in **Figure 7.3**. The volumetric shrinkage was modeled by an applied strain at the beginning of the aging step. This is the same method Benedikt used in previous studies [98, 102-104]. However, relaxation times used for the FE model, were the shear relaxation times. The motivation behind this was to account for both dimensional relaxations (applied strain), and shear relaxations (relaxations times in equations 3.22).

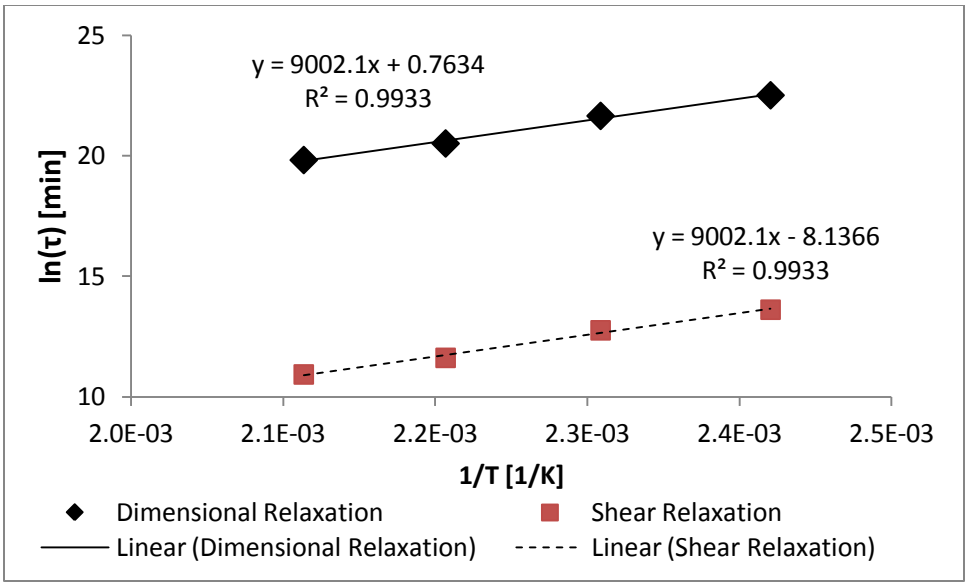

Figure 7.3: Plot of the measured dimensional relaxations and the created shear relaxations.

From **Figure 7.3** the relaxation times, τ_{shear}, can be found for any temperature. Using this, new shear relaxations were approximated for the RVE model.

7.4 RVE Modeling

Benedikt *et al.* has previously shown that viscoeleasticity must be considered when modeling aging of a polymer [98, 102-104]. Therefore, to model the viscoelasticity of the matrix, a three term Generalized Maxwell Model was fit to the dimensional relaxation data (equation 3.22).

The raw dilatometer data was fit with equation 3.22 using a nonlinear least squares regression. All viscoelastic matrix material constants can be found in **Table 6**. It should be noted here that the μ_m terms for the matrix do not sum to exactly 1. This is because with the values obtained, the correlation coefficient was very close to 1, and it was decided to retain a larger correlation coefficient (more representative of the data) rather than to force the μ_m terms to sum exactly to 1.

Table 6: Generalized Maxwell model constants used for RVE modeling.

Temp (^{o}C)	G_0 [MPa]	μ_0	μ_1	μ_2	μ_3	τ_1 [min]	τ_2 [min]	τ_3 [min]
140	665.5	0.6552	4.602×10^{-4}	1.884×10^{-3}	0.4446	302.3	2894	113800
160	583.3	0.7629	4.567×10^{-4}	1.258×10^{-3}	0.4922	307.8	2811	70300
180	669.1	0.6712	7.448×10^{-4}	2.671×10^{-3}	0.4212	254.8	2926	21420
200	647.2	0.7835	10.340×10^{-4}	1.912×10^{-3}	0.3461	177.5	1194	11410

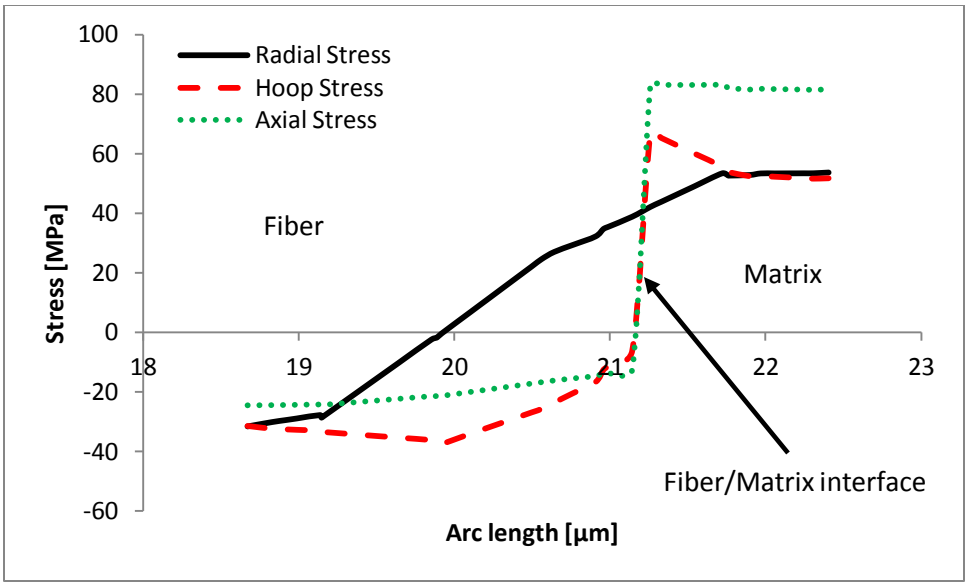

Figure 7.4: An example of the typical radial, hoop, and axial COMSOL stress plots as a function of arc length.

A typical COMSOL stress plot as a function of arc length can be seen in **Figure 7.4**. The arc length is measured from the center of the fiber and continues into the matrix up to half of the distance to the next fiber. This means that the x-axis in **Figure 7.4** is arbitrary.

Figure 7.5, **Figure 7.6**, and **Figure 7.7** compare the radial, hoop, and axial residual stresses in the matrix for the CFC and GFC from the square fiber packing arrangement FE model, with axial stress being the greatest. As time and temperature increase, so do all stresses, and the stresses were generally slightly larger in the CFC than the GFC. Stresses were calculated along both the shortest and longest distance between two fibers, and the greatest stresses were found to occur at angles of 45^{o} and 30^{o} (corresponding to the greatest distance between two fibers) for square and hexagonal

arrays respectively. To convert the stresses to radial and hoop when measured at an angle, equations 7.1 and 7.2 were used.

$$\sigma_r = \sigma_x cos^2\theta + \sigma_y sin^2\theta + 2\tau_{xy} sin\theta cos\theta \quad (7.1)$$

$$\sigma_\theta = \sigma_x cos^2\theta + \sigma_y sin^2\theta - 2\tau_{xy} sin\theta cos\theta \quad (7.2)$$

In the above equations σ_r and σ_θ are the radial and hoop stresses respectively, σ_x, σ_y, and τ_{xy} are stresses in the x, y, and shear in the xy directions respectively, and θ is the angle the stresses were measured at (i.e. 45° and 30°). A comment should be made that the radial stresses, when measured at 0°, changed sign and were compressive. Compressive stresses in the matrix are not of concern. It is the large tensile stresses that will generate cracks and create damage and thus affect the performance of the hybrid composite rods. These stresses have been shown for clarity in **Figure 7.8**, but despite having a larger magnitude, the fact that they are compressive means they were negated.

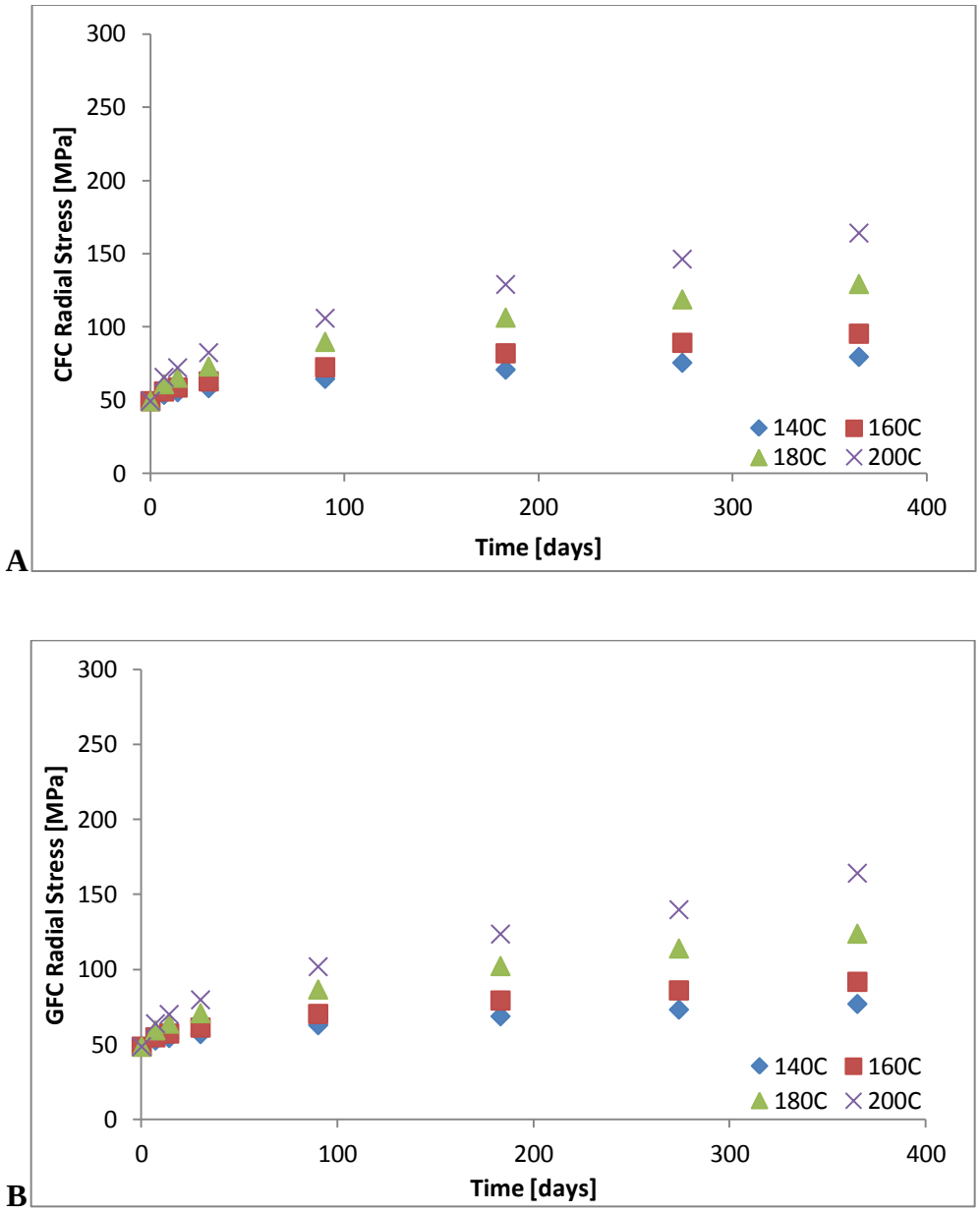

Figure 7.5. (A) Maximum radial stress of the CFC measured at 45° (B) maximum radial stress of the GFC measured at 45° for square packing. The maximum radial stresses were found to be in the matrix between two fibers.

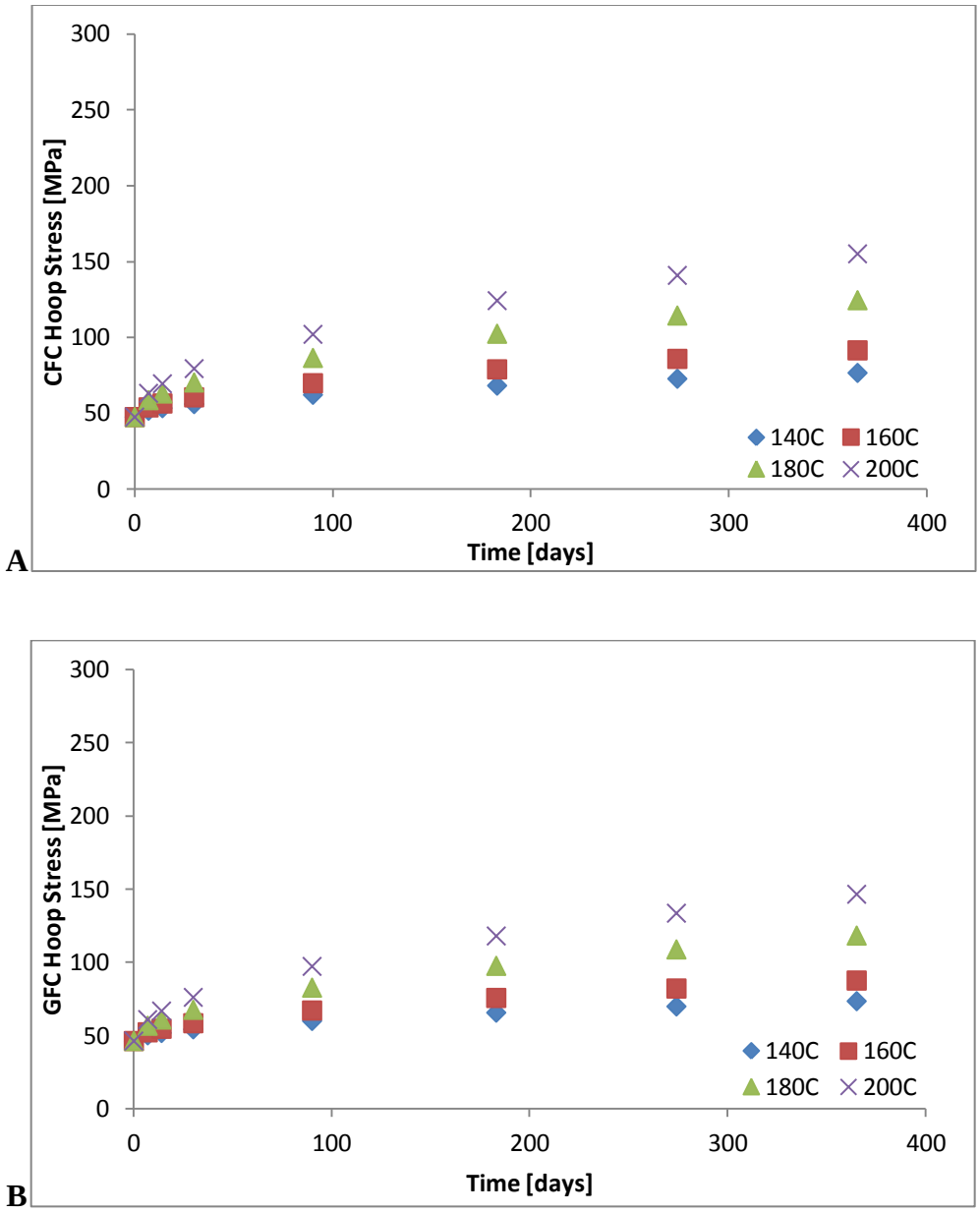

Figure 7.6: (A) Hoop stress of the CFC measured at 45° (B) hoop stress of the GFC measured at 45° for square packing.

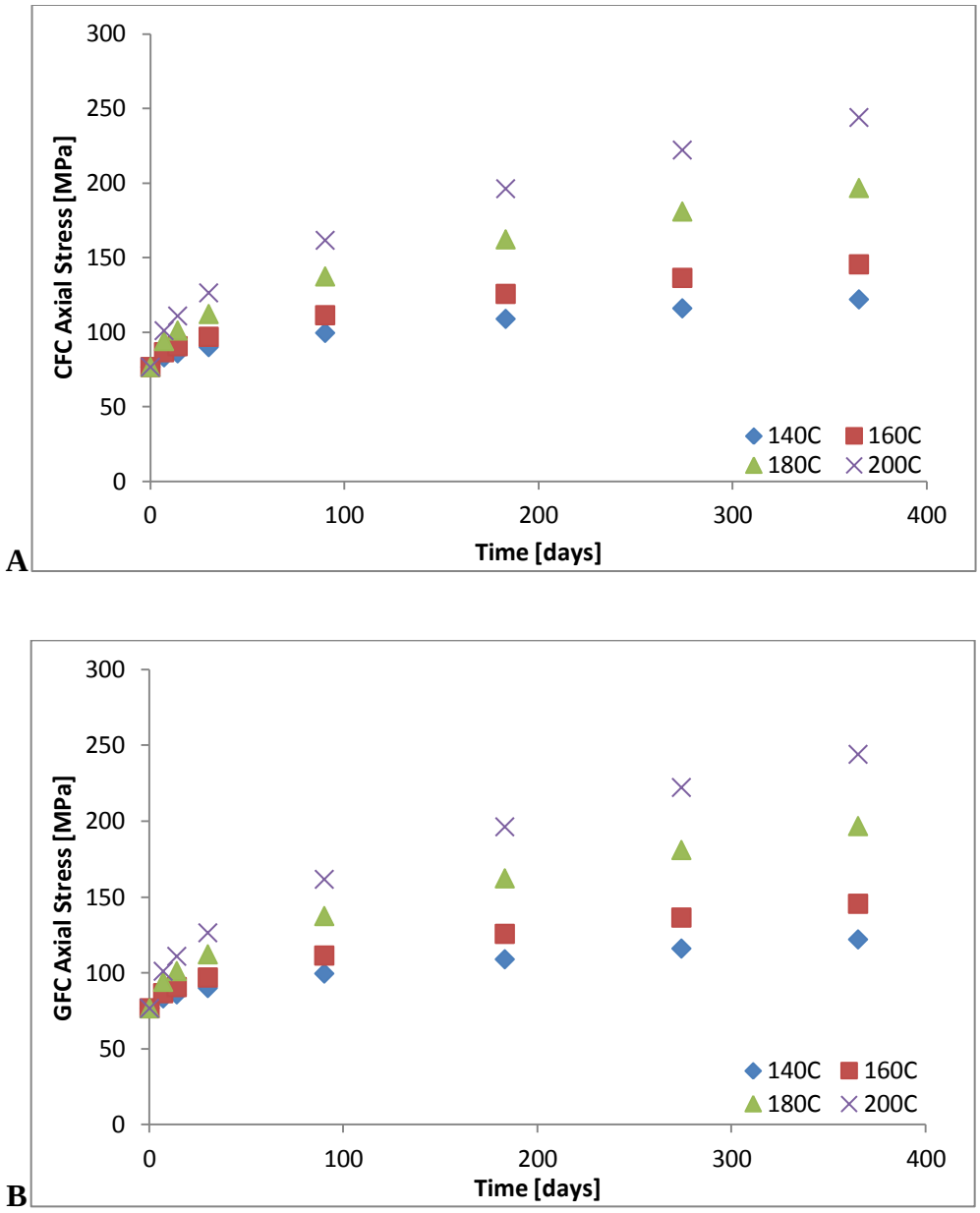

Figure 7.7: (A) Axial stress of the CFC measured at 45° (B) axial stress of the GFC measured at 45° for square packing.

The hoop and axial stresses calculated at a 0° were significantly lower than the stresses determined at a 45° or 30°. This can be seen in **Figure 7.8**, **Figure 7.9**, and

Figure 7.10. Stresses obtained along the 0° were in general approximately four to five times lower than stresses measured along the 45°. It should be noted here that all stresses presented were taken after aging and cooling back down to RT.

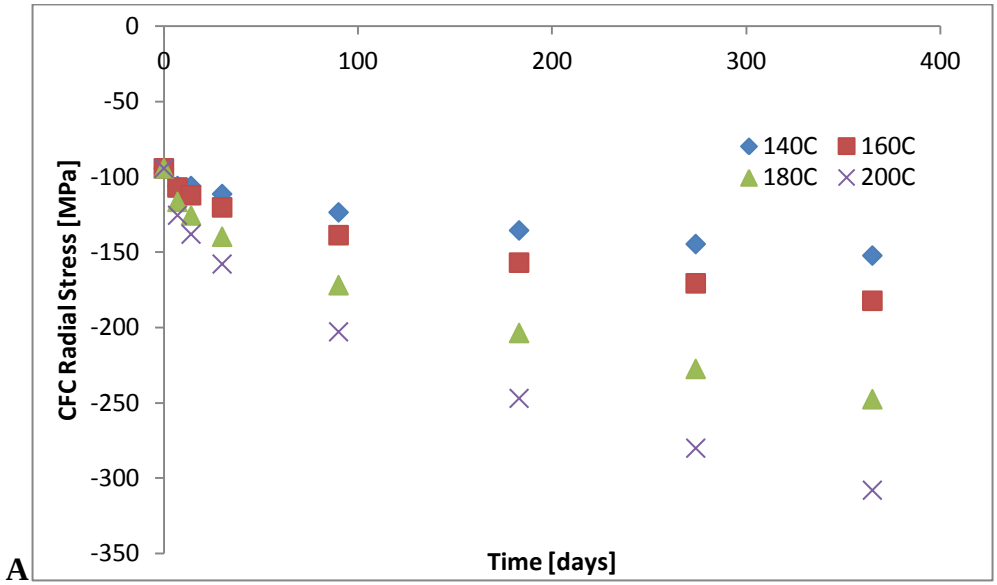

A

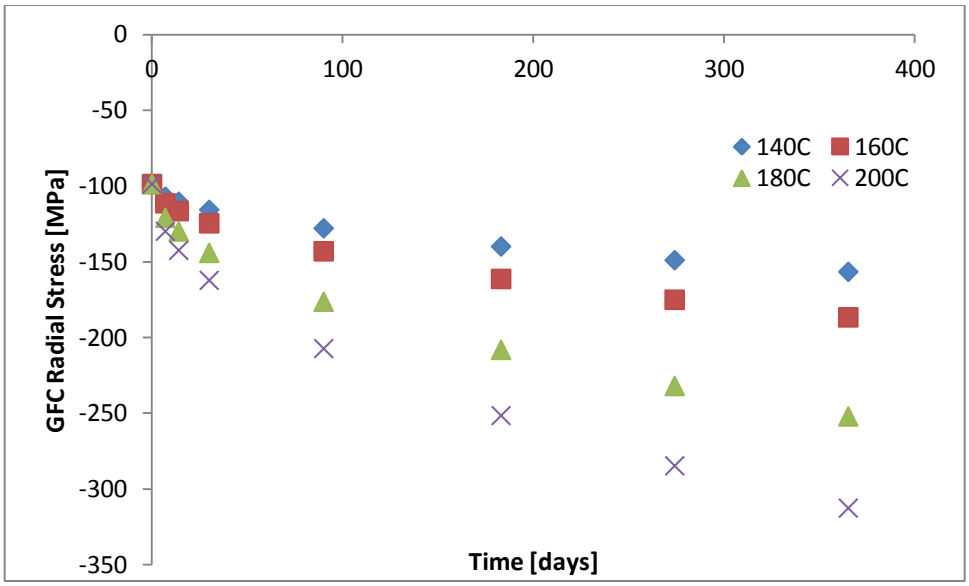

B

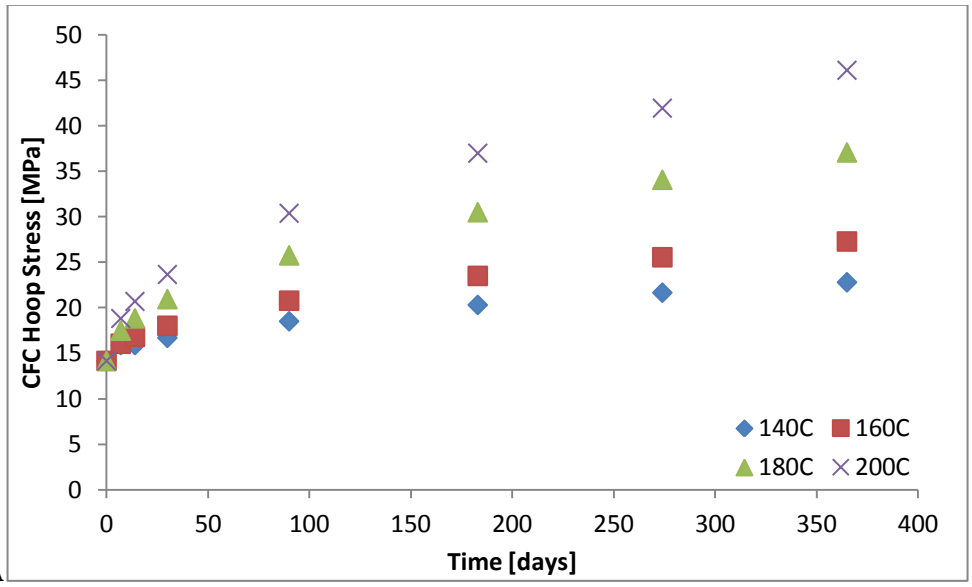

A

Figure 7.8: (A) Maximum radial stress of the CFC at 0° (B) maximum radial stress of the GFC measured at 0° for square packing. The maximum radial stresses were found to be in the matrix between two fibers.

B

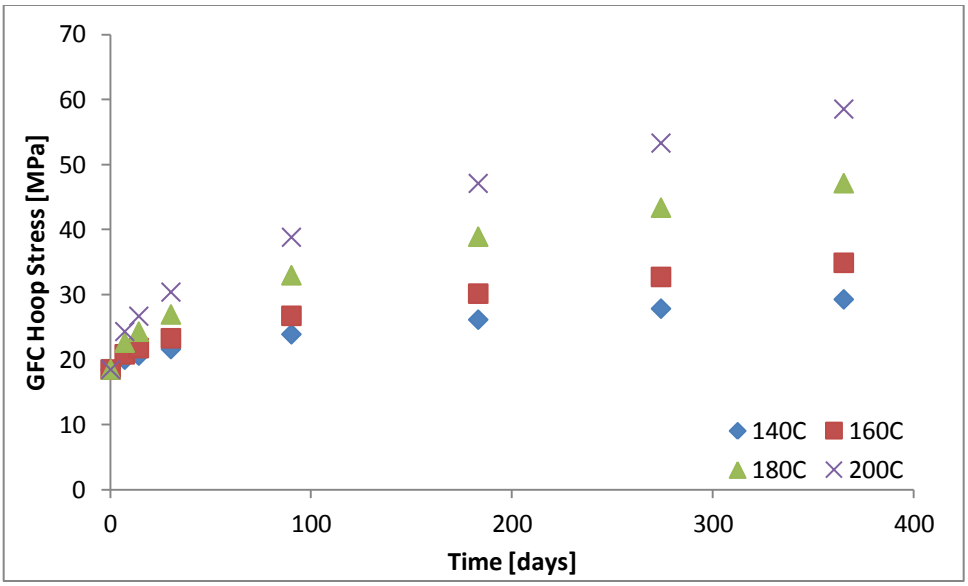

Figure 7.9: (A) Hoop stress of the CFC at 0° (B) hoop stress of the GFC at 0° for square fiber packing.

A

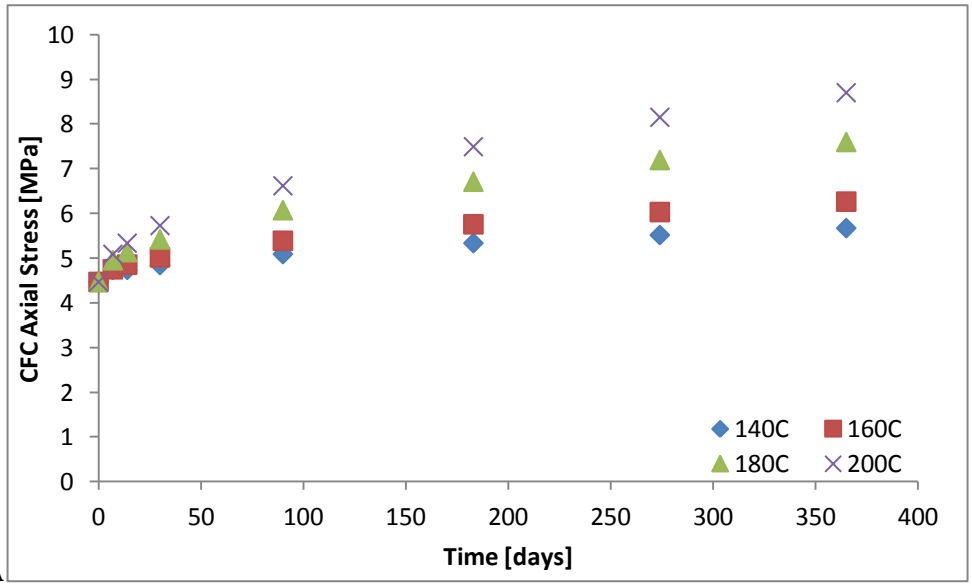

B 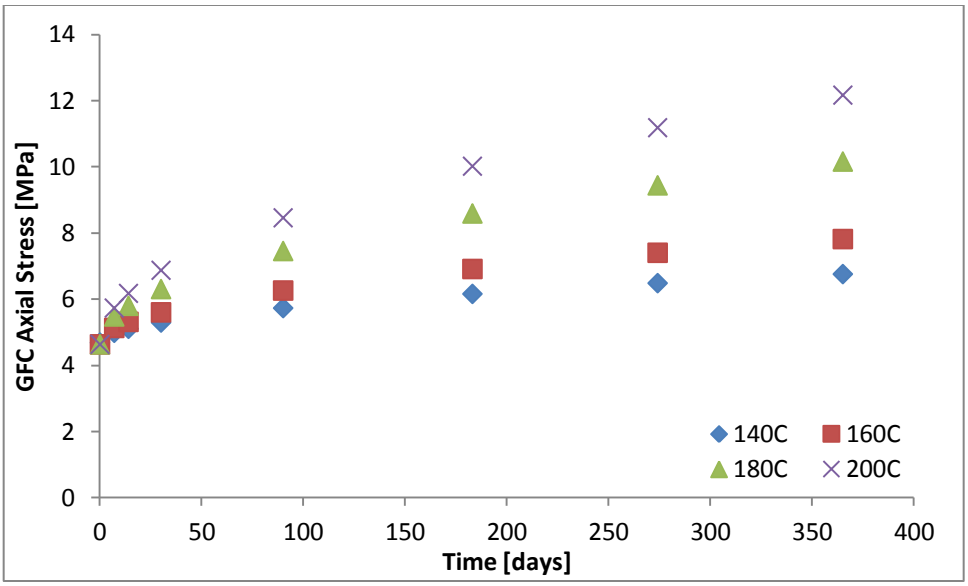

Figure 7.10: (A) Axial stress of the CFC at 0° (B) axial stress of the GFC at 0° for square fiber packing.

The hexagonal fiber packing arrangement stresses were less than square fiber packing arrangement. The radial, hoop and axial residual stresses measured along the 30° for the CFC can be seen in **Figure 7.11**, **Figure 7.12**, and **Figure 7.13**. The lower observed residual stresses found in hexagonal packing have been observed before up to a certain percent of fiber volume fraction [10]. The lower stresses observed for the hexagonal fiber packing arrangement was independent of direction. Since the hexagonal packing showed lower stresses, only the stresses measured at a 30° are presented here. This is because the hexagonal packing in general showed lower stresses, and as presented above, the maximum stress was found to be measured at the greatest distance between two fibers. In this case that is the 30° direction. A comparison of the square and

hexagonal fiber packing arrangements can be found in **Figure 7.14**. For the comparison, only the axial stresses are shown, as the axial stresses were the greatest.

A

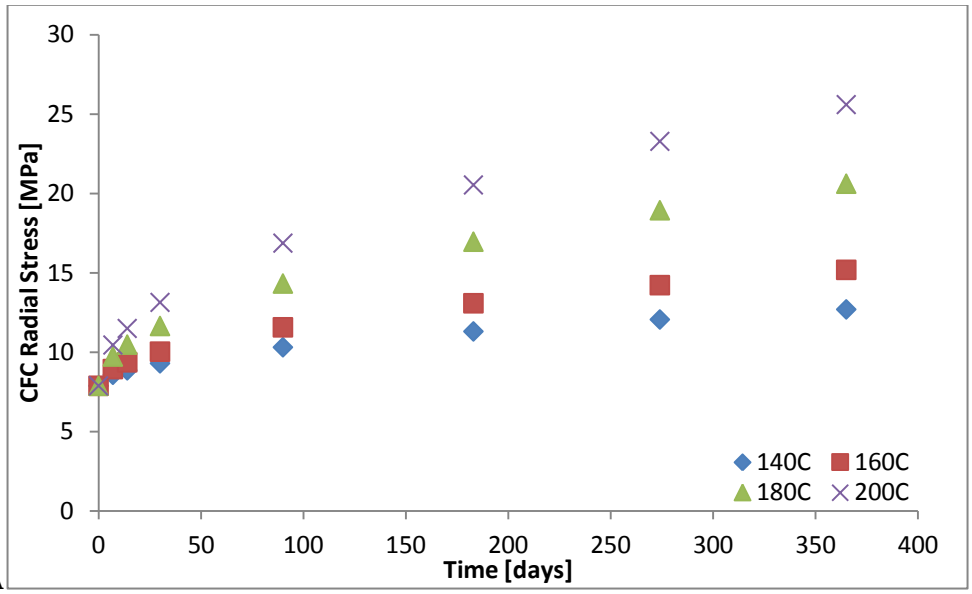

B

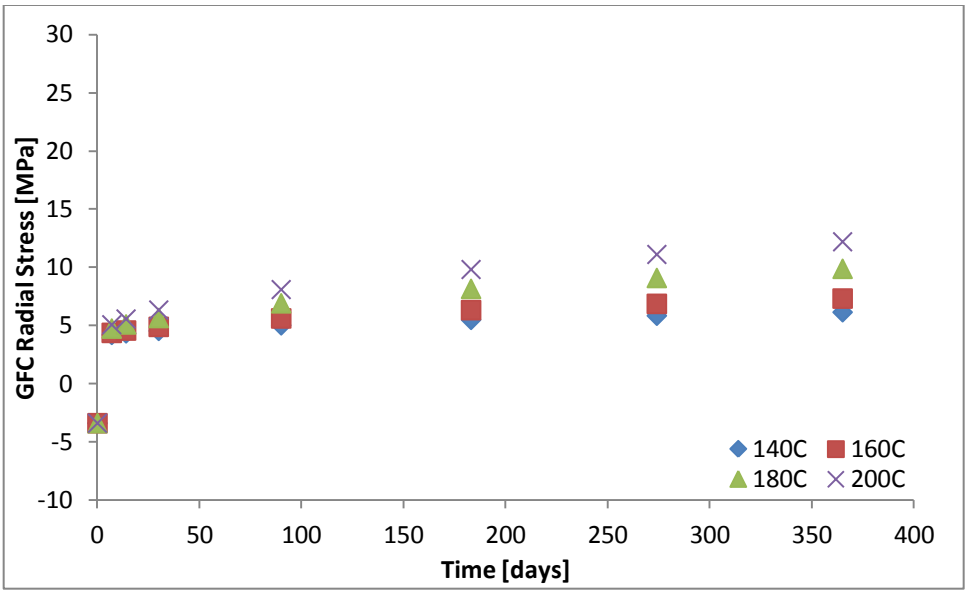

Figure 7.11: (A) Maximum radial stress of the CFC measured at 30° (B) maximum radial stress of the CFC measured at 30° for hexagonal packing. The maximum radial stresses were found to be in the matrix between two fibers.

A

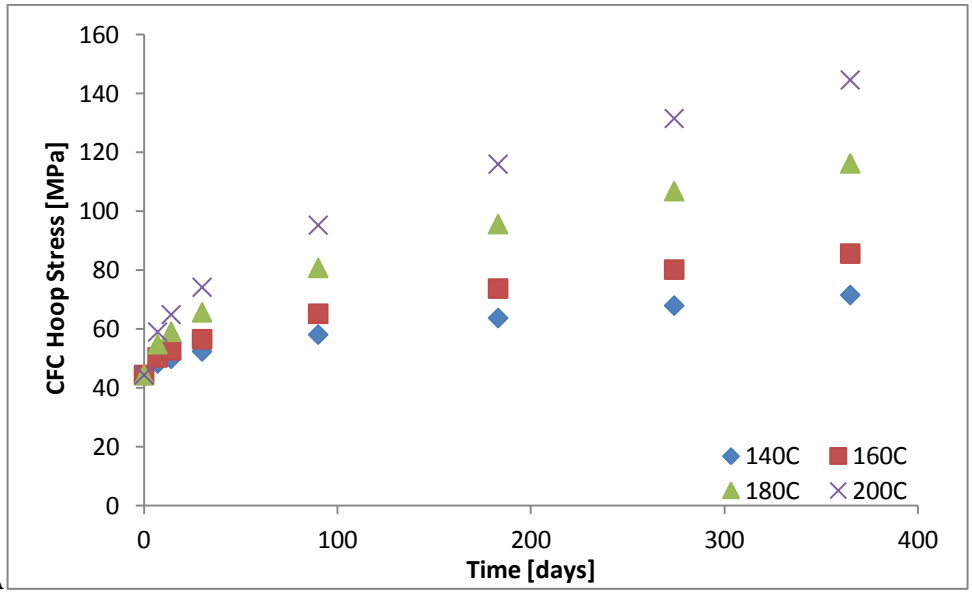

B

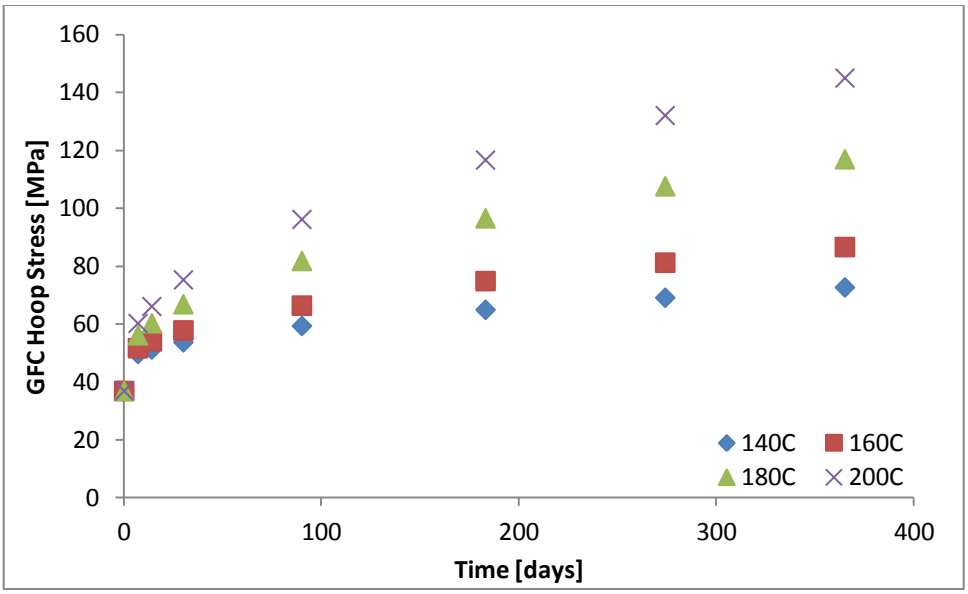

Figure 7.12: (A) Hoop stress of the CFC at 30° (B) hoop stress of the GFC at 30° for hexagonal fiber packing.

A

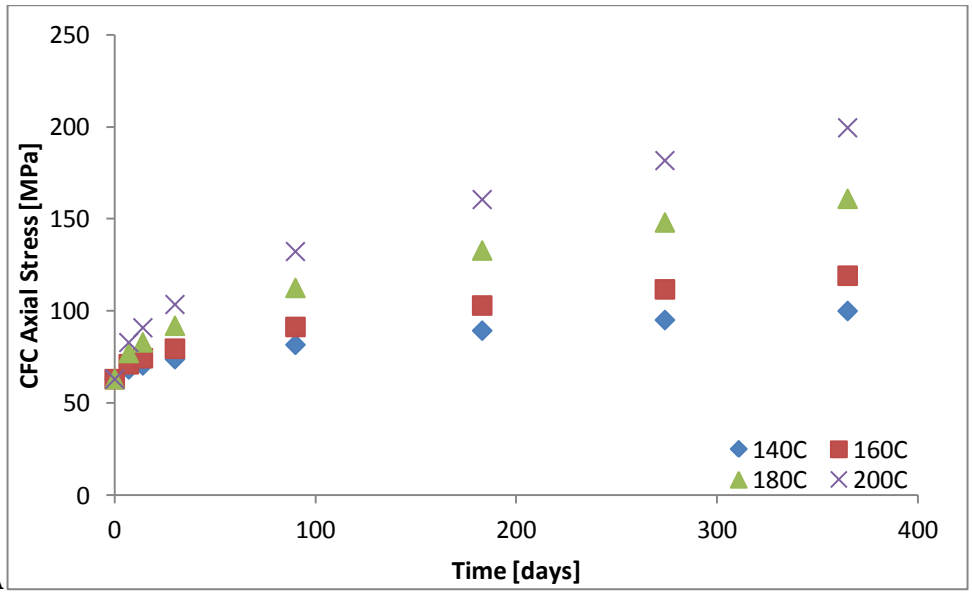

B

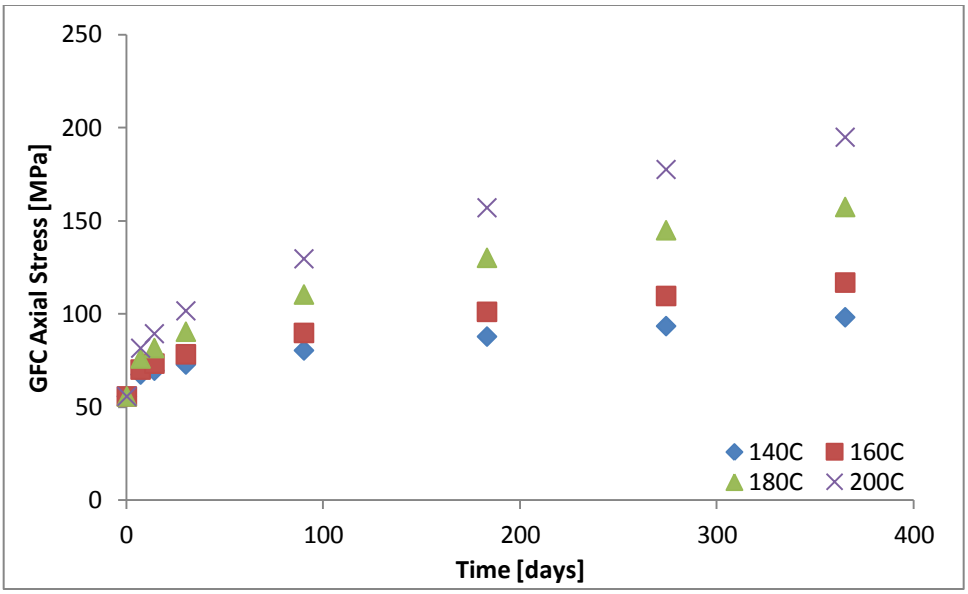

Figure 7.13: (A) Axial stress of the CFC at 30° (B) axial stress of the GFC at 30° for hexagonal fiber packing.

A

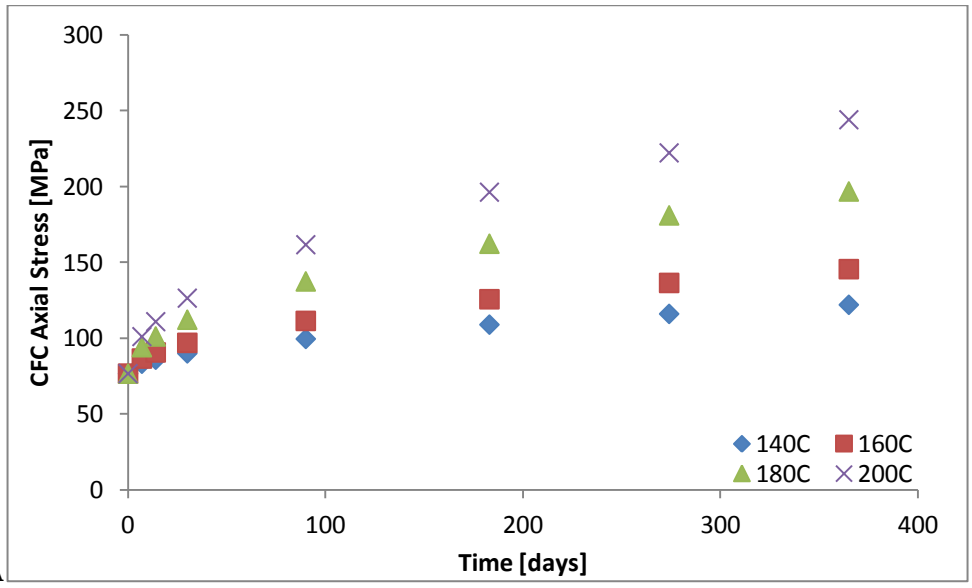

B

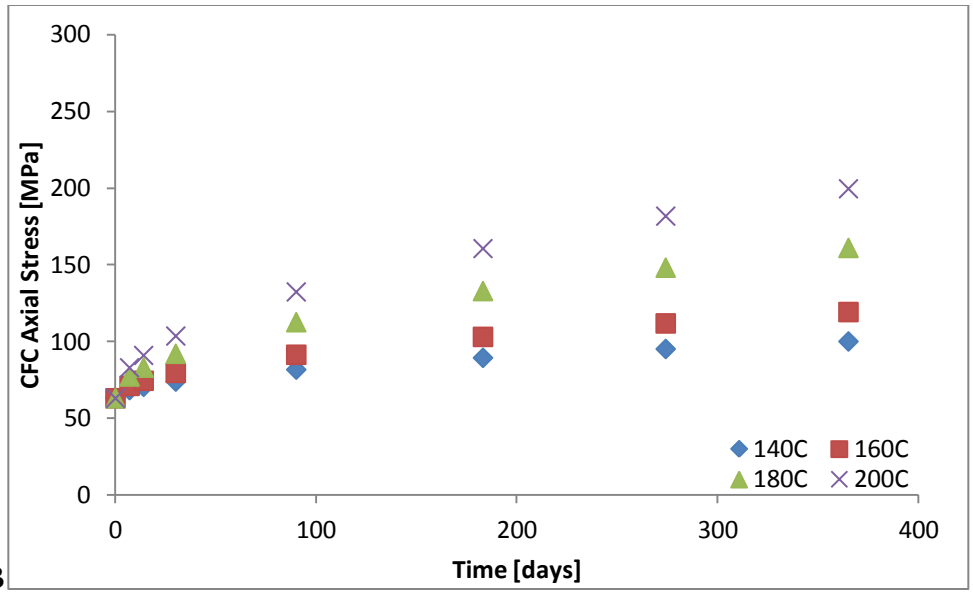

Figure 7.14: (A) Axial stress of a the CFC square packing at 45° (B) axial stress of the hexagonal packing CFC at 30°.

All the residual stresses created from aging at 140°C were relatively small compared to higher temperatures. It is possible that these stresses are low enough that there was no significant impact on flexural performance. These FE trends reflect experiment where no decrease in flexural load was observed. However, for aging temperatures above 160°C, a full year of aging increases the residual stresses by over 100%, and could easily affect flexural performance. At these high stresses it is possible that the matrix could delaminate from the fibers. This could account for the reduction in stiffness observed in the hybrid composite rods aged at 180°C (**Figure 5.3**). Burks *et al.* observed fiber/matrix delamination in a previous study [14]. SEM pictures revealed significantly degraded interfacial quality after twelve months of aging, which reduced load transfer. However, it should be stated that the stresses may account for a reduction in

load at failure, but probably do not account for the rapid decrease in flexural load at failure observed at twelve months. At this time length, there is a sudden rapid decrease in load at failure but there is only a modest increase in residual stresses. This suggests there is a change in mechanism of failure from physical aging to something else, such as chemical aging. It is possible as Burks has shown that thermo-oxidation results in loss of matrix at the surface which creates loose fibers and extensive surface damage [14]. This surface damage cannot be overlooked and must have some effect on the mechanical performance of the hybrid composite rod.

A higher temperature results in more significant dimensional relaxations, and therefore an increase in residual. However, at the lower temperatures (i.e. below 160°C), the relaxation is relatively insubstantial, and behaves asymptotically quickly. This was observed in experiment for the neat resin, where a decrease in load at failure was observed after the first week of aging, but then it was relatively unchanged at longer aging times (**Figure 6.10**). At higher temperatures, namely 180°C, there is a large reduction in load at failure in the initial weeks of aging, and then a modest decrease as aging continues. This makes sense, as the FE model shows a continual significant increase in residual stresses with aging.

A comparison of residual stresses accumulated from aging can be found in **Figure 7.15**. It can be seen that with aging temperature the residual stresses increase significantly. It appears to be an exponential increase. A comparison of the radial, hoop and axial residual stresses as a function of time can be seen in **Figure 7.16**. The residual

stresses are shown for the composite aged up to one year at 180°C. It can be seen that the axial stresses are the greatest, followed by hoop stresses, then radial.

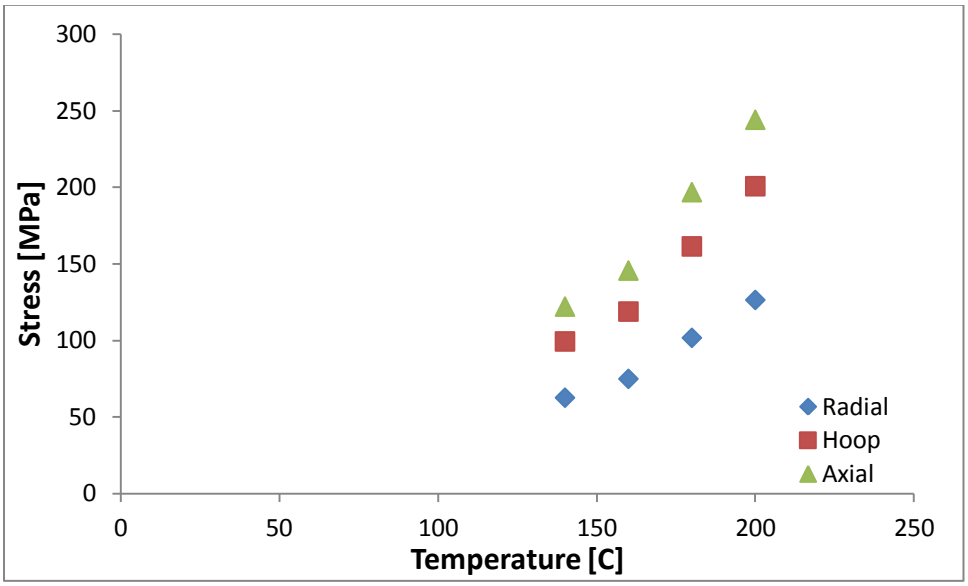

Figure 7.15: Comparison of stresses for CFC aged for 12 months at a 45° for the square fiber packing.

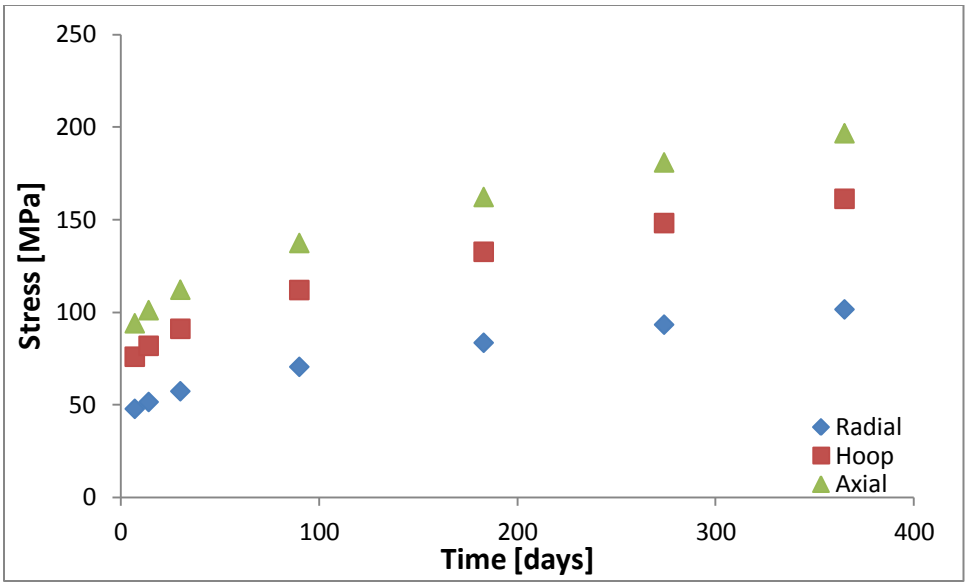

Figure 7.16: Comparison of CFC axial stresses for a specimen aged up to a year at 180°C at a 45° for the square fiber packing.

It should be noted here that the model does not account for post curing. In the manufacture of the hybrid composite rods, curing is done by pultrusion. The accelerated curing performed in pultrusion can leave behind some unreacted constituents [113]. Therefore as aging takes place, the unreacted constituents go through post curing. This process is thermally activated; as temperature increases, so does the rate of post curing. Post curing can help account for some discrepancies between the FE model and the experiment. After aging at 140°C there was a slight increase in load at failure, indicative of post curing, and the deterioration of flexural modulus and load at failure is negligible as seen in **Figure 5.3**. Yet, the FE model shows there is an increase in all the residual stresses. The increase in residual stresses shown in the FE model is probably compensated for by post curing of the resin. Contrary to this, at 180°C, there appears to

be a measurable decrease in load at failure even after only three months of aging. This suggests that the rate at which shrinkage is generating residual stresses may be exceeding the rate at which post curing is strengthening the matrix.

The residual stresses created upon cooling after curing are due to a mismatch in CTE between the fibers and the matrix. Upon reheating from RT, there is a relaxation of the stresses. With higher temperatures there is a more significant relaxation. If physical aging, or volumetric shrinkage, were not included in the model, there would be no build up of residual stresses. This would result in inaccurate residual stresses after cooling back down to room temperature. In fact, the difference between curing stresses (no physical aging), and a year of physical aging would be minimal.

The increase in residual stress follows the dimensional relaxation. Therefore, at higher temperatures, where the relaxation is more significant and faster, the residual stresses increase faster and reach greater values. However, the shear relaxation relieves stresses, but has been estimated based on previous works. The τ_{shear} could potentially be faster and more significant than has been shown here. That would result in lower observed increases in residual stresses due to more shear relaxation of the stress. On the other hand, it is possible the shear relaxations are slower than have been estimated which would result in greater residual stresses. Despite this, it is clear from the FE model that the dimensional relaxation has a much more significant effect on the residual stresses from aging, than the shear relaxation. Consequently the residual stresses increase with temperature and time.

7.3 Axis Symmetric Model

The axis symmetric model was developed as an alternative means to characterize the residual stresses created from physical aging. The concept behind this model is that, with enough layers of fiber and matrix, the innermost layer of fiber and matrix would be surrounded by what would equate to an average of the composite material properties. In other words, the innermost fiber and matrix would be surrounded by "composite" and it would be similar to looking at a single fiber with surrounding matrix in the bulk composite. A diagram of this can be found in **Figure 7.17**. In **Figure 7.17** the fiber and matrix are the innermost layers of the model and the average composite properties are the out layers that are meant to represent the composite as a whole. The stresses are characterized in the matrix portion of **Figure 7.17**.

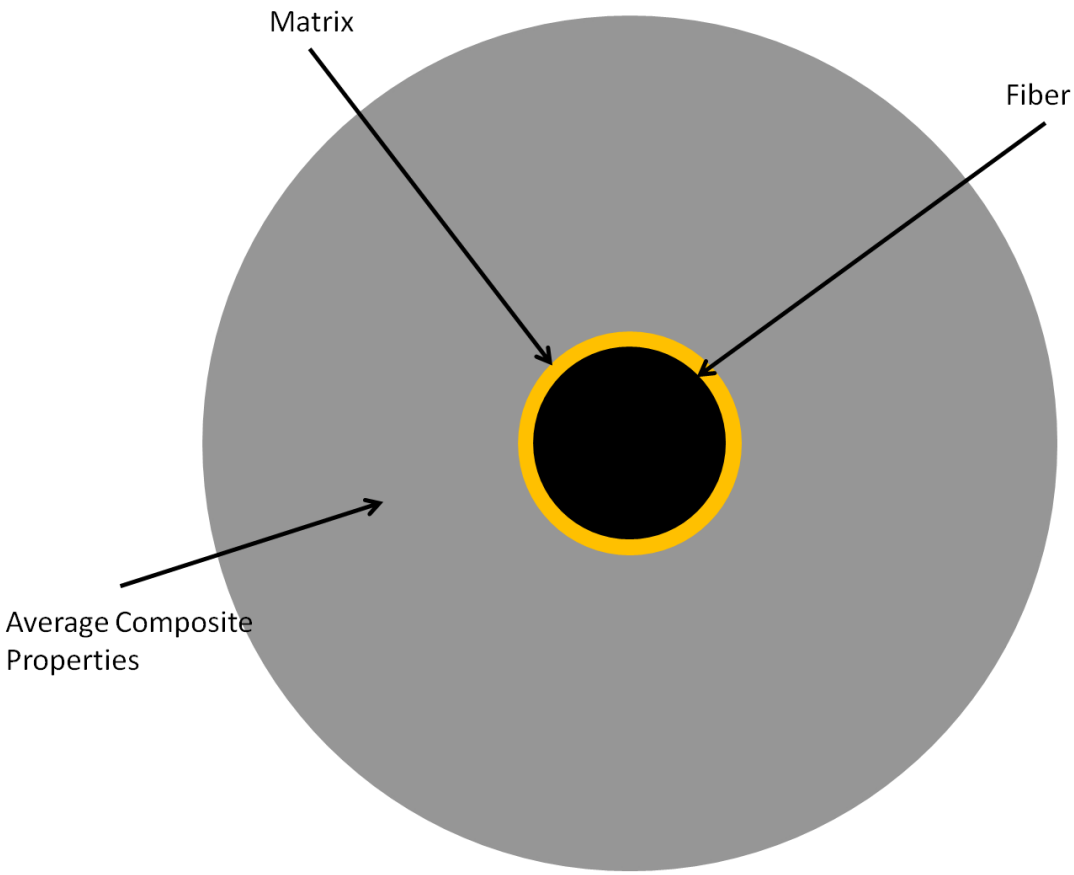

Figure 7.17: Schematic of what the axis symmetric FE model represents.

The way the model was developed was such that the model would comprise of rings, alternating between fiber and matrix. To ensure that the fiber volume fraction was constant, there were two different models developed. One had the fiber ring thickness constant, allowing for the matrix ring thickness variable, and the other model is just the opposite. The matrix ring thickness is held constant with a variable fiber ring thickness.

Convergence of the model was measured as a function of number of rings and can be seen in **Figure 7.18** and **Figure 7.19**. When the stresses were unaffected by the

inclusion of more rings, convergence was said to be achieved. The stresses were characterized only after cure cool down. There was no physical aging accounted for when considering convergence. It can be seen however, that even after 34 rings, convergence was still not fully achieved. At this point, the model was reaching the computer's physical limit, and it would run out of physical memory. Meshing could be altered, but could result in erroneous data.

It is still unclear what the meaning of this model is, if any. However, it is quite possible with the correct manipulations that it could become a very useful model. If a model could be made such that a single fiber is considered in the bulk of the material, instead of using micromechanics, better insight as to stresses developed could be achieved. This model is a step in the right direction, but as can be seen, the stresses overestimate a little too much. If these stresses could be reduced, maybe by manipulation of the material properties, perhaps a true average of the composite properties could be achieved.

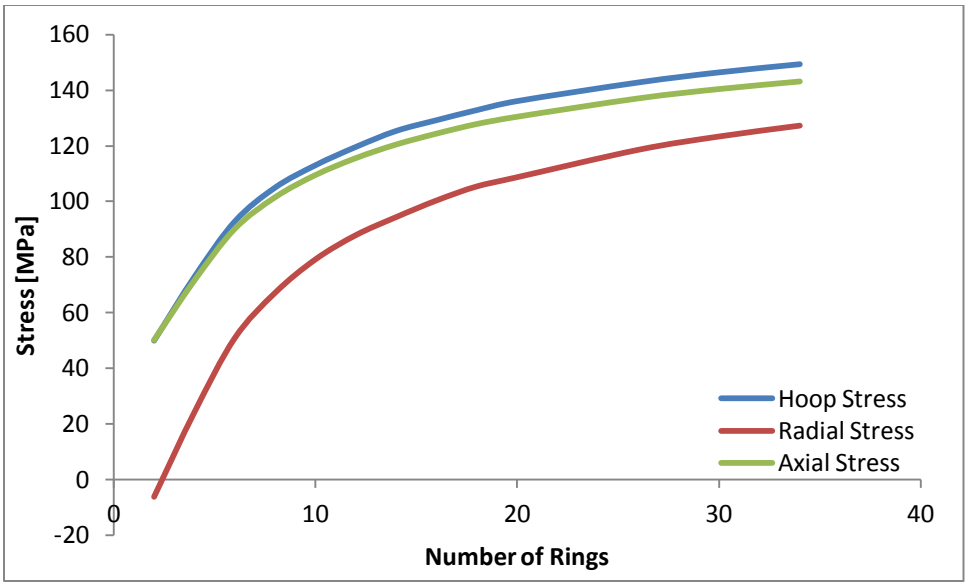

Figure 7.18: Stress convergence plot of the CFC axis symmetric model with a constant fiber radius.

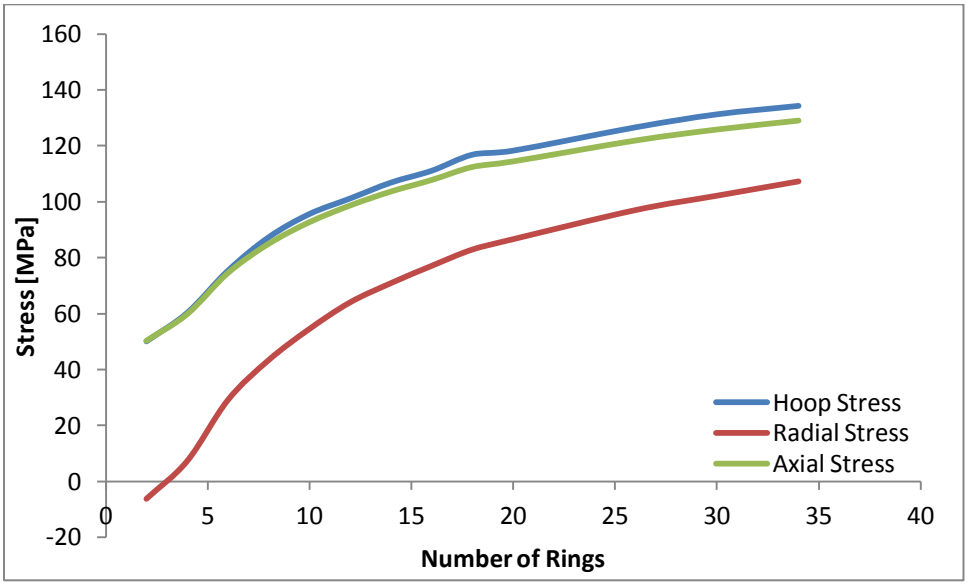

Figure 7.19: Stress convergence plot of CFC axis symmetric model with a constant matrix radius.

The convergence plots show what the stresses would be at 0 time of aging. Compared to the FE plots generated in the previous section, they are significantly larger. The RVE models from the previous section showed stress of about 55-60 MPa, while the axis symmetric model has stresses converging to a stress of nearly twice that. Interestingly, whether the matrix rings or fiber rings were held at a constant thickness had no real impact on the stresses after aging as seen in **Figure 7.20** and **Figure 7.21**. However, it did have an impact on convergence. It appears having a constant fiber ring thickness will allow the model to converge faster than with a constant matrix ring thickness. In addition, it appears that the stresses converge to a higher value with a constant fiber ring thickness.

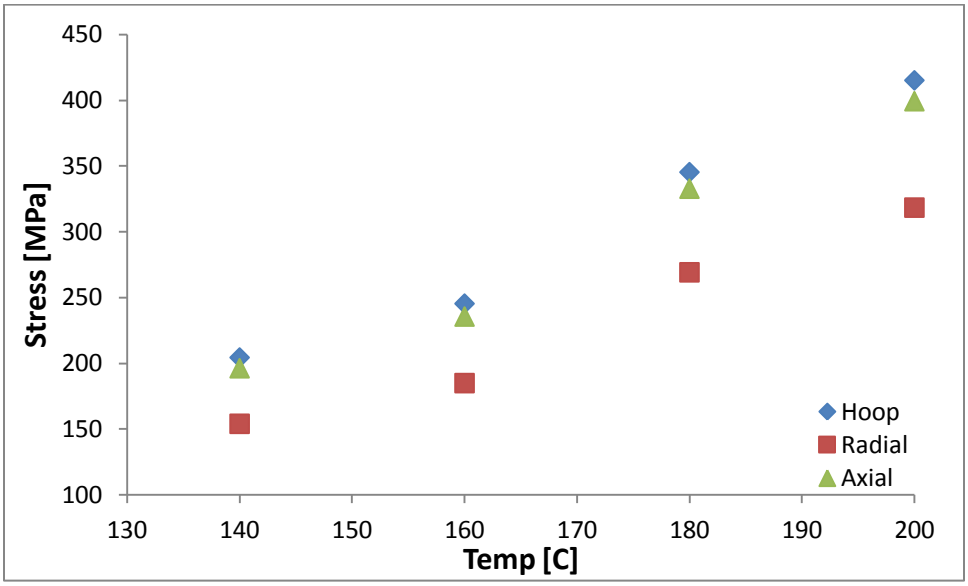

Figure 7.20: Stresses created from aging for 12 months of the CFC axis symmetric model with a constant fiber radius.

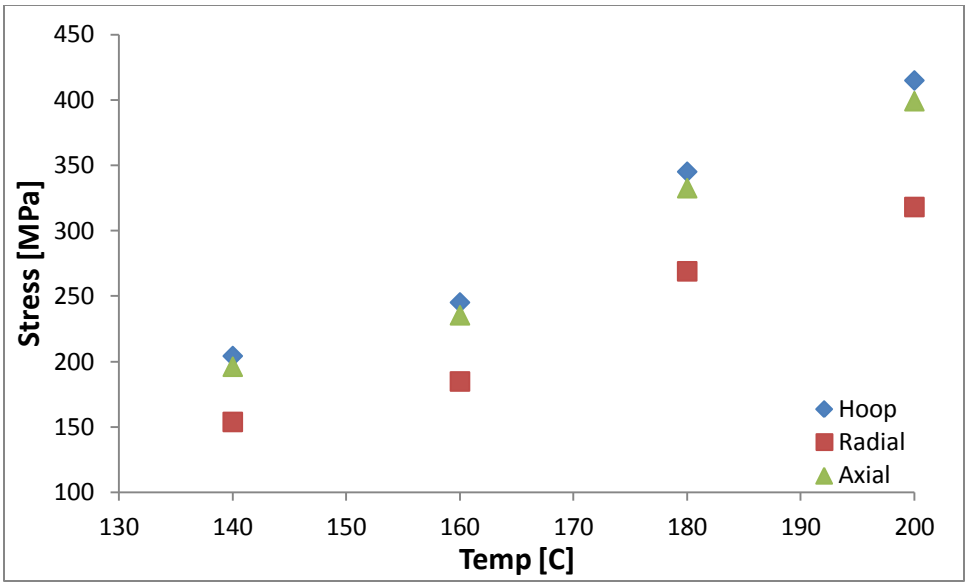

Figure 7.21: Stresses created from aging for 12 months of the CFC axis symmetric model with a constant matrix radius.

7.4 Discussion of the RVE Model

Since only temperature and physical aging were modeled, the RVE developed for this study was made to be 2-D plane strain. This was also used to accommodate the physical limit of the computer. However, this problem should eventually be modeled in three dimensions. There is an axial strain lost when assuming plane strain which is not actually the case in reality with the hybrid composite rods. This assumption is valid however. FE models in general are predictive in nature, and never truly 100% accurate. For this reason assumptions and simplifications are made to reduce on computation time, and model development time. Plane strain in this case is a valid assumption because axially the model is always the same. It should be noted here that, for the glass fiber

composite models, plane strain could potentially be a very accurate assumption. Carbon fiber has a slight negative coefficient of thermal expansion in the axial direction. Overall, the CFC may hinder the GFC expansion in the axial direction.

A second assumption made for this study was the shear relaxation times. Creep testing was not performed on the neat resin in this study. Thus a way to estimate the shear relaxations was needed. This was justified through the use of a study Gentz had previously performed [91] where the dimensional relaxation activation energy was equivalent to the shear relaxation activation energy. In other words, the slopes of the shear relaxation and dimensional relaxations were equivalent when plotted using the Arrhenius equation. However, the shear relaxations were shifted down on the same plot, but some arithmetic difference exists. In this study, the dimensional relaxations were performed; therefore the arithmetic shift between the dimensional and shear relaxations from Gentz's study could be applied to this study. This was deemed the best approximation of the shear relaxations, and therefore used. It should be noted, as discussed in Section 7.4, that the shear relaxations have a large effect on the internal residual stresses. This means a slight change in the shear relaxation times could have a large impact on the internal residual stresses. This is the reason that the shear relaxations needed to be included in the FE model. The approximation for the shear relaxations is believed to be the best that it can be, albeit still only an approximation. This means the internal residual stresses predicted by the FE model may be not completely accurate. However, the trends that the FE model predict are believed to be correct, which is what

the FE model was meant to show. Thus the model is useful for this study and shows quite clearly the trends of physical aging on the hybrid composite rods.

The model also does not account for post curing. It was shown in Chapters 4 and 5 that post curing has a large effect on both the neat resin and the hybrid composite rods. Unreacted constituents react, and improve the polymer matrix, thereby stiffening the hybrid composite rod and increasing the strength. Physical aging still occurs during the time that post curing is occurring, but in temperature dependence, post curing can be the dominant mechanism for a period of time. Developing a model that incorporates post curing was not within the scope of this study and was therefore neglected.

There is a more basic model that could have been used: an RUC that includes a two quarter fibers with matrix in between. A schematic of this can be seen in **Figure 22**. The reason an RUC was not used for this study was that the periodic boundary conditions required for this model produced erroneous stresses. The radial stresses produced from this model after aging created a discontinuity at the interface between the matrix and the fiber. This is a physical impossibility. Benedikt was able to create an RUC and consider physical aging because strains from mesoscale modeling were used as inputs for the boundary conditions. Benedikt performed multiscale modeling to achieve the correct inputs for the strains created from physical aging. This allowed for the proper production of boundary conditions that contain both periodicity and symmetry. Without those correct inputs, the proper boundary conditions cannot be applied, which yields impossible stresses after aging. An RVE was developed for that reason, and Pindera and Drago

showed that an RVE can converge to the same answer as the periodic RUC with the correct number of fibers in the array [99]. Thus the RVE was developed where the stresses were correct at the interface between the fiber and matrix.

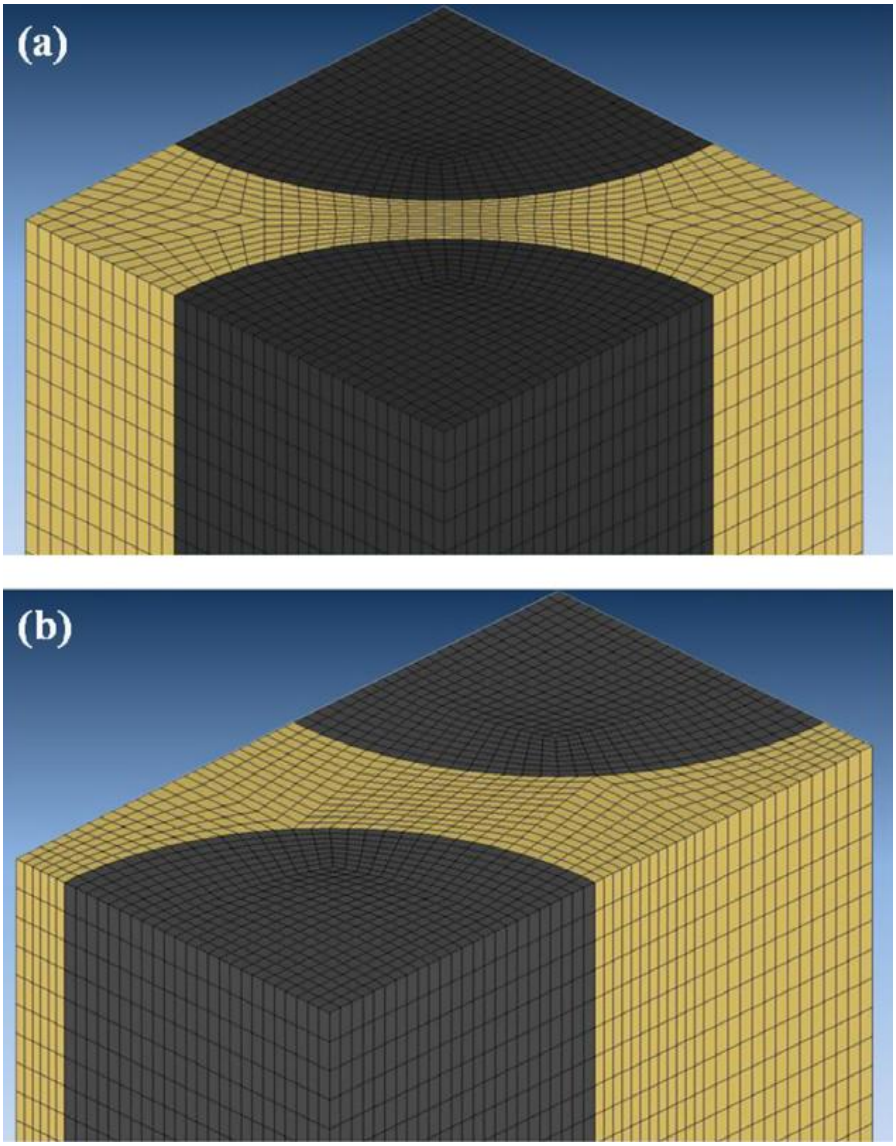

Figure 7.22: A schematic of an (a) square RUC and (b) a hexagonal RUC.[12]

[12] From [10]

7.5 CONCLUSIONS

The aging in atmospheric high temperature of a polymer core composite conductor and neat resin was performed. The activation energy for the aging process of the neat resin was found to be 74.8 kJ/mol, which is consistent with literature. Aging of a hybrid rod and neat resin at 180°C had a dramatic effect. After a full year of aging the flexural strength was reduced by 75% for the composite rod. After three months of aging the neat resin load at failure was reduced by over 60%. Aging at 140°C, on the other hand, had no observable detrimental effect up to one year of aging on the hybrid composite rod, but a moderate effect on the neat resin which showed a little over 20% reduction in load at failure after only three months of aging. The absence of reduction in load at failure for the hybrid composite rod aged at 140°C may be due to post curing, and an insignificant amount of residual stress build up. The residual stresses of aging were characterized through micromechanics with the physical aging accounted for via an applied strain. The stress relaxation times were estimated, albeit it is believed the estimation was valid because: 1). the stresses found from the finite element model reflected the mechanical performance of the neat resin, and 2) previous work done had found that the activation energy of both dimensional relaxations and shear relaxations were equivalent. Aging at 140°C and 16 °C showed only a modest increase in residual stresses after one year of aging. At higher temperatures, namely 180°C and 200°C, there was a significant impact on the residual stresses. In fact, stresses were increased over 100% after one year. This large increase in residual stresses could easily affect the

mechanical performance of the hybrid composite rods. In fact, the residual stresses are possibly high enough that the fiber/matrix interfaces had been significantly damaged and hindered load transfer, thereby reducing the overall composite stiffness. However, the internal residual stresses most likely cannot account for the sudden and rapid decrease in load at failure at twelve months of aging. This is most likely the result of a joint effect between chemical and physical aging. Thermo-oxidation, or chemical aging, results in extensive surface damage. Coupled with the large residual internal stresses, the rapid decrease in load at failure could be accounted for. This study did not cover chemical aging and therefore, more research is needed to ascertain the effect of chemical aging, physical aging, and the joint effect of both on the performance of the hybrid composite rod.

An axis symmetric FE model was also developed as a novel way to model a composite. The purpose was to create a model in which a single fiber in matrix could be observed in a surrounding bulk composite, at the micro scale. Rings of alternating fiber and matrix would represent the overall bulk composite. This model would be able to replace RVEs and RUCs. However, it was found that the model takes numerous rings for stress convergence, and the stress it converges to was over predicted by at least two times. This means this model as it is, is inaccurate. However, with more manipulation it is possible this model could become accurate and worthwhile.

CHAPTER 8: CONCLUSIONS AND RECOMMENDATIONS FOR FUTURE RESEARCH

8.1 CONCLUSIONS

8.1.1 MAJOR CONCLUSION OF THIS STUDY

The main objective of this research was to determine the most damaging aging conditions for PCCCs in service by characterizing their aging. This was accomplished by investigating the effects of ozone and temperature on the resistance to aging of PCCC rods and their epoxy resin. The study led to the following most important conclusion:

- The mechanical degradation of the neat resin and PCCC rod specimens due to aging is thermally driven and not significantly affected by the presence of ozone, both at room and elevated temperatures up to ninety days of environmental exposure.

8.1.2 OTHER IMPORTANT CONCLUSIONS

The first condition studied was 1% ozone at RT. 1% ozone was chosen because it is a high concentration that would allow for accelerated testing, but also possible. Coronal discharges could potentially create 1% ozone that the conductor would then

experience. Aside from characterizing the aging of the neat resin and hybrid composite rod in 1% ozone, another goal of this specific study was to find a high temperature epoxy that would potentially be used as the matrix of the PMC. This is important because it allows for research independence from the hybrid composite rod manufacturer. New materials, such as nanocomposites could be developed that could be more thermally stable, or more fatigue resistant. Therefore, from this study it was found that:

- The neat resin used in this study was very similar; if not the same resin used in the hybrid composite rods from the use of FTIR.
- Aging the neat resin in 1% ozone at RT had no real detrimental effect for up to three months of aging. It is possible that there is an ozone effect at greater time lengths than ninety days, albeit this study did not go to longer time lengths.
- The PCCC rods exhibited similar mechanical behavior as seen in the resins after aging in 1% ozone. This means that there was no observable detrimental effect on the hybrid composite rods.
- Most importantly, both the epoxy and the rods were found to be quite resistant to aging in 1% ozone at room temperature for up to three months.

The aging in atmospheric high temperature of 140°C had minimal effect on the hybrid composite rods and neat resin. Aging at 180°C on the other hand had a drastic effect. These temperatures are high, but it is possible the transmission lines could experience them especially during peak usage hours. This study showed:

- Aging the hybrid composite rods at atmospheric 140°C had no detrimental effect. In fact, the stiffness was modestly increased, and the load at failure from flexure tests was not reduced due to post curing.
- Aging the neat resin in 140°C had a detrimental effect on the neat resin because post curing was not present. The neat resin had been put through a rigorous cure cycle that mitigated post curing. The load at failure was reduced by a little over 20% after three months of aging.
- Aging the hybrid composite rod in 180°C had a strong effect. The thermo-oxidation resulted in loss of resin on the surfacing yielding exposed glass fibers.
- Aging the hybrid composite rods resulted in initial decrease in hardness, but no prominent trend after.
- Aging at 180°C for a year reduced the flexure load at failure by 75% and reduced the stiffness by approximately 15% of the hybrid composite rods.
- The neat resin load at failure was reduced over 60% after only three months of aging at 180°C.
- The activation energy for the aging process of the hybrid composite rods was 130.5 kJ/mol.

The characterization of neat resin and hybrid composite aged in atmospheric high temperature and 1% ozone at 140^{o}C yielded the following:

- The loads at failure were reduced for the neat resin specimens, but were increased for the hybrid composite rods.

- Both neat resin and hybrid composite rods exhibited an increase in stiffness due to postcure.
- The higher the temperature the more degradation that took place.
- Application of the t-test showed there was no statistical difference between the specimens aged in atmospheric 140^{o}C, and the specimens aged under both 1% ozone and 140^{o}C, with the exception of viscoelastic properties where the effect of ozone at 140°C on the polymer was clearly visible.
- Aging in air at 180°C was found to be especially damaging to both the rods and the neat resin specimens.

The major conclusions found from FE modeling of the residual stresses developed during the physical aging process of the hybrid composite rods are:

- The activation energy for the aging process of the neat resin is 74.8 kJ/mol.
- The absence of reduction in load at failure for the hybrid composite rod aged at 140°C may be due to post curing, and an insignificant amount of residual stress build up.
- Aging at 140°C and 160°C showed only a modest increase in residual stresses after one year of aging.
- Physical aging at 180°C and 200°C results in an increase of over 100% after one year of internal residual stress.
- The internal residual stresses most likely cannot account for the sudden and rapid decrease in load at failure at twelve months of aging. This is most likely the result of a joint effect between chemical and physical aging.

Axis symmetric FE modeling took numerous rings of alternating fiber and matrix properties for stress convergence. The model over predicts the stress by at least two times which means the model as it is, is inaccurate.

The most important conclusions of this research is as follows:

- The neat resin and hybrid composite rods were quite resilient to the presence of ozone, even when at a high temperature of 140°C.
- Stresses developed from aging at 140°C are insignificant enough that the mechanical performance of the hybrid composite rod would potentially be unaffected even after 50 years.
- 180°C aging of the hybrid composite rods has a very detrimental effect of the hybrid composite rods, and reduces flexure performance by 75%.
- The most damaging condition in this research was found to be high temperature i.e. 180°C and higher.
- The aging of the hybrid composite rods and neat resin has been characterized for up to three months of aging.

This work has characterized the aging of a hybrid composite rod and its matrix. This will have a significant impact for utility companies that may want to use the PCCC as an alternative for the current transmission line technology.

8.2 FUTURE RESEARCH SUGGESTIONS

It has been noted that the rapid decrease in load at failure observed when the hybrid composite rods are aged in air at 180°C is probably due to the joint effect of both physical and chemical aging. The chemical aging effect should therefore be studied in depth. This would include aging the hybrid composite rods in an inert environment, such as argon rich or under vacuum, and comparing those results to the results of when aged in air so that the thermo-oxidation effect can be understood. The chemical aging study should not be limited to this though. Other studies of chemical aging should be looked at, such as the effect humidity has on the hybrid composite rods. Some of the transmission lines will be through crop fields in which case pollutants such as insecticides will be present. The effect of these pollutants should be studied as well.

Thermal aging studies should be continued as well. The effect of thermal cycling should be studied. Transmission lines do not produce a constant operating temperature. In fact, the temperature cycles depending on how much power is being produced. During peak hours of the day, the temperature is either at the highest, or lowest. The effect of cycling the composite rod through these two peaks of high and low temperatures should be studied.

Struik has shown that physical aging can be fully reversed if the polymer is taken back above its T_g for approximate 10-20 minutes. Struik has called this rejuvenation. It would be of interest to see if there is a possibility of erasing some of the physical aging of the hybrid composite rods while in-service. This would require the utility companies to

test the results of running the line extremely hot for a given period of time. However, if some of the physical aging could be erased, it could potentially be to their benefit. This study would require aging in inert environments and periodically bringing the rods back up above T_g and mechanically testing them. The performance of these rejuvenated rods would then be compared to the mechanical performance of non-rejuvenated rods. This study would also require tensile testing at temperatures above T_g to determine if the lines would even be able to stay up at such high temperatures. It should be noted however, that this rejuvenation study only applies to physical aging. Chemical aging, or even fatigue of the lines would still be present and would not be mitigated by bringing the line up to high temperatures. In fact, chemical aging and fatigue could potentially be negatively affected.

This research has shown that high temperatures are of significant concern; a study about thermal and physical aging resistance is therefore needed. This research is very broad and would allow for a significant amount of further research. This is because to thermally stabilize the composite, a potential solution would be to implement nanoparticles. This opens up research into areas such as types of nanoparticles, dispersion of the nanoparticles, amount of nanoparticles etc. Mechanical properties of the nanocomposites would need to be studied as well, as the nanoparticles will change the composite and its properties.

However, thermally stabilizing may not be the best solution as it has been shown that chemical aging may be a significant problem as well. This means research into coatings of the hybrid composite rods would be useful. Protecting the composite from

oxidation and other forms of chemical attacks could potentially increase the life of the composite cores. This would be a significant study as well due to the broad subject. There are many different types of coatings, such as thin films, and ways to improve attaching the coating to the hybrid composite rod. It should be noted here that this study would include research into wear of the coating. The coating may protect the composite rod against chemical attacks, but it is possible that when in-service, abrasion between the coating and the aluminum strands could destroy the coating and render it useless.

Last, creep testing of the neat resin should be studied. This would result in a measured value for the shear relaxations, which would then allow for correct implementation into the FE model. This is important for the FE model and predicting the stresses developed during physical aging. In this research, the shear relaxations have been estimated, and therefore the trends of the FE model were of concern. However, with accurate shear relaxations, the FE model would be all that more accurate, and the stresses would start to become the true values.

The FE model in general could be improved in several ways. The first and obvious improvement would be creating a 3-D model. In this research, the model was limited by computing power, but without this limitation a 3-D model could be developed. This again would take the FE model even closer to true values. Another way the model could be improved would be changing the fiber orientations. Instead of modeling the idealized square or hexagonal fiber packing arrangements, random packing would be more representative of the true composite. This could be done by creating a random walk

the places the fibers randomly instead of orderly and structured. This would give valuable insight into what the stresses look like when fibers are clumped together, or where resin rich pockets accumulate. This could be started in a 2-D model, and evolve into a 3-D model. In the 3-D model, not just random placement of the fiber could be studied, but also if the fibers are aligned slightly off axis. In other words, instead of having all fibers perfectly aligned and parallel, some could be aligned slightly at an angle. This could give valuable insight into the effect of fiber alignment and packing.

Ultimately, from these suggested research areas, life prediction would be the overall goal. Predicting the life of the hybrid composite rod based on physical aging is useful, but it is not completely accurate. There are other factors, i.e. chemical aging that will drastically affect the performance and therefore life of the composite cores of the conductors. Thus, by performing the aforementioned studies a greater understanding of the performance of the composite rods in-service could be achieved. This would then result in a much more accurate prediction in the life of the hybrid composite rods.

REFERENCES

[1] Shackelford, James F. Introduction to Materials Science for Engineers. 6th ed. Upper Saddle River: Pearson Education, Inc, 2005. pp. 462-495.

[2] Lin, Yn-Hwang. Polymer Viscoelasticity Basics, Molecular Theories, Experiments and Simulations. 2nd. Singapore: World Scientific Publshing Co. Pte. Ltd., 2011.

[3] Simon, F. The condition of the undercooled fluidities and glasses. 1/2, 1931, Zeitschrift Fur Anorganische Und Allgemeine Chemie, Vol. 203, pp. 219-227.

[4] Struik, L.C.E. Physical Aging in amorphous polymers and other materials. s.l.: Gerbon to Capella a/d Ijssel, 1977.

[5] G.M. Odegard, A. Bandyopahyay. Physical aging of epoxy polymers and their composites. Compos Sci Technol 2012;72:1803-1811.

[6] M. Akay, G.R. Spratt. Evaluation of thermal ageing of a carbon fibre reinforced bismalemide. Compos Sci Technol 2008;68(15-16): 3081-3086.

[7] A. Lowe, B. Fox, V. Otieno-Alego. Interfacial aging of high temperature carbon/bismaleimide composites. Compos Part A 2002;33:1289-1292.

[8] M. Akay, G.R. Spratt, B. Meenan. The effects of long-term exposure to high temperature on the ILSS and impact performance of carbon faibre reinforced bismaleimide. Compos Sci Technol 2003;63:1053-1059.

[9] I. Ammar-Khodja, C. Picard, M. Fois, C. Marais, P. Netchitaïlo. Preliminary results on thermo-oxidative aging of multi-hole carbon/epoxy composites. Compos Sci Technol 2009;69(9):1427-1431.

[10] B. Burks, J. Middleton, M. Kumosa. Micromechanics modeling of fatigue failure mechanisms in a hybrid polymer matrix composite. Compos Sci Technol 2012;72(15):1863-1869.

[11] J. Middleton, B. Burks, T. Wells, A.M. Setters, I. Jasiuk, P. Predecki, J. Hoffman, M. Kumosa. The effect of ozone on polymer degradation in Polymer Core Composite Conductors. Polym Degrad Stab 2013;98(1): 436-445.

[12] B. Burks, D. Artmentrout, M. Kumosa.Characterization of the fatigue properties of a hybrid composite utilized in high voltage electric transmission. Compos Part A 2011;42(9):1138-1147.

[13] B. Burks, J. Middleton, D. Armentrout, M. Kumosa. Effects of excessive bending on residual tensile strength of hybrid composite rods. Compos Sci Technol 2010;70(10):1490-1496.

[14] B. Burks, M. Kumosa.The effects of atmospheric aging on a hybrid polymer matrix composite. Compos Sci Technol 2012;72(15):1803-1811.

[15] V.S. Rao, V. Yadav, V.K. Kumar, N. Chand. Combined effect of nanoclay and alumina addition on structure, TGA, DMA characteristics of nanoclay, and alumina-filledpolypropylene nanocomposites. Journ Thermoplastic Compos Mat 2011;25(7):851-863.

[16] S. Chartterjee, N. Nafezarefi, N.H. Tai, L. Schlagenhauf, F.A. Nuesch, B.T.T. Chu. Size and synergy effects of nanofiller hybrids including graphene nanoplatelets and carbon nanotubes in mechanical properties of epoxy composites. Carbon 2012;50(15):5380-5386.

[17] M. Norkhairunnisa, A. Azizan, M. Mariatti, H. Ismail, L.C. Sim. Thermal stability and electrical behavior of polydimethylsiloxane nanocomposites with carbon nanotubes and carbon black fillers. Journ Compos Mat 2011;46(8):903-910.

[18] P.K. Ghosh, A. Pathak, M.S. Goyat, S. Halder. Influence of nanoparticle weight fraction on morphology and thermal properties of epoxy/TiO2 nanocomposite. Journ Reinfor Plastics Compos 2012;31(17):1180-1188.

[19] Rashmi, N.M. Renukappa, R. Chikkakuntappa, N.S. Kunigal. Montmorillonite Nanoclay Filler Effects on Electrical Conductivity, Thermal and Mechanical Properties of Epoxy-Based Nanocomposites. Polym Engin Sci 2011;51(9):1827-1836.

[20] A. Allahverdi, M. Ehsani, H. Janpour, S. Ahmadi. The effect of nanosilica on mechanical, thermal and morphological properties of epoxy coating. Prog Organic Coatings 2012;75(4):543-548.

[21] P. Mederic, L. Le Pluart, T. Aubry, P.J. Madec. Structure and Rheology of Polyethylene/Imidazolium-Based Montmorillonite Nanocomposites. Journ Applied Polym Sci 2012;127(2):879-887.

[22] L. Wang, K. Wang, L. Chen, Y. Zhang and C. He. Preparation, morphology and thermal/mechanical properties of epoxy/nanoclay composite. Compos Part A 2006;37(11):1890-1896.

[23] A. Frache, O. Monticelli, M. Nocchetti, G. Tartaglione, U. Costantino. Thermal properties of epoxy resin nanocomposites based on hydrotalcites. Polym Degrad Stab 2011;96(1):164-169.

[24] S.M. Mirabedini, M. Behzadnasab and K. Kabiri. Effect of various combinations of zirconia and organoclay nanoparticles on mechanical and thermal properties of an epoxy nanocomposite coating. Compos Part A 2012;43(11):2095-2106.

[25] C.K. Reddy, T. Shekharam and D. Shailaja. Preparation and Characterization of Poly(chlorotrifluoroethylene-co-ethylvinyl ether)/Poly(styrene acrylate) Core–Shells and SiO2 Nanocomposite Films via a Solution Mixing Method. Journ Applied Poly Sci 2012;126(5):1709-1713.

[26] Th. V. Kosmidou, A. S. Vatalis, C. G. Delides, E. Logakis, P. Pissis, G. C. Papanicolaou. Structural, mechanical and electrical characterization of epoxy-amine/carbon black nanocomposites. Express Polym Letters 2008;2(5):364-372.

[27] D.S. Achilias, P. Siafaka and A.K. Nikolaidis. Polymerization kinetics and thermal properties of poly(alkyl methacrylate)/organomodified montmorillonite nanocomposites. Polym International 2012;61(10):1510-1518.

[28] O. Zabihi, A. Omrani, A. Ali Rostami. Thermo-oxidative degradation kinetics and mechanism of the system epoxy nanocomposite reinforced with nano-Al2O3. Journ Therm Analysis Calorimetry 2012;108(3):1251-1260.

[29] X. Li, ZJ. Zhan, G.R. Peng, W.K. Wang. New high-performance epoxy nanocomposites co-reinforced by two- and zero-dimensional nanoscale particles. Mat Sci Engin A 2011;530:680-684.

[30] L. Barral, J. Cano, J. Lopez, I. Lopez-Bueno, P. Nogueira, M.J. Abad, et al. Physical aging of an epoxy/cycloaliphatic amine resin. Euro Polym Journ 1999;35:403-411.

[31] Aging of quenched polypropylene. Rogers, K. Kapur and C.E. 1972, Polym Sci.

[32] D.S. Chandra, R.M.V.G.K. Rao, Kishore. Effects of post-curing on the mechanical properties and fracture features of some glass-phenolic composites. Journ Mat Sci Letters 1991;10(21):1263-1266.

[33] C.H. Chen, C.C.M. Ma. Pultruded fibre reinforced polyurethane composites II. Effect of processing parameters on mechanical and thermal properties. Compos Sci Technol 1992;45(4):345-352.

[34] D. Leveque, H. Katoh, J. Cinquin, K. Hasegawa. Durability evaluation of carbon/BMI composites after thermal aging. Jeju, Korea: s.n., August 2011, 18th International Conference on Composite Materials.

[35] J. Wolfrum, S. Eibl, L. Lietch. Rapid evaluation of long-term thermal degradation of carbon fibre epoxy composites. Compo Sci Technol 2009;69(3-4):523-530.

[36] A. Chatterjee. Thermal degradation analysis of thermoset resins. Journ Applied Poly Sci 2009;114(3):1417-1425.

[37] M.F. Ashby, D.R.H. Jones. Engineering Materials 1 an Introduction to Properties, Applications and Design. 3rd. Oxford: Elseveir Ltd, 2007.

[38] E. Barjasteh, E.J. Bosze, Y.I. Tsai, S.R. Nutt. Thermal aging of fiberglass/carbon-fiber hybrid composites. Compos Part A 2009;40(12):2038-2045.

[39] F. Samperi, C. Puglisi, R. Alicata, G. Montaudo. Thermal degradation of poly(butylenes terephthalate) at processing temperature. Polym Degrad Stab 2003;83(1):11-17.

[40] J. Wise, T. Gillen, R.L. Clough. An ultra sensitive technique for testing Arrhenius extrapolation assumption for thermally aged elastomers. Polym Degrad Stab 1995;49(3):403-418.

[41] S. Carrocio, P. Rizzarelli, G. Scaltro and C. Puglisi. Comparative investigation of photo- and thermal-oxidation processes in poly(butylenes terephthalate). Polym 2008;49(16):3371-3381.

[42] Walker, H.L. Johnston, M.K. The dissaciation of oxygen to 5000 K. Indianapolis: s.n., 1933. Meeting of the American Chemical Society.

[43] D. Allara. Aging of Polymers. Environ Health Persp 1975;11: 29-33.

[44] Y. Pei, K. Wang, M. Zhan, W.Xu and X. Ding. Thermal-oxidative aging of DGEBA/EPN/LMPA epoxy system: Chemical strucure and thermal-mechanical properties. Polym Degrad Stab 2011;96(7):1179-1186.

[45] S. Kumagai, N. Yoshimura.Impacts of thermal aging and water absorption on the surface of electrical and chemical properties of cycloaliphatic epoxy resin. IEEE Trans Dielectr Electr Insul 2000;7(3):424-431.

[46] . D. Guo, M. Zhang and K. Wang. Microstructure evolution of ammonia-catalyzed phenolic resins during thermooxidative aging. Journ Applied Poly Sci 2012;126(6):2010-2016.

[47] W. Tian, J. Hodgkin. Long term aging in a commerical aerospace composite sample: chemical and physical aging. Journ Applied Polym Sci 2010;115(5):2981-85.

[48] T.K.Tsotsis, S.M. Lee.Long-term thermo-oxidative aging in composite materials: failure mechanisms. Compos Sci Technol 1998;58:355-68.

[49] K. Pochiraju, G.P. Tandon. Interaction of oxidation and damage in high temperature polymeric matrix composites. Compos Part A 2009;40:1931-40.

[50] G.P. Tandon, K.V. Pochiraju, G.A. Schoeppner. Thermo-oxidative behavior of high-temperature PMR-15 resin and composites. Mat Sci Engin A 2008;489(1-2):150-161.

[51] H. Parvatareddy, J.Z. Wang, D.A. Dillard, T.C. Ward, M.E. Rogalski. Environmental aging of high-performance polymeric composites: effects on durability. Compos Sci Technol 1995;53:399-409.

[52] L. Frank-Lacaze, C. Bonnet, S. Besse, F. Lapicquw. Effects of ozone on the performance of a polymer electrolyte membrane fuel cell. Fuel Cells 2009;9(5):562-569.

[53] F. Cataldo. On the action of ozone on polyaniline. Polym Degrad Stab 2001;75(1):93-98.

[54] F. Cataldo, G. Angelini. Some aspects of ozone degradation of poly(vinyl alcohol). Polym Degrad Stab 2006;91(11):2793-2800.

[55] F. Cataldo, M. Omastova. On the ozone degradation of polypyrrole. Polym Degrad Stab 2003;82(3):487-495.

[56] J.M. Torres, C.M. Stafford, B.D. Vogt. Manipulation of the elastic modulus of polymers at the nanoscale: Influence of UV-ozone cross-linking and plasticizer. ACS Nano 2010;4:5357.

[57] T. Nair, M. Kumaran, G. Unnikrishnan. Mechanical and aging properties of cross-linked ethylene propylene diene rubber styrene butadiene rubber blends. Joun Applied Polym Sci 2004;93(6):2606-2621.

[58] Y.K. Choi, Y. Gotoh, K. Sugimoto, S.M. Song, T. Yanagisawa, M. Endo. Processing and characterization of epoxy nanocomposites reinforced by cup-stacked carbon nanotubes. Polym 2005;46(25):11489-11498.

[59] Z. Jin, Z. Zhang, L. Meng. Effects of ozone method treating carbon fibers on mechanical properties of carbon/carbon composites. Mat Chem Phys 2005;97(1):167-172.

[60] G. Peng, H. Wang, H. Wang, Q. Liu, W. Hao. Influence of carbonyl Fe on degradation of epoxy in ozone environment. Journ Polym Environ 2009;17(3):159-164.

[61] R. Kultzow, S. Foxhill. Cycloaliphatic epoxy resins. 2007. Thermoset Resin Formulators Association.

[62] Q. Liao, H.J. Zhang, K. Wu, H.Y. Li, S.N. Bao, P. He. Oxidation of graphene on Ru(0001) studied by scanning tunneling microscopy. Applied Surf Sci 2010;257(1):82-86.

[63] . S. M. Lee, Y.H. Hwang, J.R. Hahn, H. Kang. Defect-induced oxidation of graphite. Phys Review Letters 1999;82(1):217-220.

[64] S.P. Lonkar, S. Therias, N. Caperaa, F. Leroux, J.L. Gardette. Photooxidation of polypropylene/layered double hydroxide nanocomposites: Influence of ontralamellar cations. Euro Polym Journ 2010;498(1-2):1456-1464.

[65] . G.P. Tandon, K.V. Pochiraju, G.A. Schoeppner.Thermo-oxidative behavior of high-temperature PMR-15 resin and composites. Mat Sci Engin A 2008;498(1-2):150-161.

[66] G. Zhang, W.G. Pitt, S.R. Goates, N.L. Owen.Studies on oxidative photodegradation of epoxy resins by IR-ATR spectrscopy. Journ Applied Polym Sci 1994;54:419-427.

[67] Study of the degradation of an epoxy/aminerResin, 1 - photo and thermo-chemical mechanisms. 2005, Macromolecular Chemistry and Physics, Vol. 206, pp. 575-584.

[68] B. Mailhot, S. Morlat-Therias, M. Ouahioune, J.L. Gardette. Study of the drgradation of epoxy/amine resin, 2 kinetics and depth-profiles. Macromol Chem Phys 2005;206:585-591.

[69] G.Z. Xiao, M.E.R. Shanahan. Irreversible effects of hygrothermal aging on DGEBA/DDA epoxy resin. Journ Applied Polym Sci 1998;69(2):363-369.

[70] B. Guo, D. Jia, W. Fu, Q. Qiu. Hygrothermal stability of dicyanate-novolac epoxy resin blends. Polym Degrad Stab 2003;79(3):521-528.

[71] S.G. Miller, G.D. Rpberts, J.L. Bail, L.W. Kohlman, W.K. Binienda. Effects of hygrothermal cycling on the chemical, thermal and mechanical properties of 862/W epoxy resin. High Perform Polym 2012;24(6):470-477.

[72] G. Xian, H. Li, X. Su. Water absportion and hygrothermal ageing of ultraviolet cured glass-fiber reinforced acrylate composites. Polym Compos 2012;33:1120-1128.

[73] S. Jana, W.H. Zhong. FTIR study of ageing of epoxy resin reinforced by reactive graphitic nanofibers. Journ Applied Polym Sci 2007;106:3555-3563.

[74] S. Pillay, U.K. Vaidya, G.M. Janoski. Effects of moisture and UV exposure on liquid molded carbon fabric reinforced nylon 5 composite laminates. Compos Sci Technol 2009;69:839-846.

[75] R.J. Morgan, J.E. O'Neal, D.L. Fanter. Effect of moisture on the physical and mechanical integrity of epoxies. Journ Mat Sci 1980;15(3):751-764.

[76] E.L. McKague, J.E. Halkias and J.D. Reynolds. Moisture in composites - Effects of supersonic service on diffusion. Journ Compos Mat 1975;9:2-9.

[77] J.A. Hough, Z.D. Xiang F.R. Jones. The effect of thermal spiking and resultant enhanced moisture absorption on the mechanical and viscoelastic properties of carbon fibre reinforced epoxy laminates. Experim Techniq Design Compos Mat 1998;144(3):27-41.

[78] Gupta, Alka. Polymer Chemistry. Meerut: Global Media, 2010.

[79] U.S. Energy Information Administration. Annual Energy Review. EIA. [Online] September 27, 2012. [Cited: October 2, 2012.] http://www.eia.gov/totalenergy/data/annual/#summary.

[80] MatWeb Material Property Data. Aluminum 6061-T6; 6061-T651 . MatWeb. [Online] 2012. [Cited: September 10, 2012.] http://matweb.com/search/datasheet.aspx?MatGUID=1b8c06d0ca7c456694c7777d9e10be5b.

[81] B. Burks, D. Armentrout, J. Buckley, M. Baldwin, M. Kumosa. Hybrid composite rods subjected to excessive bending loads. Compos Sci Technol 2009;69(15-16):2625-32.

[82] B. Burks, D. Armentrout, M. Kumosa. Characterization of the fatigue properties of a hybrid composite utilized in high voltage electric transmission. Compos Part A 2011;42(9):1138-1147.

[83] D. Hull, T.W Clyne. An Introduction to Composite Materials. 2nd. New York: Cambridge University Press, 1996. p. 11.

[84] P. Rupnowski and M. Kumosa. Meso- and micro-stress analyses in an 8HS graphite/polyimide woven composite subjected to biaxial in-plane loads at room temperature. Compos Sci Technol 2003;63:785-99.

[85] B. Burks, M. Kumosa. The effects of atmospheric aging on a hybrid polymer matrix composite. Compos Sci Technol 2012;72(15):1803-11.

[86] B. Burks, J. Middleton, M. Kumosa. A model for bending stress amplitude prediction from Aeolian vibrations of a polymer matrix composite core conductor. August 2011, IEEE Transact Power Deliv. in review.

[87] B. Burks, J. Middleton, M. Kumosa. Effects of aging of the flexural strengths of the ACCC core. October 2011. Technical Report.

[88] J.P. Habas, J.M. Arrouy, F. Perrot. Effect of electrical partial dicharges on the rheological and chemical properties of polymers used in HV composite insulators after railway service. IEEE Transact Dialec Electric Insul 2009;16(9):1444-1445.

[89] W. Bu, J. Yin, F. Tian, G. Li, Q. Lei. Effect of corona ageing on the structure changes of polyimide and polyimide/Al2O3 nanocomposite films. Journ Electrostatics 2011;69:141-145.

[90] Gentz, M. Polyimide composites at elevated temperatures. 2004. PhD Dissertation. University of Denver.

[91] Residual stresses in inidiractional graphite fibers/polyimide composites as a function of aging. M. Gentz, B. Benedikt, J.K. Sutter and M. Kumosa. 10-11, 2004, Composite Science and Technology, Vol. 64, pp. 1671-1677.

[92] . E. Barjahsteh, N. Kar, S.R. Nutt. Effect of filler on thermal aging of composites for the next-generation power lines. Compos Part A 2011;42(12):1873-1882.

[93] ASTM Annual Book of Standards. ASTM D790-07 standard test methods for flexural properties of unreinforced and reinforced plastics and electrical insulating materials. 2008.

[94] N.K. Kar, E. Barjasteh, Y. Hu and S.R. Nutt. Bending fatigue of hybrid composute rods. Compos Part A 2011;42(3):328-336.

[95] M. Kumosa. Failure analysis of a 345kV ACCC conductor. June 2011. Final Failure Report for Populus-Terminal Transmission Partners under contract #163128.78.0116.

[96] ASTM D4476-03 standard test method for flexural properties of fiber reinforced pultruded plastic rods. ASTM Annual Book of Standards. 2009.

[97] Fischer-Cripps, Anthony C. Nanoindentation. Secaucus: Springer, 2002.

[98] B. Benedikt, M. Gentz, L. Kumosa, P. Rupnowski, J. Sutter, M. Kumosa. X-ray diffraction experiments on aged graphite fiber/polyimide composites with embedded aluminum inclusions. Compos Part A 2004;35(6):667-681.

[99] A. Drago, M.J. Pindera.Micro-macromechanical analysis of hetergeneous materials: Macroscopically homogeneous vs periodic microstructures. Compos Sci Technol 2007;67:1243-1263.

[100] A.Nayfeh. Wave Propogation in Layered Anisotropic Media With Applications to Composites. 1. Amsterdam: Elsevier Science B.V., 1995.

[101] Ferry, J.D. Viscoelastic Properties of Polymers. 2nd. New York: John Wiley & Sons, Inc, 1970. pp. 302-307.

[102] B. Benedikt, M. Kumosa, D. Armentrout, L. Kumosa, J.K. Sutter, P.K. Predecki. Analysis of stresses in aluminum particles embedded inside unidirectional and woven graphite/polyimide composites subjected to large bending loads. Mech Adv Mat Structures 2004;11(1):31-49.

[103] B. Benedikt, M. Kumosa, P.K. Predecki, L. Kumosa. An analysis of residual thermal stresses in unidirectional graphite/PMR-15 composite based on the E-ray diffraction measurements. Compos Sci Technol 2001;61(14):1977.

[104] B. Benedikt, P. Rupnowski, L. Kumosa, J.K. Sutter, P.K. Predecki, M. Kumosa. Determination of interlaminar residual thermal stresses in waven 8HS graphite/PMR-15 composite using X-ray diffraction measurements. Mech Compos Mat Structures 2002;9(4):375-394.

[105] Menard, K.P. Dynamic Mechanical Analysis. s.l.: Encyclopedia of Polymer Science and Technology, 2004.

[106] G.A. Schoeppner, G.P. Tandon, E.R. Ripberger. Anisotropic oxidation and weight loss in PMR-15 composites. Compos Part A 2007;38(3):890-904.

[107] . N.S. Allena, M. Edgea, D. Mourelatoua, A. Wilkinsona, C.M. Liawua, M.D. Paralladab, J.A. Barriob and V. Ruiz Santa Quiteriab. Influence of ozone on styrene-ethylene-butykene-styrene (SEBS) copolymer. Polym Degrad Stab 2003;79(3):297-307.

[108] P.C. Lucas, R.S. Porter.Hydroperoxide from phenyl ring reactions of photooxidized polystyrene. Polym Degrad Stab 1988;22(2):175-184.

[109] W.P. Keavey, P.V. Rush, J.J. Pappas. Glyoxal from ozonolysis of benzene. Ind Eng Chem Prod Res Dev 1969;8(1):68.

[110] J. Stowe, P. Predecki, P. Laz, B. Burks, M. Kumosa. Probabilistic molecular dynamics evaluation of the stress-strain behavior of polyethylene. Acta Materialia 2009;57(12):3615-3622.

[111] . J. Middleton, J. Hoffman, B. Burks, P.K. Predecki, M. Kumosa. Aging of a Polymer Core Composite Conductor: Mechanical Properties and Residual Stresses. s.l. : Submitted for Review Compos Part A, May 2014.

[112] . J. Middleton, B. Burks, T. Wells, A. M. Setters, I. Jasiuk, M. Kumosa. The effect of ozone and high temperature on polymer degradation in polymer core composite conductors Polym Degrad Stability 2013;98:2282-2290.

[113] MatWeb Material Property Data. Overview of Materials for Epoxy, High Temperature. [Online] MatWeb. http://matweb.com/search/DataSheet.aspx?MatGUID=7edc700f902841f29d5578fd5f182f5b&ckck=1.

[114] G.M. Odegard, A. Bandyopadhyay. Physical Aging of Epoxy Polymers and Their Composites. Journ Polym Sci Part B: Polym Phys 2011;49(24):1695-1716.

[115] M. Gentz, B. Benedikt, J.K. Sutter, M. Kumosa. Residual stresses in inidiractional graphite fibers/polyimide composites as a function of aging. Compos Sci Technol 2003;64(10-11):1671-1677.